



TENDL: Complete Nuclear Data Library for Innovative Nuclear Science and Technology

A.J. Koning^{1,2,*}, D. Rochman³, J.-Ch. Sublet¹, N. Dzysiuk^{4,5}, M. Fleming^{6,7} and S. van der Marck⁴¹*Nuclear Data Section, International Atomic Energy Agency, P.O. Box 100, 1400 Vienna, Austria*²*Department of Physics and Astronomy, Uppsala University, Uppsala, Sweden*³*Laboratory for Reactor Physics Systems Behaviour, Paul Scherrer Institut, Villigen, Switzerland*⁴*NRG, Westerduinweg 3, 1755 LE Petten, Netherlands*⁵*Taras Shevchenko National University of Kyiv, Kyiv, Ukraine*⁶*Nuclear Energy Agency, OECD, 92100 Boulogne-Billancourt, France*⁷*United Kingdom Atomic Energy Authority, Culham Science Centre, Abingdon OX14 3DB, United Kingdom*

(Received 3 August 2018; revised received 7 November 2018; accepted 29 November 2018)

The TENDL library is now established as one of the major nuclear data libraries in the world, striving for completeness and quality of nuclear data files for all isotopes, evaluation methods, processing and applied performance. To reach this status, some basic principles have been applied which sets it apart from other libraries: reproducible dedicated evaluations when differential data are available, through determination of nuclear models implemented in TALYS and their parameters, completeness (with or without experimental data), format and processing standardization, automation of production and reproducibility. In this paper, we will outline how such an approach has become a reality, and recall some of the past successes since the first TENDL release in 2008. Next, we will demonstrate the performance of the latest TENDL releases for different application fields, as well as new approaches for uncertainty quantification based on Bayesian inference methods and possible differential and integral adjustments. Also, current limitations of the library performances due to modelling and needs for new and more precise experimental data will be outlined.

CONTENTS

| | |
|--|----|
| I. INTRODUCTION | 2 |
| A. General Philosophy of TENDL | 3 |
| B. Current TENDL Use Worldwide | 3 |
| C. Conceptual Differences with Other World Libraries | 4 |
| D. This Paper | 4 |
| II. RESOLVED AND UNRESOLVED RESONANCES | 5 |
| A. Source of Resonance Parameters | 5 |
| 1. A Resonance Compiler Code: TARES | 5 |
| 2. Stable and Long-lived Isotopes | 7 |
| 3. Isotopes with Significant Missing Resonances | 7 |
| 4. Shorter-lived Isotopes | 7 |
| B. High-Fidelity Resonances with CALENDF | 7 |
| 1. Prior to the HFR: Smooth, Radiator and the SRA | 7 |
| 2. Next Step: the HFR | 10 |
| C. Retroactive SAMMY Fitting | 10 |

| | |
|---|----|
| III. TALYS | 11 |
| A. Brief Summary of Nuclear Models | 13 |
| 1. Optical Model | 13 |
| 2. Level Density | 14 |
| 3. Gamma-ray Strength Function | 14 |
| 4. Compound Nucleus Model | 14 |
| 5. Pre-equilibrium Model | 15 |
| 6. Fission | 15 |
| IV. UNCERTAINTIES | 15 |
| A. Bayesian Monte Carlo for Covariances | 15 |
| 1. Goodness-Of-Fit Estimator | 17 |
| 2. Pseudo-Experimental Data | 18 |
| 3. Summary | 19 |
| B. Covariances for Resonance Regions | 19 |
| 1. Parameters Covariance for Stable and Long-lived Isotopes | 19 |
| C. Covariances for nubar and PFNS | 21 |
| V. LIBRARY PRODUCTION | 22 |
| A. Production Flow for TENDL with ‘T6’ | 22 |
| 1. T6 Software | 22 |
| 2. Required Input for the TENDL Data Files | 25 |
| B. Optimized Input Parameters for TALYS ‘Best’ Input Files | 25 |

* Corresponding author: a.koning@iaea.org

| | |
|--|----|
| C. TENDL Neutron Data Library | 26 |
| D. TENDL Photonuclear Data Library | 27 |
| E. TENDL Charged Particle Data Libraries | 27 |
| 1. Proton Sublibrary | 28 |
| 2. Deuteron Sublibrary | 29 |
| 3. Triton Sublibrary | 30 |
| 4. Helium-3 Sublibrary | 30 |
| 5. Alpha Sublibrary | 30 |
| F. Differential Validation with EXFOR | 31 |
| G. Validation with Compiled Experimental Data Sets | 33 |
| 1. Thermal Cross Sections | 33 |
| 2. Resonance Integrals | 34 |
| 3. MACS and the KADoNiS Database | 34 |
| VI. ADJUSTMENT | 35 |
| A. Prior Nuclear Data | 36 |
| B. Inference via Differential Data and Monte Carlo | 37 |
| C. Inference via Integral Benchmarks and Monte Carlo | 39 |
| VII. PROCESSING ROUTES | 40 |
| A. PREPRO | 40 |
| 1. Data Formats for Applications | 41 |
| B. NJOY Processing | 41 |
| C. CALENDF Processing | 42 |
| VIII. BENCHMARKING | 42 |
| A. ICSBEP | 42 |
| B. Shielding | 44 |
| C. Delayed Neutron Data Testing | 45 |
| D. Integral Activation Data | 46 |
| 1. JAEA FNS Decay Heat Data | 46 |
| 2. Integro-differential Validation | 46 |
| IX. APPLICATIONS | 48 |
| A. Use in Nuclear Software | 48 |
| B. Use in Nuclear Libraries | 48 |
| C. Total Monte Carlo | 48 |
| D. Other Applications | 50 |
| X. FUTURE | 50 |
| A. Systematic Evaluation of Experimental Reaction Data | 50 |
| B. Solving Deficiencies in Uncertainty Quantification | 50 |
| C. Systematic Integral Data Evaluation | 50 |
| D. Upgrade to Microscopic Nuclear Models used in TALYS | 50 |
| E. Cleaning up the Software | 51 |
| ACKNOWLEDGEMENTS | 51 |
| References | 51 |

I. INTRODUCTION

The field which we now call ‘nuclear data’ was already present in the 1950’s and 1960’s when the development of nuclear technology required a systematic use of basic nuclear scientific information. Information from nuclear reaction and structure experiments were stored in numerical databases for preservation of knowledge and foremost for use in applications. These databases were fed into the first prototypes of computer codes which, subject to severe memory and speed limitations, managed to simulate the behavior of several nuclear devices at a basic but essential level.

Jumping straight to 2019, we can certainly say that the nuclear data field has matured. Large experimental databases like EXFOR [1] for reactions and XUNDL for structure reach an impressive degree of completeness of compilation with respect to historical and new measurements. Nuclear simulation codes have the latest nuclear models implemented and challenge the current day computer power, and the amount of evaluated, ENSDF, ENDF data in libraries and processed nuclear data libraries is entering the Gb range. After its trendsetting role in the 1960’s, the nuclear data field has been passed by other organizations, companies and industries when it comes to IT-related development. This is probably due to the decreasing popularity of, and financial input in, nuclear data evaluation. This lagging behind relates among others to the most used data format, ENDF-6, which indeed still stems from the 1960’s and must look totally archaic to newcomers. Fortunately, there are now initiatives such as the Generalized Nuclear Data (GND) format [2] to modernize this situation. The TENDL approach outlined in this paper relies on a firm control over information and knowledge in the whole nuclear data chain. Information management throws light on data and information, while knowledge management does upon knowledge, understanding and wisdom. Thereby, it is important to not only store and use information but also knowledge and to make optimal use of what we and our predecessors have measured, invented, evaluated and developed, without reinventing the wheel every time.

The information management side of nuclear data is relatively well-developed. (Well-)established databases are available, or processed into, ready to use forms. In the nuclear data world, one would categorize the EXFOR data compilation as information, while its interpretation, or evaluation (which so far has not yet been recorded in a systematic way), would rank as knowledge. Similarly, on the theoretical side, various nuclear models and their parameters have been accepted by the community as the current state-of-the-art until eventually some better model comes along. That means that the use of these models should basically be trivial; after the research stage comes the implementation and production stage, and these two phases should be strictly separated. The TALYS code [3] aims to fulfill this goal: several years after the research stage of theoretical nuclear reaction mod-

elling, a particular model should be so well established and accepted that there should be no discussion about its implementation in software. Again knowledge has been transformed into (the production of) information in the sense of validated, frozen software. Mixing research, development and production usually leads to failure, which is why for example a new version of TALYS is only released once per two years.

The knowledge management side of nuclear data is quite. Each component of the nuclear data chain has its own experts who know best the details, and which available information is more right or more wrong. This knowledge is should actually be quantified, in the sense that judgment about particular experimental data sets and the performance of nuclear models in certain energy and mass ranges, together with their parameters would be safely stored in ‘expert databases’, after which the standard automated flow of software and data can produce the next version of the data library. In short, the key to efficient, high-quality nuclear data evaluation is quantifying knowledge of the experts.

The aim of the system built around TALYS is to implement this information and knowledge flow as much as possible. The TENDL library is merely one output of the system built around TALYS. This should not be read as a case of false modesty; the rapidly increasing use of TENDL worldwide is something to be proud of, but retrospectively we conclude that it is nothing more than pouring the output of this software and knowledge system into a specific format, albeit a complicated one. Also it should be noted here that parts of TENDL still come from other existing libraries, since these parts clearly outperform current TALYS capabilities. For example, this is the case for the major actinides which are adopted from the ENDF/B-VIII data library [4]. The production of ENDF-6 formatted TENDL files opens up many possibilities for simulation of integral processes, as shown in this paper. Although the emphasis in this paper will be on the TENDL library, the systematic and automated approach built around TALYS gives rise to possibilities which can not easily be found elsewhere, for example

- Uncertainty propagation with Total Monte Carlo [5]: varying experimental data, resonance and nuclear model parameters inside their uncertainty margins at the beginning of the entire chain of software and databases for nuclear technology results in exact probability distributions and correlations of technologically relevant parameters, without the necessity to drag along (processed) covariance matrices throughout the chain. Instead, one has a statistical ensemble of ENDF-6 and processed libraries
- Complete verification and validation of the EXFOR database [6] to a certain global depth of detail.
- Large scale comparisons of different nuclear models by comparing the relative ratio of the results for a wide range of nuclides.
- Complete libraries with astrophysical reaction rates [7], medical isotope production data,
- Worldwide use of TALYS and its satellite software, for basic nuclear science and applications, *etc.*

and it is to be expected that the availability of such a system gives rise to ‘sudden’ new ideas (*e.g.*, visualization possibilities, useful computer Apps, *etc.*), analogous to the new concepts in the above list which emerged unplanned and only a few years apart. Each of the topics above probably deserves, or is already outlined in, a separate publication. In this paper we will focus on the TENDL nuclear data library, including the physics behind it, its uncertainty quantification, and applied use.

A. General Philosophy of TENDL

The first versions of the various nuclear data libraries in the world contained evaluations which had only specified parts of the libraries filled with data, often those reaction channels for which experimental data existed and/or those parts which were deemed important for applications (otherwise differential measurements would probably not exist). Not so long ago, a detailed look into a nuclear data library gave the impression that the generally adopted point of view was “If it has not been measured, it does not exist”, since only specific parts of a nuclear data library were filled. Thanks to the development of nuclear models, in combination with demands from users which could not afford gaps in their nuclear data tables, this point of view is slowly but surely being abandoned by all major nuclear data libraries. TENDL takes a rather extreme point of view here: every nuclear reaction process which is expected to take place in reality should be present in a nuclear data library, measured or not measured. In short, that means, all projectiles, all nuclides, all reaction channels and all energies. This entails a heavy reliance on nuclear modeling with predictive power for all reaction channels and secondary distributions, and a globally reliable approach for uncertainty quantification. Where possible, and preferably, simulated results should be overruled by high-quality experimental data, either directly, or by TALYS calculations with parameters that have been adjusted to match the experimental data. As detailed in this paper, this approach of completeness, with as much quality as possible, is applied to both the resonance range and the fast energy range.

B. Current TENDL Use Worldwide

In Fig. 1, the worldwide use of the TENDL libraries in the past decade is depicted, while Fig. 2 shows a, somewhat arbitrary, distribution over fields of application.

A welcome observation is that in more and more nuclear analyses, both with regards to differential data and applications, TENDL is now compared with other world

data libraries with respect to its performance. This means that TENDL is beyond the stage of only being used when "there is nothing else available", although it is perhaps hard to believe that a complete nuclear data library can also deliver quality on an individual nuclide basis. In this paper, we will show why use of TENDL for individual nuclide-by-nuclide analyses is justified. Nevertheless, Fig. 2 shows that the use of TENDL is dominated by non-criticality analyses for applications as non-proliferation, activation, decay heat, radiation damage, *etc.* which require neutron data that is generally not available in other libraries, and applications with charged particles and photons for which there is often nothing else available.

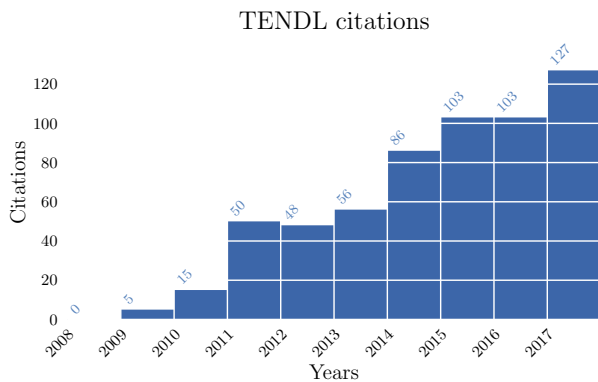


FIG. 1. Time-dependence of TENDL citations, from the first library release in 2008.

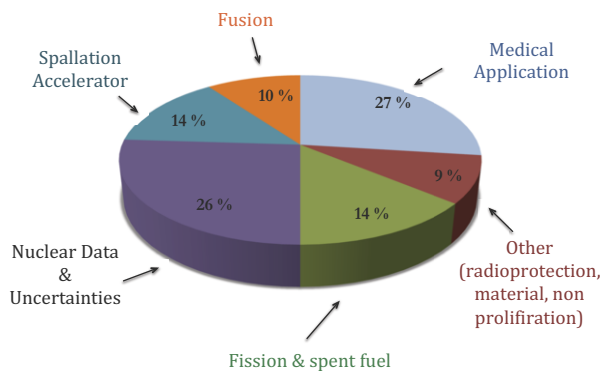


FIG. 2. (Color online) Segmentation of TENDL publications by application area, over the years 2008-2017.

C. Conceptual Differences with Other World Libraries

The production process of TENDL is different from all other nuclear data libraries in the world. In both approaches the evaluation effort is shared between people. Only for TENDL this happens at a level deeper than that of filling the ENDF library with data, namely with fundamental input files for the evaluation: Databases relative to EXFOR, containing pointers to include or exclude experimental data, a 'best' TALYS input file for each target nuclide, a specific chosen resonance parameter set and a file with specific, better data from other world libraries. The entire library is produced at once, while for other nuclear data libraries different evaluators deliver isotopic ENDF-6 data files at different times, using different ENDF-6 procedures, at one central place. This leads to a rather fundamental question: Can an evaluated isotopic file in TENDL perform better than that of other world libraries, knowing that in TENDL the evaluation effort has to be more equally shared over all nuclides, while in the approach of other world libraries one invests more expert knowledge in that particular isotope but one does not make use of this efficient system which produces a very complete and consistent file? The current paper aims to give some answers to that. Important to remember is that for all other world libraries an 'evaluation' is equal to an ENDF-6 formatted file, since knowledge has gone straight into the latter which is not reproducible anymore. Hence, we like to say that *e.g.*, ENDF/B-VIII has 556 evaluations (or isotopic data files), while TENDL-2017 has 2813 isotopic data files.

D. This Paper

This paper is organized as follows. In Section II, we will start with an outline of the low-energy reaction part of the system and describe the treatment of the resolved and unresolved resonance ranges. In Section III, the fast and high energies will be covered, and this part is dominated by the TALYS code. A brief review of the used nuclear models and parameters will be given. Section IV contains a description of the methods used to assign uncertainties to the nuclear data. In Section V the entire software system, 'T6', to produce the TENDL libraries is described, together with an explanation of the method to come to best results from a differential data point of view, and a description of all TENDL sublibraries. Section VI deals with nuclear data adjustment to both differential and integral data. In Section VII the processing codes and routes for the TENDL libraries are described, while the subsequent benchmarking is outlined in Section VIII. Section IX gives an overview of the most important applications of TENDL that we are aware of. Finally, Section X is devoted to the future of TENDL and conclusions.

II. RESOLVED AND UNRESOLVED RESONANCES

The resolved and unresolved resonance range (later called RRR and URR, respectively) is of major importance for the correct simulation of all systems heavily relying on thermal reactions. In the following, we will describe the specific approach taken in the TENDL library.

Our goal is to provide the users with a set of resonance parameters for all isotopes included in TENDL (neutron sublibrary). As easily understood, the origin of these parameters cannot be the same for *e.g.*, ^{73}As or ^{75}As which are both given in TENDL (one is short lived with 80 days half-life, the other one is stable). This is why we can distinguish a few categories:

1. isotopes with measured resonance parameters and measured “*integral*” values. Here, integral values can be thermal cross sections, capture integrals or Maxwellian averaged cross sections,
2. isotopes with “*integral*” values only,
3. isotopes without any experimental information.

Examples for the two mentioned isotopes are presented in Fig. 3. As seen on these figures, both isotopes seem to possess “*evaluated*” resolved resonances. If looked more into details, the ^{75}As isotopes have very similar resonances between the two presented libraries. Given that ^{75}As is the only stable isotope of Arsenic, these resonances are certainly derived from transmission and capture measurements at time-of-flight facilities. In the case of ^{73}As , one can see that the resonances are very different between the two libraries. In the case of ENDF/B-VIII.0 [4], they even follow a regular pattern, derived from a fixed D_0 (averaged spacing between resonances). This indicates that these resonances are not measured, but created to provide a resonance aspect to the cross section, possibly scaled to reproduced a thermal value. In the case of TENDL-2017, even if the resonances appear to be real, they are also derived from systematics and statistical patterns. The way to obtain them will be presented below. These two examples are representative of the global approach often taken in a library, and systematically in TENDL.

Additionally, the reality is a bit more complicated, since for some isotopes, only a few resonances are reported, and it is known that an important amount is missing. Additionally, TENDL is also provided with covariance information. In the resonance range, the evaluation of the covariances entails some particularities compared to the fast neutron range, as the cross sections strongly vary in small energy steps. These aspects will be presented in more details in the following sections, hopefully providing TENDL users with the necessary information to build up confidence in the presented data.

A. Source of Resonance Parameters

As presented above, the origin of the resonance parameters in the TENDL libraries vary, depending on the degree of knowledge for the given isotope. In any case, a resolved resonance region is always given. In the production of TENDL, the resonance range is handled by a specific code called TARES.

1. A Resonance Compiler Code: TARES

TARES is a program to obtain cross section information in the resonance range, solely used for the production of resonance parameters in the context of the TENDL library. Its primary goal was to be connected with the software TALYS [8] to complete the low energy region. As TARES is used in the production of the TENDL library, it is part of the “T6” package, which will be described later. Since then, TARES is used in the production of the TENDL libraries and in the production of the so-called “random ENDF files”, used to propagate nuclear data uncertainties following the “Total Monte Carlo” (TMC) approach [5]. It does not only perform original resonance analysis, but TARES is also using other codes such as SAMMY [9] for the fitting of pointwise cross sections, CALENDF [10] for the generation of ladder of resonances and PREPRO [11] for the reconstruction of pointwise resonances. One of the particularity of TARES is to successfully linked all these codes for all isotopes of interest in TENDL.

It can be used from $Z = 3$ to $Z = 118$ to

- produce resonance parameters in the ENDF format (called MF2 or file 2). Mainly three formats are used: multi-level Breit Wigner (for actinides), Reich-Moore (for some non actinides) and LRF7 (for the majority of non actinides),
- produce resonance parameter uncertainties in the ENDF format (called MF32),
- produce cross section uncertainties in the resolved resonance range in the ENDF format (called MF33),
- produce random resonance parameters based on parameter uncertainties,
- reconstruct pointwise cross sections based on the resonance parameters in tabulated x-y format,
- reconstruct pointwise cross sections based on the resonance parameters in ENDF format (called MF3),
- produce grouped cross sections based on the resonance parameters in tabulated x-y format,
- apply the retroactive method to update the resonance parameter covariances (using SAMMY),

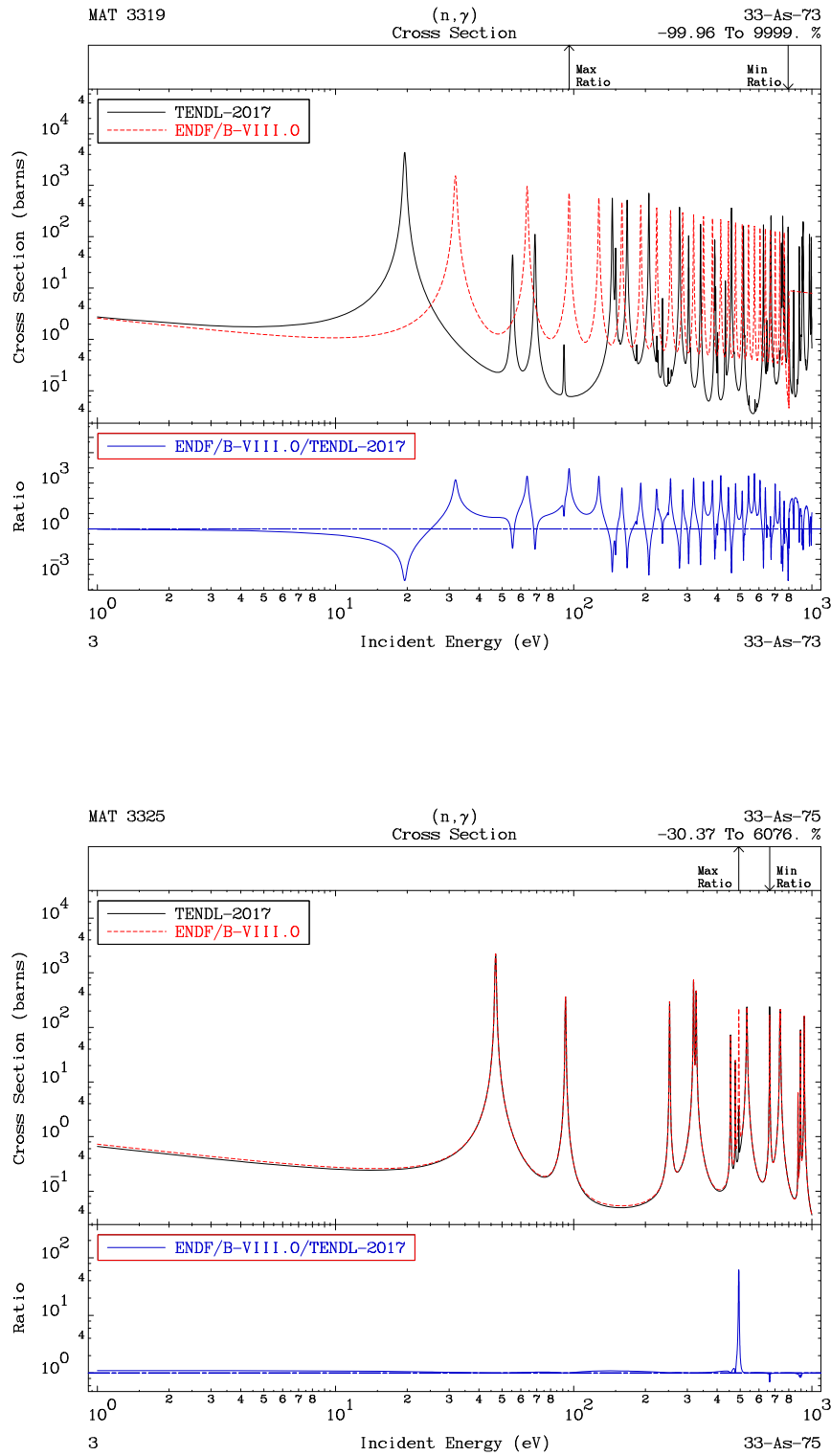


FIG. 3. (Color online) Resonance range for ^{73}As (top) and ^{75}As (bottom) from TENDL-2017 and ENDF/B-VIII.0.

- and produce angular distributions in the resonance range (also using SAMMY, or more precisely SAMRML).

Details of the application of TARES for TENDL will be developed in the following sections.

2. Stable and Long-lived Isotopes

In the case of stable and long-lived isotopes, the resonance parameters are taken either from existing libraries, or from compilations such as the Atlas of Neutron Resonances [12]. In these cases, a complete evaluation in the sense of performing a SAMMY [9] or REFIT [13] analysis is not done. Such approach is justified for isotopes heavier than $A \simeq 19$, including actinides. These parameters, together with a specific formalism approximation will define what enters in the so-called “file 2” (also called MF2) of the ENDF file. For the formalism, only two are used for the resolved resonance range (Reich-Moore or Multi-level Breit-Wigner). For the unresolved resonance range, the same procedure is followed: if a URR domain exists in another library, it is adopted in TENDL. If none are given, we either also do not provide a URR, or we propose one coming from TALYS calculations (see next section).

In some cases, the calculated thermal cross section from the resonance contribution does not correspond to the measured thermal value. In this case, the missing cross sections are added by using negative resonances. In TENDL, we are using an automatic procedure to calculate the resonance parameters of the negative resonances in order to match a specific thermal value. Very good results for the elastic, total and capture cross sections can be obtained, but it is not always successful in the case of actinides, where manual adjustments need to be done. Still, once the resonance parameters are found, they are stored in a simple table, ready for the next use of TARES.

In the case of light elements, the MF2 is often not used, but the pointwise cross sections are given in the “file 3”, of MF3. In TENDL, we do not have for the time being the capability to perform our own evaluations of these important isotopes. A very pragmatic solution is followed: simply adopting a full evaluated ENDF file from other libraries. This is for instance the case for ^1H , ^{16}O . This being said, for light isotopes not provided in other libraries, we believe that it is (still) worth providing some values in the shape of MF2, based on resonance compilations, or on the High Fidelity Resonances approach (HFR, see next section). This is the case for instance for ^{16}N .

In parallel, the estimation of the uncertainties and correlations are also done taking into account the experimental, or compiled uncertainties for thermal cross sections and resonance integrals.

3. Isotopes with Significant Missing Resonances

For some isotopes, some relatively large ranges of energy are not covered by measured resonances, even at low energy. This is for instance the case of ^{106}Cd , or ^{108}Cd . For such isotopes, two possibilities exist: either ignore the missing resonances (resulting in a strong decrease of the cross section), or filling the gap with statistical resonances. The origin of these statistical resonances is presented in the HFR section, but an example for $^{106}\text{Cd}(n,\gamma)$ is presented in Fig. 4. One can see the impact of the missing resonances for a specific energy range. One of the drawbacks of creating statistical resonances is to provide the impression that there is no need of additional measurements. It is therefore important to understand the origin of such resonances and to flag them as being calculated and not measured.

4. Shorter-lived Isotopes

Continuing towards the path of missing more and more information for the thermal and resonance range, it is very common that resonances of short-lived isotopes are not known. In many cases, their thermal cross sections are also not known. In general, such isotopes are not important for reactor applications, but can become relevant for short-term processes (such as the calculation of decay heat up to minutes after the shutdown of a reactor, or in environments with very high neutron flux [14]). The way to deal with such isotopes in TENDL is explained in the HFR section, with the guiding idea that all isotopes have a resolved resonance range in TENDL.

B. High-Fidelity Resonances with CALENDF

The global methodology of the High Fidelity Resonance approach (or HFR) is presented in details in Ref. [15]. An overview will be presented here with the specific link to TENDL.

As mentioned before, every single isotope in TENDL has a resolved resonance range. For missing resonances, these RRR are populated by statistical resonances with the HFR method. As in the case of TALYS, there no manual intervention required in the case of TARES and the HFR. TARES already contains the necessary information to provide statistical resonances for each single isotope. This procedure is used each time there is no (or missing) resonances, and each time a random MF2 is needed. A schematic view of the whole process is given in Fig. 2 of Ref. [15].

1. Prior to the HFR: Smooth, Radiator and the SRA

Filling the resonance range with calculated resonances is not new. The first solution consists in extending the

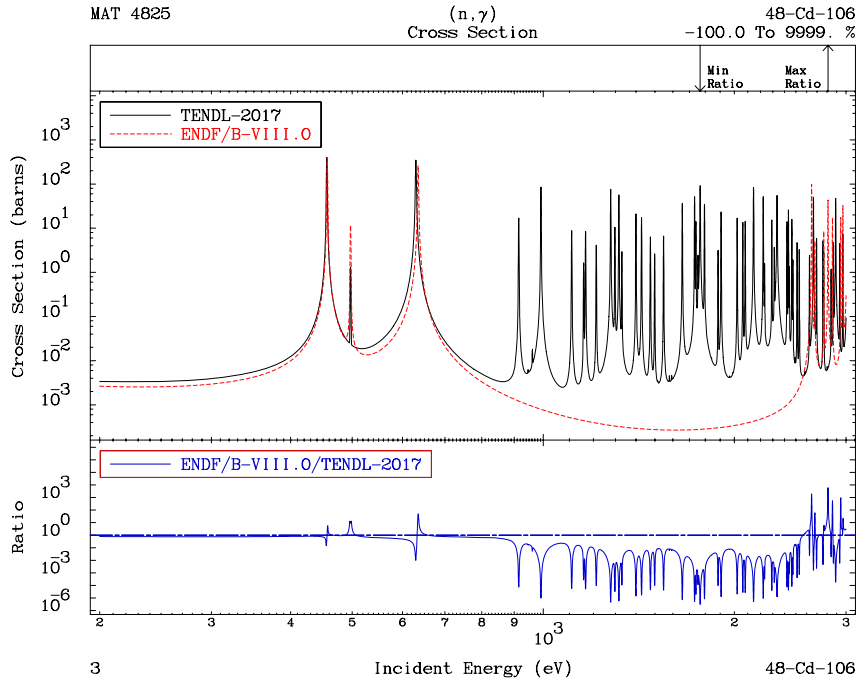


FIG. 4. (Color online) Example of the “filling” of missing resonances for $^{106}\text{Cd}(n,\gamma)$: comparison between TENDL-2017 and ENDF/B-VIII.0.

optical model calculation from a few hundreds of keV down to 0.01 eV, thus obtaining smooth cross sections. Obviously no resonance structure can be obtained, but such calculations could be adjusted in order to reproduce a measured thermal value (*e.g.*, by adjusting optical model and level density parameters). An example of such method is presented in Fig. 5 for the $^{90}\text{Sr}(n,\gamma)$ cross section. In this example, one can clearly see the drawback of this method: there is a non-physical discontinuity between the resonance and fast-neutron ranges, due to the different adjustments made in these two energy ranges.

Another simple approach to mimic resonance behavior is to create one resonance at every D_0 , D_0 being the s-wave average level spacing (see for instance Ref. [16]). In this case, resonances appear on a regular basis and were said to follow a “radiator behaviour”. This method was applied in the first releases of the TENDL libraries. A short description is given here, as it helps to understand the evolution towards the HFR.

For radiator-like resonances, the following assumptions were made for the six resonance parameters (l , j , E , Γ_n , Γ_γ and possibly Γ_f). The l value is assumed to be zero, and the spin of resonances j is the spin of the target nucleus plus 0.5. The four other parameters are changing with the resonance numbers i . The resonance energy E_i

is equal to

$$E_i = D_0 \times i, \quad (1)$$

with D_0 the s-wave average level spacing. For the neutron width Γ_n , according to the extreme compound, or black, nucleus model [17] the strength function is constant for all nuclei, and for s-wave neutrons is given by

$$\frac{\langle \Gamma_n^0 \rangle}{D_0} = \frac{2k_0}{\pi K} = 1 \times 10^{-4}, \quad (2)$$

where $\langle \Gamma_n^0 \rangle$ is the average s-wave reduced neutron width, D_0 is the average s-wave level spacing, k_0 is the wave number for a 1 eV neutron while K is the wave number inside the nucleus. For a potential well depth of 42 MeV, the black nucleus value of the strength function is 1×10^{-4} (Note that the strength function is a dimensionless quantity). It is then assumed that

$$\langle \Gamma_n^0 \rangle \simeq \Gamma_{nj}^{\ell=0} = \sqrt{\frac{1 \text{ eV}}{E_0} \frac{\Gamma_{nj}}{V_{\ell=0}}}, \quad (3)$$

with the penetrability $V_\ell = 1$ for s-waves ($l = 0$). We can then extract the neutron widths for the i^{th} resonance being:

$$\Gamma_{ni} = S_0 \times D_0 \times \sqrt{D_0 \times i}, \quad (4)$$

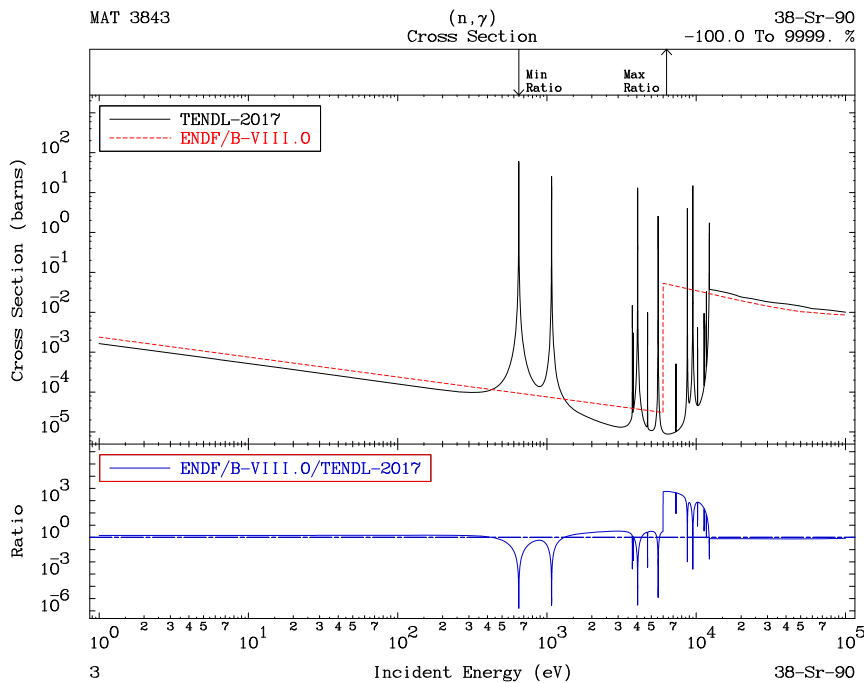


FIG. 5. (Color online) Example of smooth and resonance cross sections for $^{90}\text{Sr}(n,\gamma)$: comparison between TENDL-2017 and ENDF/B-VIII.0.

with S_0 the strength function for s-wave resonances. As an example, the case of ^{205}Pb is presented in Fig. 6 with 20 hypothetical resonance levels added to the bound level to simulate the elastic and capture cross sections up to 100 keV [16]. It was assumed a s-wave strength function S_0 of 10^{-4} , an average level spacing D_0 of 5 keV, a radiative width Γ_γ of 10 eV and a scattering radius of 8.7 fm. The fission width is simply related to the capture width with the following formula [12]:

$$\langle \Gamma_f \rangle = \langle \Gamma_\gamma \rangle \times \frac{\sigma_{\text{th}}(n, f)}{\sigma_{\text{th}}(n, \gamma)}. \quad (5)$$

In this approach, the shape of the resonances is also not physical as it can be seen in Fig. 6. A refinement can be found in the Single Resonance Approach (SRA), as originally presented in Refs. [18, 19]. The idea was to use a unique resonance plus a $1/v$ background to reproduce a known thermal cross section. One of the advantages is to be able to reproduce thermal values as well as resonance integrals when no other information are available. If no experimental values are known, systematics are applied as also presented in Ref. [16]. An example of such capture cross section is presented in Fig. 7 for $^{90}\text{Sr}(n,\gamma)$. One can see that the SRA represents an improvement for the RRR representation compared to a smooth cross section. Still,

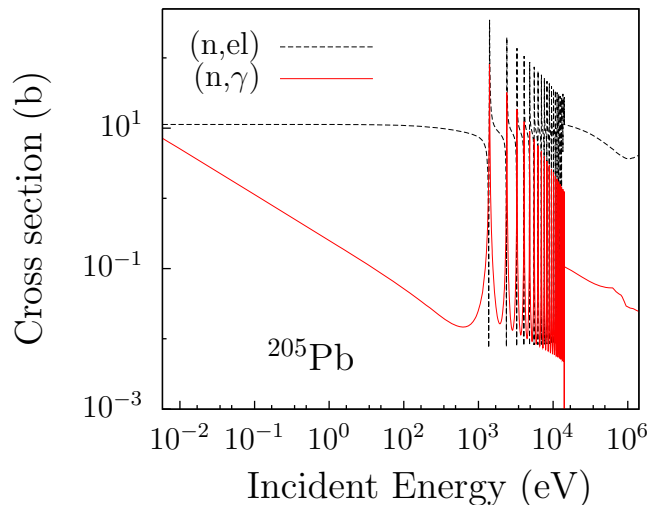


FIG. 6. (Color online) Example of radiator-like resonances for ^{205}Pb , see Ref. [16] for details.

a strong and non physical abrupt step appears between the resonance treatment and the fast neutron range. Additionally, the SRA does not address how to provide an

unresolved resonance range, if needed.

2. Next Step: the HFR

The HFR approach had as an original goal to create a link between the resolved resonance range and the fast neutron range. In the absence of experimental data in the resonance range, the idea is to extend the optical model calculation virtually down to 0 eV, to extract energy-dependent average parameters and to use these parameters to produce statistical resonances based on the ladder approach. Details are given below.

Such approach can be applied to isotopes without any experimental information, to isotopes with known thermal cross sections only, and also to isotopes with known resonances up to a certain energy. In the last case, the HFR would simply mean to “reconstruct” the URR into resolved resonances (see a good example for ^{238}U in Ref. [20]). A set of parameters are needed with their energy-dependent variations:

- scattering radius r ,
- average level spacing D_0 ,
- average reduced neutron width Γ_n^0 ,
- average radiation width Γ_γ ,
- and if needed the average fission width Γ_f .

As explained, these parameters are obtained by extending the necessary model calculations at low energy (*optical mode*). This is realized by using TALYS and the so-called “urr.dat” output file which contains the necessary information on a specific energy grid. In the TENDL libraries, the default optical model is the Koning-Delaroche [21], either local or global, depending on the isotopes (with some exceptions such as the stable Hf isotopes and some actinides). Therefore, the above parameters are simple derived from this optical model. An outline of the standard options of the optical model potential, level densities and photon strength function is given in the next Section on TALYS.

Once these parameters are available, they are given as input for the generation of random ladders of resonances, using the statistical properties of the unresolved resonance range. As presented in Ref. [16], “*ladders can be generated at an energy E by randomly selecting a starting resonance energy for one (l, j) sequence, and also randomly selecting a set of widths for that resonance using the appropriate average widths and χ^2 distribution functions. The next higher resonance energy can be selected by sampling from the Wigner distribution for resonance spacings, and a new set of widths for that resonance can be chosen. The process is continued until a long ladder of resonances for that (l, j) is obtained. The process for the other (l, j) sequences is then repeated, each such sequence*

being uncorrelated in positions from the others.” In practice, the CALENDF code [10] is used inside TARES, applying a Gaussian Orthogonal Ensemble random matrix for each (l, j) couple to generate random resonance energies [22]. The advantage of using CALENDF compared to NJOY for the resonance generation is that CALENDF follows the Wigner law and to include correlations between successive resonances. Energy “segments” are determined in CALENDF with a few tens of s -wave resonances in each of them. Based on stratified random numbers, the widths of the resonances are also obtained.

One needs to realize that the resonances created with this method are not real but their parameters are derived from specific distributions, in agreement with the optical model used at higher energy. If the seed of the random number generator is changing, different resonances will be obtained for a specific isotope.

Examples of these statistical resonances can be found in the recent TENDL libraries and the case of $^{90}\text{Sr}(n, \gamma)$ is also presented in Fig. 5. The impact of the HFR compared to the normal Hauser-Feshbach (HF) calculations have been extensively presented in Ref. [14], where it is demonstrated that the deviation between HF and HFR calculations is increasing when going further away from the valley of stability. In Ref. [14], a specific choice of level density model and gamma-strength function was made (Back-shifted Fermi gas model and Hartree-Fock BCS tables). Many other selections can be used to generate statistical resonances. In Fig. 8, the ratios of HFR/HF in terms of Maxwellian Average Cross Section (MACS) are presented for a different choice: using Hartree-Fock-Bogolyubov tables for the gamma-strength functions and Microscopic level densities (Skyrme force) from Hilaire’s combinatorial tables. The results presented here are very similar to those of Ref. [14]: the HFR leads to higher resonant captures compared to the HF model when the nuclear level densities are increasing. This indicates the importance of using cross sections having a resonance behaviour compared to smooth cross sections. In TENDL, the HFR is applied for all, either completely or partially missing from experiment, resolved and unresolved resonance ranges, for all nuclides.

C. Retroactive SAMMY Fitting

The retroactive method helps to analyse existing resonance parameters, without using the original experimental data (for instance from transmission measurements). It is therefore an approximate method and cannot replace a complete data study, as it is usually done for resonance analysis. With a certain number of assumptions, one can use the SAMMY fitting program [9] to obtain covariance matrices for the resonance parameters, or for the reconstructed cross sections. With the knowledge on the thermal cross sections (and uncertainties) and possibly other integral data (resonance integral, MACS), one can make sure that the reconstructed cross sections and uncertain-

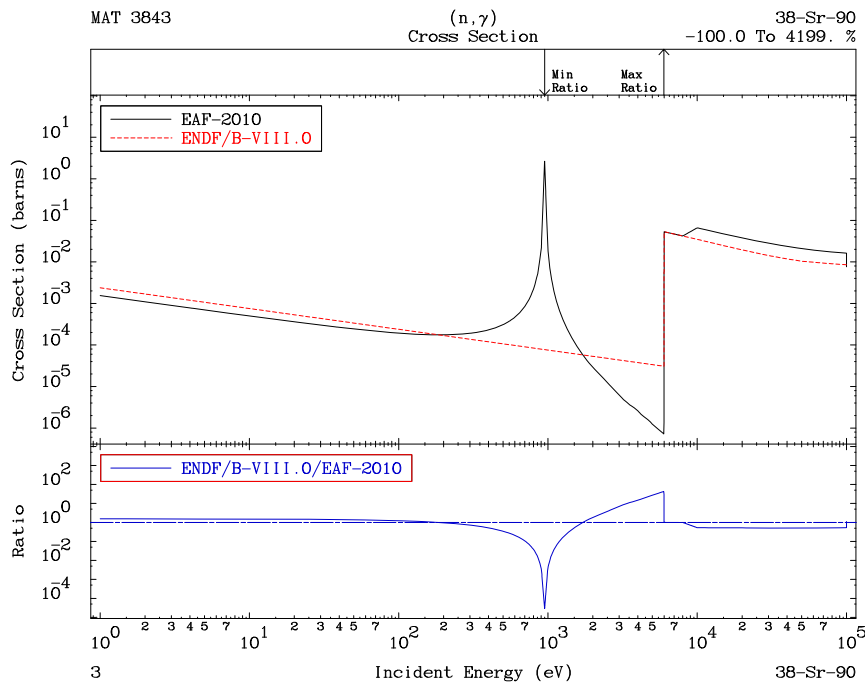


FIG. 7. (Color online) Same as Fig. 5 but with EAF-2010 for the Single Resonance Approach.

ties will match the thermal points. Such procedure is used in TARES for the production of the resonance parameters and their covariances.

Recently (since TENDL-2017), some features of SAMMY are also used to produce a set of cross section covariances (MF33) instead of resonance parameter covariances. Such covariance matrices for group cross sections in the resonance range are also merged with the MF33 for the fast neutron range. Therefore, only MF33 from 0 to 200 MeV is now provided in TENDL. In Ref. [23] it was shown that it is better for some applications to use the MF32 covariance file regarding self-shielding effects, but from a user perspective the processing of MF33 can be performed without specific knowledge (such solution is also accepted in the ENDF/B-VIII.0 library [4]). Examples for the use of the retroactive method can be found in the SAMMY manual (*e.g.*, sample case *t097k*). The retroactive method is applied as follows in the case of TENDL:

- Existing resonance parameters are provided to SAMMY for cross section reconstruction,
- artificial uncertainties are given to the reconstructed cross sections (relatively small value, in the order of percent),
- a new fitting is performed, thus providing new res-

onance parameters (almost equal to the previous ones) with an energy-energy correlation matrix and a resonance parameter correlation matrix,

- the uncertainties for the reconstructed group cross sections can artificially be adjusted to match thermal values.

Following these steps, new resonance parameter ENDF files can be obtained: for the parameters (in different formalism, multi-level Breit Wigner, Reich Moore or limited LRF7), and the uncertainties (for parameters as well as for group cross sections).

This procedure is applied for the majority of isotopes in TENDL, but not for the main ones such as $^{235,238}\text{U}$ or ^{239}Pu .

III. TALYS

The nuclear model code TALYS[3] is designed to analyse and predict nuclear reactions. The physical models implemented in TALYS have been validated for the simulation of nuclear reactions that involve neutrons, photons, protons, deuterons, tritons, ^3He - and alpha-particles, in the keV - 200 MeV energy range and for target nuclides of mass 19 and heavier. Formally, the ranges are even more

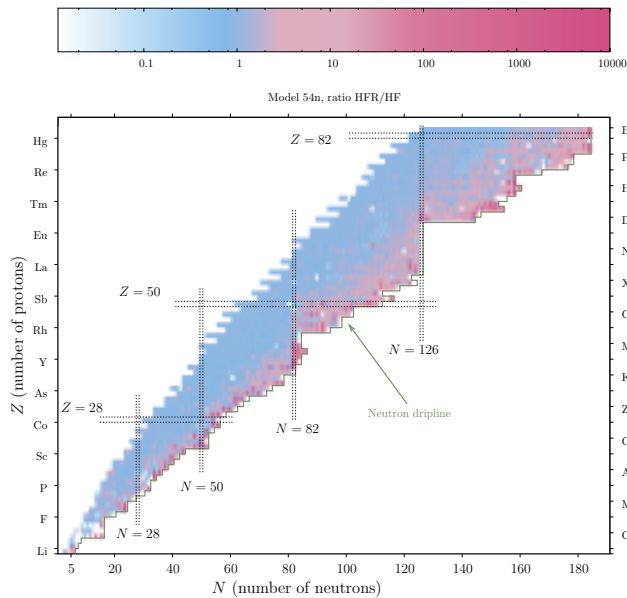


FIG. 8. (Color online) (N, Z) plane for the ratios of the HFR over the HF MACS at 30keV for about 3300 nuclei between Li and Bi lying between the valley of β -stability and the neutron drip line. A different choice of level density and gamma-strength function was made compared to a similar figure presented in Ref. [14]. Colors indicates the order of magnitude of the HFR/HF ratio for each isotope.

extensive than this: Using external resonance information the code now produces meaningful results already in the meV range, and the code can even be used for targets as light as ${}^6\text{Li}$ and up to incident energies of 1 GeV. Note however that the optical and statistical models implemented in TALYS are known to break down for nuclides with masses below about 20. Also, above several hundreds of MeV the omission of pion production in TALYS will become obvious. Other limitations are the absence of a sound model for gamma-ray transitions at thermal energies, and explicit treatment of break-up reactions such as (d,p) to discrete states, and the latest models for quantum-mechanical pre-equilibrium emission. The code aims at quality and completeness at the same time: Sophisticated nuclear reaction models have been implemented, using a vast range of microscopical nuclear structure ingredients, but at the same time allows to add enough phenomenology to always produce desired answers.

TALYS has been extensively validated over the past 20 years in fields ranging from fundamental nuclear reaction studies to data evaluation for nuclear reactors, medical isotope production and astrophysics, among others. This validation was not only performed by the authors but also by thousands of users who often do not hesitate to report both positive and negative feedback, including

bugs, to the authors which has made this open source code very robust. Figure 9 shows the number of papers per year that make use of TALYS. Obviously, at the time of printing the current paper, the numbers for 2018 are not definite yet, but we can state that currently on average about 2 papers per day are released that use TALYS in some way, and that the total number of papers citing TALYS is now beyond 5000. An extensive description of the various applications of TALYS can be found in [8]. Fig. 10 gives a breakdown per application.

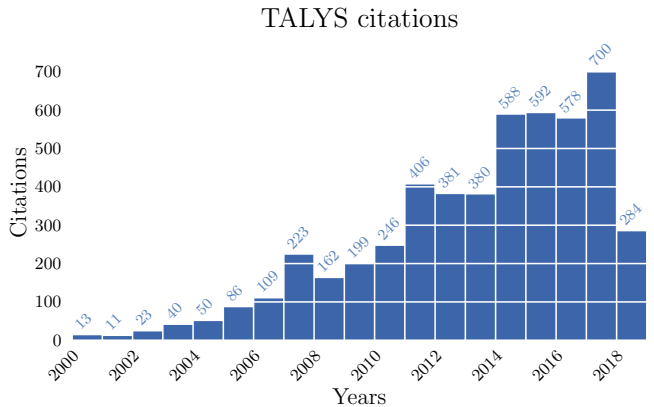


FIG. 9. Time-dependence of TALYS citations, from the first beta release in 2001.

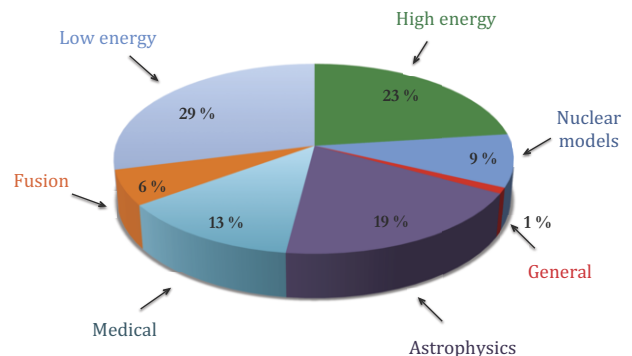


FIG. 10. (Color online) Segmentation of TALYS publications by application area, over the years 2001-2017.

Since all models used for the nuclear reaction mechanisms implemented in TALYS are limited, it can not be expected that TALYS can ab initio reproduce high-quality experimental data, and therefore adjustable model parameters are needed. More than 400 different keywords are available, though not all for adjustable model parameters but also for model and output options

etc., to let TALYS do what the user desires. And even with that, reproduction of experimental data may not always be successful, if the nuclear model is “too wrong”. This holds especially for actinides and the modeling of the fission channel, for which it is still difficult to use TALYS as a routine production tool. An advantage of TALYS is that it can generate data for any reaction channel regardless of whether it has been measured or not. The quality of the final nuclear reaction simulation is then represented by the ability of TALYS to match, interpolate between, and extrapolate beyond the existing experimental data.

TALYS can be used for many purposes, not only nuclear data evaluation. For completeness, we here list the TALYS output that is required for the production of the TENDL libraries. As output, for a single projectile + target combination and a range of incident energies, TALYS produces cross sections (assuming incident neutrons here) for:

- total (n,tot), elastic (n,el) and non-elastic (n,non) reactions,
- capture channel (n, γ),
- single particle production channels (n,n'), (n,p), (n,d), (n,t), (n,h), (n, α),
- discrete level inelastic reactions, (n,n'₁), (n,n'₂), *etc.* and the continuum (n,n'_{cont}), and similarly for all other ejectiles,
- multi-particle production (n,2n), (n,np), *etc.*,
- total fission (n,f) and its subdivision into first, second, *etc.* chance partial fission,
- residual production (n,x)_A^ZEl, mostly relevant at higher energies, as far as not yet covered by the exclusive channels mentioned above,
- production of the ground state and isomers, if present, e.g. (n,n'^g), (n,n'^m), and similarly for all other channels and residual products,
- total particle production (n,xn), (n,xp), *etc.* mostly relevant at higher energies.

As for secondary distributions, TALYS produces:

- the elastic scattering angular distribution,
- the angular distributions for inelastic scattering per discrete level, and similarly for the other ejectiles,
- double-differential emission spectra for all outgoing particles,
- recoil distributions for the residual nuclides,
- particle production yields,
- discrete and continuum gamma-ray distributions for all open channels.

As detailed elsewhere in this paper, the only output that TALYS does not (yet) provide, and which makes TENDL a truly complete general purpose library, is resonance information (provided by TARES), average number of neutrons from fission (provided by TAFIS), prompt fission neutron spectrum (provided by TANES), and complete covariance information (provided by TASMAN).

A. Brief Summary of Nuclear Models

We will not repeat the more extensive description of all nuclear models that are implemented in TALYS, and refer to Ref. [8] for that. Rather we constrain ourselves to describing the essential models and parameters that are used for a typical TENDL file.

1. Optical Model

The most important quantities calculated by the optical model are

- the shape elastic angular distribution,
- the reaction cross section,
- the total cross section,
- inelastic cross sections and angular distributions using either a coupled-channels (deformed nuclei) or DWBA (spherical nuclei) approach,
- transmission coefficients, for compound nucleus decay and pre-equilibrium emission,

and a good optical model is expected to reliably predict these quantities for energies and nuclides for which no measurements exist. All optical model calculations in TALYS are performed by ECIS-06 [24], which is implemented as a subroutine. Unless otherwise specified, the optical model potential is that of Koning-Delaroche [21] for non-actinides and Soukhovitskii *et al.* [25] for actinides. As detailed in [21], local parameterizations, *i.e.*, per target nuclide, are used as preference, and if they do not exist due to absence of experimental data the global parameterization is used. In addition, by default the dispersive (unpublished) variant of the potential is taken with the parameters as stored in the optical model database of TALYS.

For every nuclide at or near the valley of stability, a coupling scheme has been stored in the TALYS database, so that upon request automatically a coupled-channels calculation can be invoked. If a specific deformed potential is not available in the database, then for deformed non-fissile nuclides, *e.g.*, in the rare earth region, we take the local or global spherical potential of Koning-Delaroche and subtract 15% from the imaginary surface potential parameter.

The other direct reaction methods used, depending on the target nucleus, such as DWBA, weak-coupling and various rotational and vibrational coupled-channels schemes are discussed at length in [21].

For deuterons, tritons, and Helium-3 particles, we use a simplification of the folding approach of Watanabe [26], see also Ref. [27]. We take the nucleon OMPs described above, either local or global, as the basis for these complex particle potentials. A change compared to some of the recent TENDL versions is that for alpha particles we now use the potential of Avrigeanu *et al.* [28], which provides a globally good description of alpha particles for both projectiles as ejectiles.

2. Level Density

For most nuclides, the level density is taken to be of the Backshifted Fermi Gas form, although for some nuclides we use a combined Constant Temperature + Fermi gas form, as detailed in Ref. [29]. There is a level density prescription for the target nucleus, compound nucleus and all residual nuclides that can be reached in the reaction, and for each of these nuclides this involves typically 3 or 4 parameters: the level density parameter a , the spin cutoff parameter σ^2 , and the pairing shift P (or E_0 and T in the constant temperature model). For deformed nuclides, extra parameters for collective enhancement are involved. For nuclides that may fission, the above number of parameters is multiplied by the number of fission barriers, since on top of each barrier a discrete and continuum level scheme is built. Although models for using microscopic level density tables are available, the current TENDL versions are still based on phenomenological models, since there is more experience with parameter adjustment for these models, as changes from nucleus to nucleus are smoother for global phenomenological models. Since these microscopical level densities, which we will call ρ_{micro} , have not been adjusted to experimental data, we add adjustment flexibility through a scaling function, *i.e.*,

$$\rho(E_x, J, \pi) = \exp(c\sqrt{E_x - \delta})\rho_{\text{HFM}}(E_x - \delta, J, \pi), \quad (6)$$

where by default $c = 0$ and $\delta = 0$ (*i.e.*, unaltered values from the tables). The “pairing shift” δ simply implies obtaining the level density from the table at a different energy. The constant c plays a role similar to that of the level density parameter a of phenomenological models. Adjusting c and δ together gives adjustment flexibility at both low and higher energies.

3. Gamma-ray Strength Function

The gamma-ray strength function is often taken as that of Kopecky-Uhl [30], of which the most important pa-

rameters are the height, width, and energy of the Giant Dipole Resonance. Like the particle transmission coefficients that emerge from the optical model, gamma-ray transmission coefficients enter the Hauser-Feshbach model for the calculation of the competition of photons with other particles. For $E1$ -transitions, GDR parameters for various individual nuclides exist in the RIPL database, and these are stored in the nuclear structure database of TALYS. Some nuclides have a split GDR, *i.e.*, a second set of Lorentzian parameters. For these cases, the incoherent sum of two strength functions is taken. For all transitions other than $E1$, systematic formulae compiled by Kopecky [31], for the resonance parameters are used.

At sufficiently low incident neutron energies, the average radiative capture width Γ_γ is due entirely to the s -wave interaction, and this width at the neutron separation energy is used to normalize the gamma-ray transmission coefficients. These Γ_γ values are, when available, read from our nuclear structure database. For nuclides for which no experimental value is available, values come from interpolation, in mass, between available experimental values.

Similar to level densities, TALYS also provides microscopic options for $E1$ radiation, with gamma-ray strength functions calculated according to the QRPA model, see Ref. [32]. Here, the adjustment is as follows:

$$f_{E1}(E_\gamma) = f^{\text{nor}} f_{\text{micro}}(E_\gamma + E_{\text{shift}}), \quad (7)$$

where by default $f^{\text{nor}} = 1$ and $E_{\text{shift}} = 0$ (*i.e.*, unaltered values from the tables). Since these microscopical strength functions have not yet been adjusted to experimental data, they are not yet used for TENDL, but in the near future they will be.

4. Compound Nucleus Model

For low incident energies, the Hauser-Feshbach model with width fluctuation correction has been implemented. We still stick to the conclusion of [33] that Moldauer’s model is appropriate for this. For compound nucleus angular distributions, the Blatt-Biedenharn model is included. TALYS adds the resulting Legendre coefficients to those of the shape elastic scattering and direct inelastic scattering to yield the total Legendre coefficients at each incident energy. At higher incident energies, the binary compound nucleus cross section becomes small, and compound nucleus evaporation proceeds mainly via the multiple emission Hauser-Feshbach model, which is a bit simpler than that of the binary reaction since width fluctuation corrections and angular distributions are not included. A lot of effort has been invested in the early years of TALYS development to make these calculations as efficient as possible, since often more than 95% of the calculation time is spent inside the Hauser-Feshbach loops. Essential is to store intermediate data, containing a combination of level densities and transmission coefficients,

in arrays outside the various loops, and to use integer, instead of real, manipulation for angular momentum variables.

5. Pre-equilibrium Model

For pre-equilibrium reactions, TALYS makes use of the two-component exciton model model[34], involving one general matrix element M^2 steering the damping from simple to more complex exciton states, and the single-particle state density parameters g_ν and g_π which determine the particle-hole state density for each nuclide considered in the reaction chain. The latter two parameters are often used to adjust (n,2n) and (n,p) cross sections. The emission rates that appear in the exciton model are based on the same OMP transmission coefficients as those used in the other reaction mechanisms, such as compound nucleus decay. The pre-equilibrium stage takes place after the first stage of the reaction but long before statistical equilibrium of the compound nucleus is attained. It is imagined that the incident particle step-by-step creates more complex states in the compound system and gradually loses its memory of the initial energy and direction. The two-component exciton model has been proven to be a powerful method to describe this process. As described in [21], for deuteron up to alpha emission also stripping, pick-up, break-up and knock-out parameters are required as additions to the aforementioned exciton model. Also an exciton model for photon emission and multiple pre-equilibrium reactions are included.

6. Fission

For fission, the default model implemented in TALYS is based on the transition state hypothesis of Bohr and the Hill-Wheeler expression. As described in *e.g.*, Ref. [8], this represents the probability of tunneling through a single barrier with height B_f and width $\hbar\omega_f$ for a compound nucleus with excitation energy E_x . It reads

$$T_f(E_x) = \frac{1}{1 + \exp\left[-2\pi\frac{(E_x - B_f)}{\hbar\omega_f}\right]}. \quad (8)$$

For a transition state with excitation energy ε_i above the top of the same barrier, one has

$$T_f(E_x, \varepsilon_i) = \frac{1}{1 + \exp\left[-2\pi\frac{(E_x - B_f - \varepsilon_i)}{\hbar\omega_f}\right]}, \quad (9)$$

which means that the barrier is simply shifted up by ε_i .

This provides the input for formulae for double and triple humped barriers. These transmission coefficients enter the Hauser-Feshbach model to compete with the particle and photon transmission coefficients. The fission calculation in TALYS is steered by many parameters, such as for each fission barrier its height, width and

level density parameters for each nuclide in the chain. In addition class II/III states for resonance structure in between the wells may alter the prediction. Experimental parameters are taken from the RIPL database [31], which contains a large collection of actinide fission barrier heights and curvatures for both the inner and outer barrier based on a fit to experimental data. It has to be noted here that even with a seemingly robust set of parameters for all these fission and level density parameters it is very hard to describe the fission channel, and we consider this as one of the weak points of TENDL. Often, we have to normalize the TALYS calculations to other well-evaluated nuclear data libraries to get a satisfactory answer.

IV. UNCERTAINTIES

A. Bayesian Monte Carlo for Covariances

The uncertainty quantification of TENDL follows a method called Bayesian Monte Carlo (BMC), see *e.g.*, [35] and proceeds in various steps of inference. The full framework has been described in [36] and here only the essential steps are repeated. Note that the outline below holds for the fast energy range. A mathematically rigorous description is given in Ref. [37]. The combination of Bayesian updating, using likelihood functions, and Monte Carlo sampling of parameters applied to nuclear model codes has first been applied by Smith, [38], Capote *et al.* [39] in a method called UMC-B. and Bauge *et al.* [40] in a method called BFMC. Our approach is inspired by all these initiatives, but differs in a few aspects.

The probability that an experimental data set with uncertainties, represented by the vector \mathbf{x} is described by a nuclear model calculation driven by a parameter vector \mathbf{p} , is given by the likelihood function

$$\mathcal{L}(\mathbf{p}; \mathbf{x}) = \exp(-\chi^2/2), \quad (10)$$

where χ^2 , an abbreviation of $\chi^2(\mathbf{p}; \mathbf{x})$, is a measure for the deviation of model from experiment, weighted by the experimental covariance matrix. The choice of χ^2 is discussed below in Section IV A 1. We have omitted factors that cancel out in the final formulae, see Eq. (12). As outlined in [36], the Bayesian update integral needed to go from prior to posterior uncertainties is calculated by the Monte Carlo technique. In more practical terms, we take a total of K random parameter samples and for each sample k , all L nuclear model parameters are randomly sampled from a uniform probability density function,

$$P(p_l) = \frac{1}{p_l^{\max} - p_l^{\min}}, \quad \text{for } p_l^{\min} \leq p_l \leq p_l^{\max}, \\ 0 \text{ elsewhere, } l = 1, L. \quad (11)$$

Hence, for each individual TALYS run. L may represent hundreds of parameters, to which the calculated cross sections are sensitive or not (the sensitivity is less relevant

in a Monte Carlo approach). With these random parameter samples the TALYS code is run to produce all cross sections, spectra, angular distributions *etc.* of interest. The $\chi^{2(k)}$ for the entire experimental data set under consideration is calculated so that the weight of each random TALYS sample is given by

$$w^{(k)} = \frac{\mathcal{L}(\mathbf{p}^{(k)}; \mathbf{x})}{\sum_{k=1}^K \mathcal{L}(\mathbf{p}^{(k)}; \mathbf{x})}, \quad (12)$$

which automatically entails that $\sum_{k=1}^K w^{(k)} = 1$. Values of K around 3000 are used to obtain proper posterior parameter distributions.

The concept of BMC is thus rather straightforward: Run a model code K times and calculate $w^{(k)}$ for $k=1, K$. Each random sample k contains information about the specific combination of parameters that leads to a certain set of cross sections, and thus a value $\chi^{2(k)}$. Clearly, a large deviation between TALYS and experiment means a large χ^2 value and low \mathcal{L} and $w^{(k)}$ for that particular combination of parameters. In this sense, knowledge on the parameter distribution is gradually built up. We obtain the full posterior probability distribution for each parameter, simply by applying the weights $w^{(k)}$ to each value of the sampled parameters. For completeness, we mention that by averaging over the K samples, we also obtain converged values for average, variance and covariances for the model parameters, although we do not need these moments in our approach. The weighted average of each of the L model parameters is

$$\bar{p}_l \approx \sum_{k=1}^K w^{(k)} p_l^{(k)}, \quad l = 1, L, \quad (13)$$

the variance,

$$\text{Var}(p_l) \approx \sum_{k=1}^K w^{(k)} (p_l^{(k)} - \bar{p}_l)^2, \quad l = 1, L, \quad (14)$$

and the covariance,

$$\text{Cov}(p_l, p_m) \approx \sum_{k=1}^K w^{(k)} (p_l^{(k)} - \bar{p}_l)(p_m^{(k)} - \bar{p}_m), \quad l, m = 1, L. \quad (15)$$

The process is depicted in Fig. 11. We start with a sufficiently wide uniform probability distributions for the model parameters. Each random sample leads to a particular weight by considering the deviation from model to experiment for all channels, and applying that weight to all parameters of the sample gives the final numerical parameter distribution. In principle, the posterior parameter distribution is such that subsequent sampling from it no longer leads to unrealistic cross sections, since those parameter combinations have been filtered out in the first step which starts from the uniform parameter distribution. Hence, the final probability distribution for

the cross sections is obtained by starting from the numerical parameter histograms that were obtained in the first step. That process is depicted in Fig. refBMC2. The random TALYS cross sections are now closer to the experimental data than after uniform parameter sampling, and we obtain weighted posterior probability distributions for the cross sections this time. This is also the step in the process where for each sample of the parameter vector the random ENDF library for use in Total Monte Carlo is obtained. Also, for this second step the number of random runs is typically a 1000, although practical experience shows that results converge rather well after 300 runs already. It is important to restart with a credible parameter distribution because Total Monte Carlo is computationally expensive and so is the computation of the covariance matrix. Again, the first moments of the distributions can also be obtained, which are relevant since traditional uncertainty propagation makes use of covariance data in ENDF-6 format, as also used in the TENDL libraries. Hence, the weighted average of each theoretical (T) cross section i is

$$\bar{\sigma}_{Ti} \approx \sum_{k=1}^K w^{(k)} \sigma_{Ti}^{(k)}, \quad i = 1, N, \quad (16)$$

the variance,

$$\text{Var}(\sigma_{Ti}) \approx \sum_{k=1}^K w^{(k)} (\sigma_{Ti}^{(k)} - \bar{\sigma}_{Ti})^2, \quad i = 1, N, \quad (17)$$

and the covariance,

$$\text{Cov}(\sigma_{Ti}, \sigma_{Tj}) \approx \sum_{k=1}^K w^{(k)} (\sigma_{Ti}^{(k)} - \bar{\sigma}_{Ti})(\sigma_{Tj}^{(k)} - \bar{\sigma}_{Tj}), \quad i, j = 1, N. \quad (18)$$

The above is the entire uncertainty propagation procedure. It is very straightforward, but it contains some awkward issues which we discuss below. First on the method, although the most exact for uncertainty propagation, the disadvantage is that it is generally not easy to identify which actual parameter(s) are responsible for *e.g.*, large χ^2 values, as in simple linear sensitivity methods, although the particular parameters which have a large impact on the cross sections, and thus χ^2 , eventually emerge through strongly non-uniform posterior probability distributions, after sampling enough times. Prior and posterior correlations between parameters are also irrelevant, apart from possible academic interest in that they confirm expected correlations, such as *e.g.*, the correlation between the optical model real potential depth and radius ($V.r^2 = \text{constant}$, which is expected from OMP volume integral considerations). Hence, parameter correlations are output, not input, of the method. The only disadvantage of sampling the model parameters uncorrelated is that the process is somewhat less efficient, since certain parameter combinations which should have been sampled correlated may give a large distance of model

from experiment and thus a smaller weight, but these do not count in the end result anyway. Parameter combinations which lead to physical results, *i.e.*, theoretical cross sections close to measurement, automatically emerge in the parameter covariance matrix of Eq. (15) as strongly correlated.

1. Goodness-Of-Fit Estimator

We think that the main problem of BMC resides in the correct definition of the goodness-of-fit estimator χ^2 , and a solution for this has not been found yet. Obviously, with a weighting function like $\exp(-\chi^2/2)$ no statistical convergence, or even meaningful results, are obtained if the distribution of χ^2 values is too wide. Suppose that after random sampling all K values of χ^2 vary between 10 and 30, then more than 99% of the $w^{(k)}$ values correspond to useless parameter combinations resulting in very small weights and the final posterior distribution for both cross sections and parameters is too wide. Of course, statistical theory dictates that models leading to such large $\chi^2 \gg 1$ values should be rejected, but models missing the experimental uncertainty band by several factors are not uncommon in nuclear data, and we have no choice but to use the models to provide complete data libraries!

There are both experimental and theoretical causes for this χ^2 problem:

- In general, a full covariance matrix for the experimental data used in the evaluation is not available from the original work or not (even approximately) assigned by someone else, like an evaluator. Sometimes, the distinction between statistical and several sources of systematical uncertainties is given. If data points are treated as completely uncorrelated, by lack of better option or hesitation to assign correlations, it is easy to see that the total χ^2 may become huge. In addition, the total χ^2 will be even larger if wrong experimental data sets are not filtered out.
- The limitation of the nuclear model, also called the model defect. Even if the problem of the previous item, a consistent experimental covariance matrix to keep χ^2 constrained, would be solved, a deviation of the model of several factors larger than the experimental uncertainty, and which can not be solved by model parameter variation inside physically acceptable limits, will again lead to high χ^2 values and thus low and widely scattered values for $w^{(k)}$.

In sum, we try to relate limited nuclear models to good and wrong experimental data without proper experimental covariance assessment. It was outlined in [21] that automatic data fitting is hopeless in such cases.

Since we feel that the proper definition of the GOF estimator χ^2 is more important for the final result than the particular variant of Bayesian inference, whether it is

BMC, UMC-B or BFMC, we will make this a bit more explicit. The generalized χ^2 formula for N calculated cross section points σ_{Ti} , put in vector $\sigma_{\mathbf{T}}$ and N experimental cross section points σ_{Ei} , put in vector $\sigma_{\mathbf{E}}$ is

$$\chi^2 = (\sigma_{\mathbf{T}} - \sigma_{\mathbf{E}})^T \mathbf{E}^{-1} (\sigma_{\mathbf{T}} - \sigma_{\mathbf{E}}). \quad (19)$$

If the $N \times N$ matrix span one experimental data set, *e.g.*, cross sections for N incident energies of an excitation function, then the full experimental covariance matrix \mathbf{E} may be available, if we are lucky. This is, or should be, published as the outcome of one measurement, and be available in EXFOR. If the correlations between points are reasonable, then the \mathbf{E} matrix in Eq. (19) can be inverted. If the $N \times N$ matrix spans various measurements of the same reaction channel, the situation is already more complicated, This occurs for the evaluation of neutron standard reactions, where some correlation between experimental data sets, via *e.g.*, common monitor reactions or other common experimental circumstances, need to be included to get a proper complete covariance matrix. If the $N \times N$ matrix spans all available experimental data sets for all reaction channels of a target nucleus, the situation is already running out of hand, even though a full covariance matrix would be the only consistent entity to take into account when making an evaluated data file for one target isotope. To fill \mathbf{E} , assumptions on cross channel correlations will have to be made (including the simple assumption of keeping them zero). And finally, if the $N \times N$ matrix spans many nuclides and reactions simultaneously, a proper evaluation is (so far) out of reach. For all these scenarios, \mathbf{E} needs to be inverted to come to a χ^2 value, and it is not at all guaranteed that the assumptions we impose on the cross correlations will keep a constrained χ^2 value, if \mathbf{E} can be inverted at all. In addition, low-quality or suspicious experimental data sets need to be discarded.

The most extreme assumption that can be made for Eq. (19) is that all values in the data set are entirely uncorrelated. In that case the matrix elements $E_{i,j}$ are 0 if $i \neq j$, with the diagonal elements of \mathbf{E} given by the square of the total, *i.e.*, systematic + statistical, uncertainty of the experimental cross section, *i.e.*, $d\sigma_{Ei}$. This leads to

$$\chi^2 = \sum_{i=1}^N \left(\frac{\sigma_{Ti} - \sigma_{Ei}}{d\sigma_{Ei}} \right)^2. \quad (20)$$

What becomes clear is that assuming uncorrelated values will directly lead to large total χ^2 values. Nevertheless, this assumption is often imposed when there are *e.g.*, various different measurements for the same incident energy, and the experimental values + uncertainties are compared with a model calculation or the value given by a data library.

Even if the above problem of establishing a credible experimental covariance matrix would be solved, we still

have the problem that all nuclear models are limited. A significant deviation of the model values from the experimental data will directly give large χ^2 values.

Promising developments are underway to tackle these issues. A recipe for assuming and including experimental uncertainties and their correlations has been proposed by [37]. Model defects can be taken into account by using Gaussian processes, as detailed by [41].

Unfortunately, neither of these promising developments has yet made it into the TENDL evaluation scheme. Until that time, model defects and the absence of experimental covariance data has been taken into account in a more approximate way by the following pragmatic formula for χ^2 for each random sample k ,

$$\chi^{2(k)} = \frac{N}{\chi^{2(0)}} \sum_{c=1}^C \sum_{m=1}^{M_c} \frac{w_m}{N_{Mc}} \sum_{i=1}^{N_{Mc}} \left(\frac{\sigma_{Tci}^{(k)} - \sigma_{Ecmi}}{d\sigma_{Ecmi}} \right)^2 + \frac{1}{N_{Tc}} \sum_{i=1}^{N_{Tc}} \left(\frac{\sigma_{Tci}^{(k)} - \sigma_{Tc0}}{d\sigma_{Tc0}} \right)^2, \quad (21)$$

where $\chi^{2(0)}$ serves as a damping value belonging to the TALYS run with central values for all parameters, as a remedy for the model defect, c runs over the C reaction channels with experimental data, m runs over M_c experimental data sets per reaction channel, where each data set has N_{Mc} data points, N is the total number of data points and w_m is a weight to discard or include particular experimental data sets. The second term can be considered as the prior since it covers pseudo-experimental data (of which we give more details below), with N_{Tc} the number of data points for each theoretical, or pseudo-experimental, channel. The establishment of Eq. (21) is explained in much more detail in Ref. [36].

2. Pseudo-Experimental Data

The uncertainty quantification of evaluated data in TENDL goes according to the following scheme. Before doing a TENDL evaluation of one particular isotope in a Bayesian framework, we wish to establish a prior that is independent of the experimental data for that particular isotope. For that we have two valuable assets:

- A universal nuclear model code, TALYS
- The entire EXFOR database for all nuclides and reactions (including the particular isotope under evaluation, but that is statistically irrelevant)

In Ref. [36] it was outlined how we established the predictive power of TALYS for neutron-induced reactions. We perform one 'blind' TALYS calculation for each target nuclide with all nuclear model parameters taking on their global, default values and compare the results with the entire EXFOR database for cross sections. By binning the deviations of model from experiment in histograms

we establish the average deviation of TALYS from experiment, as a function of reaction channel and incident energy, averaged over all nuclides close to the stability line with experimental data. The predictive power of TALYS for neutron-induced reactions is then given by the following function for the standard deviation s , in %, per reaction channel,

$$s(E) = s_{min} + (a - s_{min}) \exp(-bE') + \max(c - s_{min}, 0) \frac{E''^2}{(E''^2 + d^2)}, \quad (22)$$

where s_{min} is the minimal standard deviation for the global prediction, often obtained near the peak of the excitation function, and generally somewhat lower than the average value for the reaction channel s_{ave} . The second term depends on $E' = E - E_{thr}$, with E_{thr} the threshold incident energy, in practice taken as the energy where the TALYS cross section crosses the value of 1 mb. (For reactions with positive Q-values, like (n, p) and (n, α) channels, we obviously apply this only to the rising part of the excitation function, and not in the thermal range). The exponent, scaled by parameter b , mimics the sharp decrease in relative deviation between TALYS and experimental data when the energy exceeds threshold. Parameter a is a measure for the uncertainty at threshold. The last term mimics the change in uncertainty at higher energies, depending on parameters c and d , and $E'' = E' - E_c$, where E_c is a measure for the energy at which the relative uncertainty is minimal, *i.e.*, generally at the highest cross section value. The parameters for the various reaction channels are given in Table I.

TABLE I. Global cross section uncertainties per reaction channel from default TALYS calculations; average deviation and parameters for energy-dependent variation, see Eq. (22). The relative deviations s_{ave} , s_{min} , a and c are given in %, b is a dimensionless factor, while the energies d and E_c are given in MeV.

| Reaction | s_{ave} | s_{min} | a | b | c | d | E_c |
|----------------|-----------|-----------|-----|-----|-----|----|-------|
| (n,tot) | 6 | 8 | 60 | 0.3 | 0 | 12 | 6 |
| (n,el) | 10 | 12 | 60 | 0.3 | 0 | 12 | 6 |
| (n,non) | 10 | 12 | 60 | 0.3 | 0 | 12 | 6 |
| (n,inl) | 50 | 12 | 100 | 1 | 100 | 12 | 5 |
| (n, γ) | 62 | 40 | 60 | 0.3 | 0 | 20 | 20 |
| (n,2n) | 25 | 24 | 100 | 1 | 100 | 15 | 6 |
| (n,3n) | 150 | 40 | 100 | 1 | 100 | 12 | 6 |
| (n,f) | 110 | 50 | 100 | 1 | 100 | 12 | 6 |
| (n,p) | 53 | 34 | 100 | 1 | 100 | 12 | 6 |
| (n, α) | 120 | 45 | 100 | 1 | 100 | 12 | 6 |

Note that almost *all* EXFOR data, *i.e.*, neutron reactions on all target nuclides between F and Fm, determine the parameters of this global formula. Eq. (22) can then be applied to one nuclide in particular to create pseudo-experimental data for that target nucleus, *i.e.*, we fill every reaction channel with central values provided by the global TALYS calculation for that nucleus and assign uncertainties to each point using formula (22). In

some sense, we create an entire "EXFOR" database with pseudo-experimental data.

A perhaps controversial way of explaining Eq. (22) is: if a measurement is less precise than the uncertainty given by the predictive power, then one can better take a TALYS estimate instead! Of course, in practice experimental uncertainties of good measurements are significantly smaller than that associated to the global predictive power of TALYS, so this seldom occurs. Creating these sets of pseudo-experimental data for all reaction channels of a nucleus has two purposes:

A. It can be used for the first zoom-in of parameter uncertainties, as illustrated in Fig. 11. We start with a very wide uniform distribution for each TALYS parameter, representing an uninformative prior for the parameters ('knowing nothing'). Each weight is now determined by a χ^2 that is obtained relative to the pseudo-experimental data for this nucleus. By means of the Bayesian Monte Carlo update, the wide uniform parameter distribution is reduced to a non-uniform, narrower distribution which corresponds to a final cross section distribution that overlaps more or less with the uncertainties of the pseudo-experimental data. If for a particular reaction no real experimental data exists, the final evaluation including covariance data is hereby already obtained.

B. We need to keep the pseudo-data on board as essential information when we further zoom in on well-measured data per nuclide. We must include pseudo-data for unmeasured reaction channels or energy ranges. Otherwise one may obtain unrealistic cross section results since the optimization process will steer certain parameters to any unrealistic value if they are not constrained by data. In other words, if for a nuclide *e.g.*, only some experimental (n,γ) data points exist and no (n,α) data while hundreds of TALYS parameters are varied simultaneously to produce the optimal result, then specific parameters for *e.g.*, the alpha knock-out reaction may reach unphysical values, since the optimization process is not penalized for attaining unrealistic theoretical (n,α) cross sections. Filling the entire reaction channel space with pseudo-data remedies this. Once credible real experimental data sets are included for a particular reaction channel, it will make the pseudo-data for that channel and energy range directly irrelevant since the uncertainty of the real experimental data will be much smaller and thus have a larger weight to the χ^2 .

3. Summary

In sum, we first create pseudo-experimental data for all nuclides, energies and reaction channels. This leads to the parameter distribution of Step 1, *i.e.*, the one that reproduces the pseudo-experimental data from global TALYS calculations. Next, if real experimental data from EXFOR exist for various reaction channels of a nucleus, they will, thanks to their smaller uncertainties, dominate the Bayesian updating process and the parameter distribu-

tions will become narrower and the posterior parameter and cross section pdf's for this nucleus are obtained. Next, after assigning weights based on well-selected experimental data for the particular nucleus under study, the posterior parameter distribution is used for producing the covariance matrix for this target nucleus and for random ENDF data files for Total Monte Carlo (TMC) application.

B. Covariances for Resonance Regions

Similar to the section on the resonance parameters, the uncertainties (or covariance) approach varies depending on the level of knowledge of the isotope.

1. Parameters Covariance for Stable and Long-lived Isotopes

In the case of covariance information for the resonance range, different possibilities have been explored in the past TENDL releases. The first choice was to provide so-called "file 32" (or MF32) together with a compact version (smaller in size, but retaining only part of the MF32 information), being the uncertainties and correlations for (and between) resonance parameters. To be useful to users, such information needs to be processed (for instance with NJOY [42]), implying that the right processing of MF32 had to be done by persons not always familiarized with the specifics of MF32, and with specific NJOY versions, not always verified for this type of processing. An example of such processed MF32 in terms of cross section is presented in Fig. 13 (top) as it was included in TENDL-2010. More recently, a different approach was taken, following the development of the ENDF/B-VII.0 library, using MF33 only. It was shown in Ref. [23] that the use of MF33 instead of MF32 can present some limitations for the calculations of uncertainties on self-shielded cross sections. In practice, this drawback is partly compensated by the convenience of the MF33 processing. The process to produce a MF33 in the resonance range is based on SAMMY:

- The existing resonance parameters are provided to SAMMY to reconstruct the cross sections. The uncertainties on these parameters were first assessed to reproduce pointwise cross sections uncertainties, as for instance provided in the thermal range by the Atlas of Neutron Resonances [12]. For higher energy, a general concept of increasing cross section uncertainties with energy is used, assuming that the thermal cross sections are better known than other ones in the resonance range.
- SAMMY is also fitting the obtained cross sections, leading to energy-energy cross section correlations based on a specific energy grid.

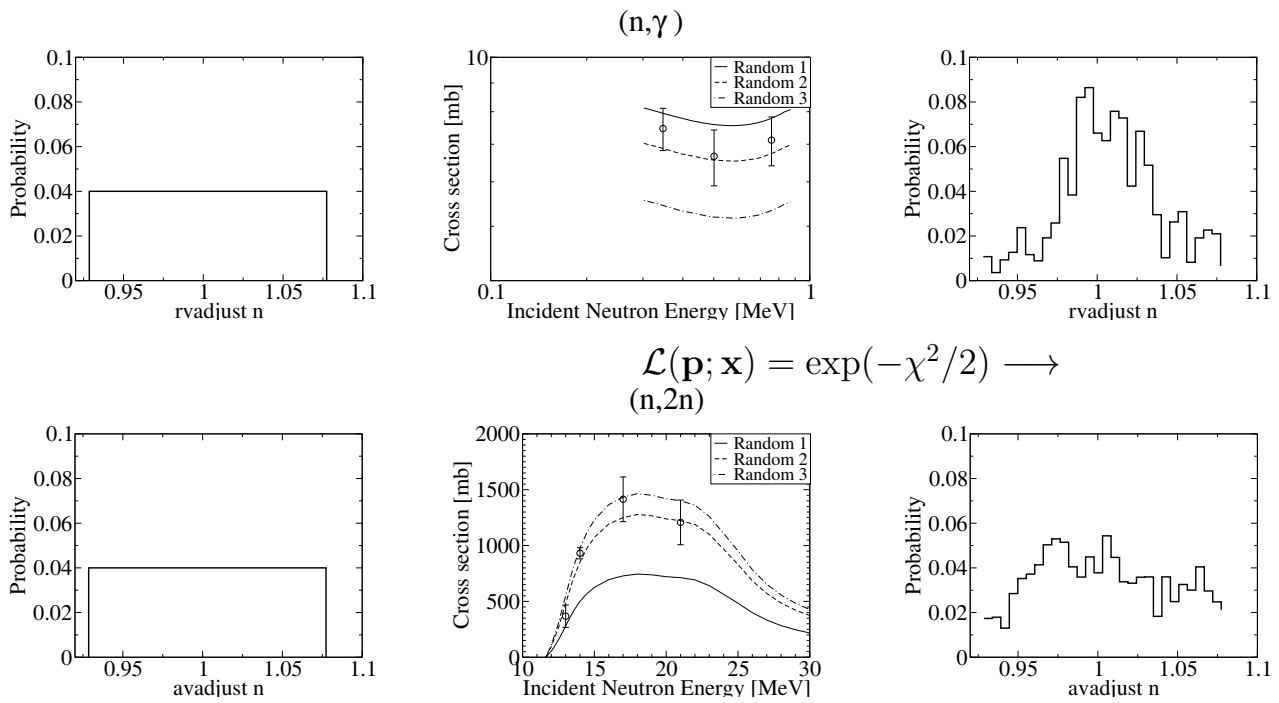


FIG. 11. Bayesian update of model parameters. Eq. (10) is used to denote the weighting.

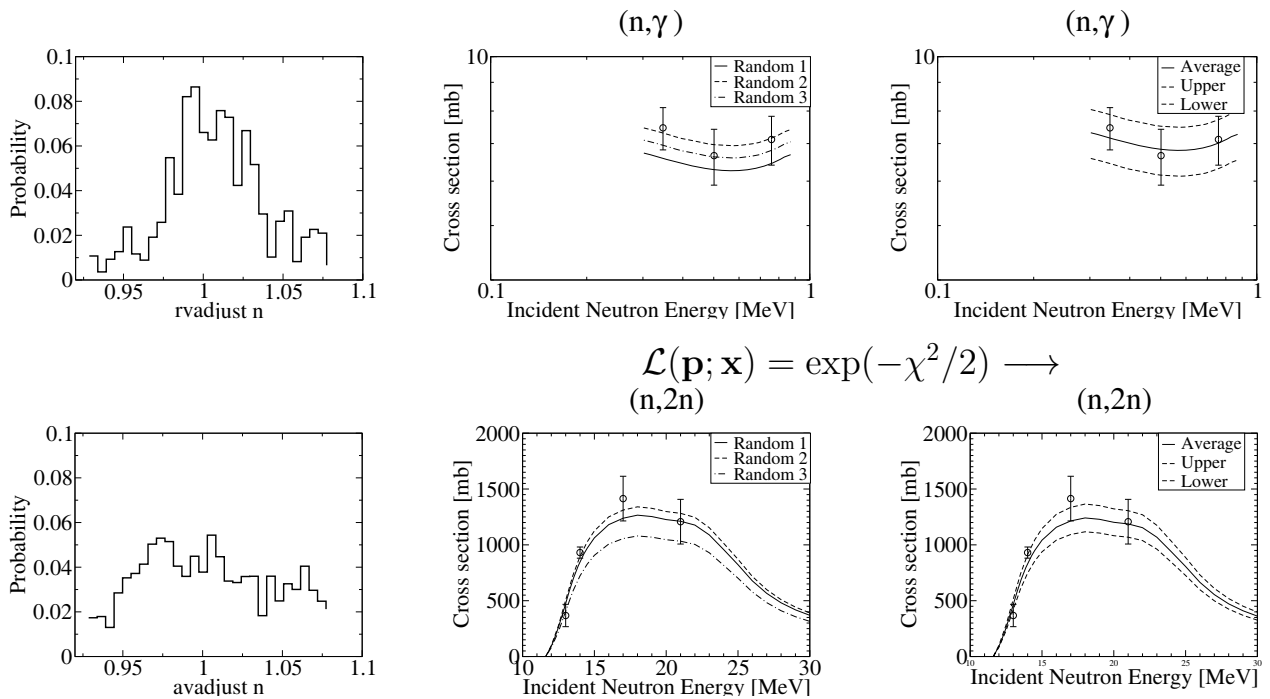


FIG. 12. Probability distributions for cross sections. Eq. (10) is used to denote the weighting.

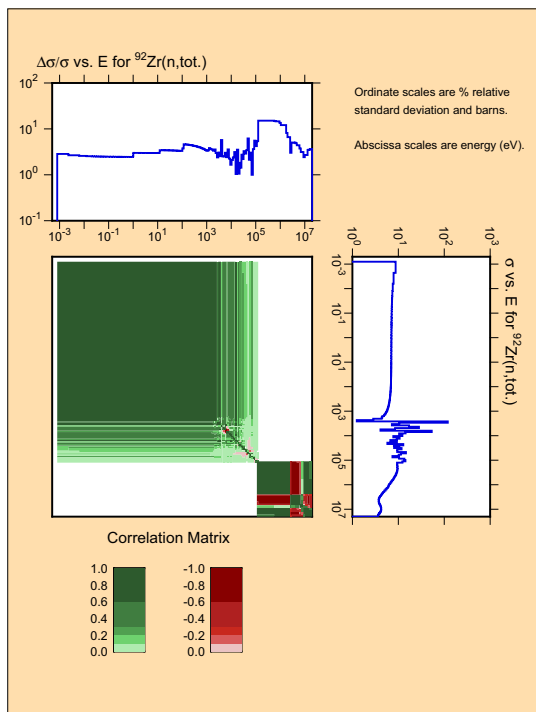
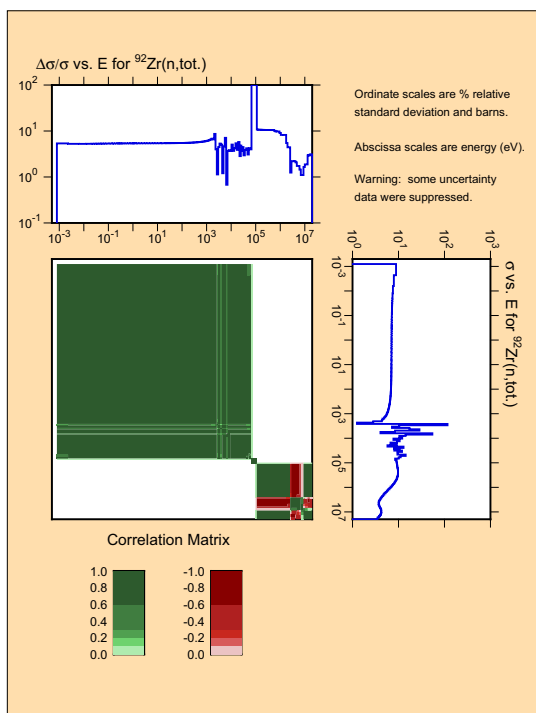


FIG. 13. (Color online) Uncertainties and correlations for $^{92}\text{Zr}(n,\text{tot})$ from MF32 (top) and MF33 (bottom).

- The uncertainties of the thermal cross sections are reproduced by multiplying the whole range by a specific factor. This is possibly one of the most crucial steps in this process. For many applications, the thermal neutron region is of prime importance. Having a good educated guess for the uncertainties in this region will determine the quality of the covariance files for a large number of users. In the majority of cases, we follow the recommendations of the Atlas [12] for uncertainties of the thermal cross sections. If no values are given, other considerations are involved (such as the isotope half-life, its abundance, its relevance for specific applications). At this point, it is difficult to list all the possible cases and we invite the reader to visit the TENDL website. Specific examples for Pb and Bi can be found in Ref. [16], and in Ref. [43] for ^{147}Nd .
- The new correlations and uncertainties are included in a MF33 file.

This approach is very pragmatic and is far from a correct analysis of the resonance range. It is anyway not its purpose. In practice, the obtained correlations and uncertainties can be considered satisfactory as long as it is not proven otherwise. An example is presented in Fig. 13 (bottom) for the $^{92}\text{Zr}(n,\text{tot})$ cross section, where two versions of a TENDL covariance file, one with MF32 and one with MF33, are compared.

C. Covariances for nubar and PFNS

As for the other nuclear data quantities, the covariance information for nubar and the prompt fission neutron spectra (or pfns) are produced based on the variation of model parameters. Different models can be used, from very simplified considerations [44] to more advanced principles [45], leading to very different results, for uncertainties as well as for energy-energy correlations. In TENDL, the Madland-Nix model is used for all actinides [46], and various developments are being currently done to use the GEF code. As the Madland-Nix model is not linked to other models (for instance for cross section calculations), the nubar and the pfns are not correlated with other nuclear data quantities. Such correlations can only be “created” with the use of integral benchmarks, as presented in Ref. [47] (for the time being, these additional correlations are not included in the TENDL library). Examples of the uncertainties and correlations for the nubar and pfns of ^{235}U are presented in Fig. 14.

The shape of the correlations is typical from the variations of the parameters of the Madland-Nix model, with one rigid point at high energy, and anti-correlated variations from each side of this point. In a complete evaluation, these strong correlations would be attenuated by the use of experimental data. In the future, more dedicated model codes for fission fragment distributions, such as the GEF code but also newer approaches, will offer an al-

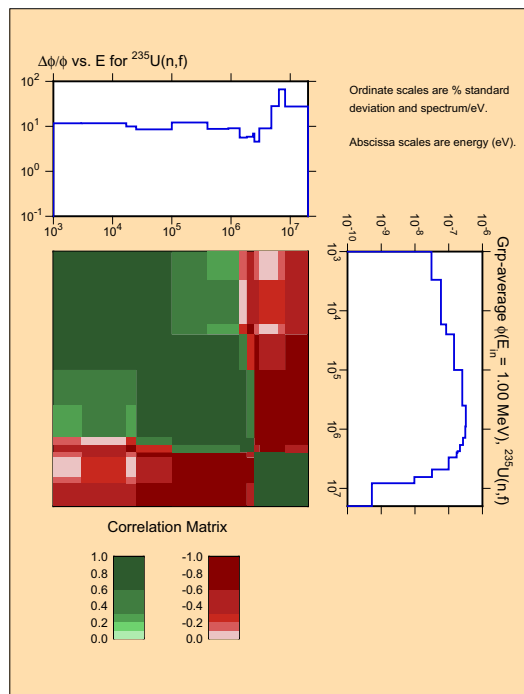
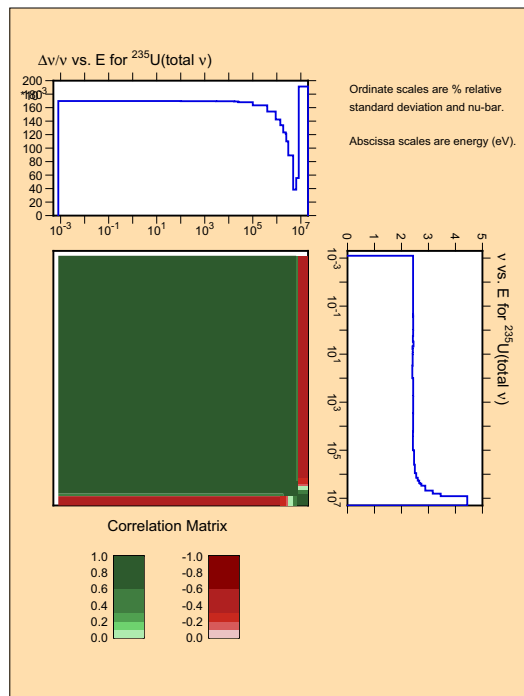


FIG. 14. (Color online) Example of the uncertainties and correlations for the nubar of ^{235}U in 44 groups, at thermal energy for nubar (top) and 1 MeV for the pfns (bottom).

ternative approach, especially once connected to TALYS. This would provide the possibility to obtain correlations between different quantities (fission yields, nubar, pfns, and cross sections).

V. LIBRARY PRODUCTION

A. Production Flow for TENDL with ‘T6’

This section contains a description of the various tools which are needed for the production of TENDL. The software system built around TALYS is called T6, which is named after the six core codes which are needed to produce a complete nuclear data library.

1. T6 Software

The four major (in the sense of possibilities, development effort and size) codes are:

- **TALYS**
The nuclear reaction code TALYS has been extensively described in Section III.
- **TEFAL**
The ENDF-6 formatting code TEFAL processes the nuclear reaction results of TALYS, and data from other sources if TALYS is not used, into ENDF-6 nuclear data libraries. TEFAL was constructed to avoid any error-prone human interference in the creation of nuclear data files: the whole ENDF-6 file is created at once, on the basis of all nuclear reaction info that we feed it. Hence, the idea is to first run TALYS for a projectile-target combination and a range of incident energies, and to obtain a ready to use nuclear data library from the TEFAL code through processing of the TALYS results, possibly by merging it with experimental data or data from existing data libraries. All possible covariance data that the ENDF-6 format allows is included as well. For all this, a significant part of the ENDF-6 formats manual [48] was implemented in TEFAL.
- **TASMAN**
TASMAN is statistical software for TALYS. The most used function of TASMAN is the generation of probability distributions for all the outputs of TALYS such as cross sections, spectra, angular distributions *etc.* and their related first moments such as averages, variances and covariances. It does this on basis on Monte Carlo sampling of the TALYS input parameters. The Bayesian Monte Carlo method described in Section IV is now the preferred method for uncertainty quantification and propagation. TASMAN is thus able to sample from arbitrary, tabulated probability distributions obtained in a first inference stage and is also the driver

for the generation of random ENDF files which form the basis of Total Monte Carlo uncertainty propagation. In addition, TASMANT can create parameter sensitivity profiles for all cross sections, spectra *etc.* that TALYS produces and it can automatically fit TALYS cross sections to experimental data from the EXFOR database through deterministic or stochastic (simulated annealing) search methods on the model parameters. For the BMC method, TASMANT is run a first time to produce the weighted parameter distributions, starting from a uniform prior parameter distribution. After that, TASMANT is restarted and samples from the weighted distribution.

- **TARES**
TARES is a code to generate resonance information in the ENDF-6 format, including covariance information. In short, it produces a full set of RRR and URR parameters for MF2, and a complete set of covariance information in MF32, which is stored either in the “regular” covariance format or in the compact format, or in MF33 (which is the default in TENDL-2017). It is discussed in more detail in Section II.

Two additional codes are needed,

- **TANES**
TANES is a simple program to calculate the fission neutron spectrum based on the Los Alamos model [49]. The original Madland-Nix [46] or Los Alamos model for the calculation of prompt fission neutrons characteristics (spectra and multiplicity) has been implemented in a stand-alone module. The TANES code is using this stand-alone module, combined with parameter uncertainties (on the total kinetic energy, released energy and multi-chance fission probabilities) to reproduce and randomize the fission neutron spectrum. The program provides the central and random values for the fission neutron spectra at different incident energies (MF5) and their covariances (MF35). For covariance files, a simple Monte Carlo variation of the parameters is performed, using the Madland-Nix model. The random spectra (or more specifically their standard deviations) are then formatted into MF35.
- **TAFIS**
TAFIS calculates fission yields, prompt neutron emission from fission and other necessary fission quantities (kinetic energy of the fission products, kinetic energy of the prompt and delayed fission neutrons, total energy released by prompt and delayed gamma rays). For fission yields, it is using the systematics of fission-product yields from A.C. Wahl [44], combined with *ad hoc* uncertainties. It calculates the independent and cumulative fission yields at any incident energy up to 200 MeV and for different incident particles (spontaneous, neutrons,

protons, deuterons, *etc.*). Empirical equations representing systematics of fission-product yields are derived from experimental data. The systematics give some insight into nuclear-structure effects on yields, and the equations allow estimation of yields from fission of any nuclide in the range $Z = 90$ to 98 and $A = 230$ to 252. For neutron emission, different models are used depending on the energy range and are presented in Ref. [44]. The output of this program is a fission yield file with uncertainties, prompt and delayed neutron emission files for central and random values (MF1 MT452), a list of central and random fission quantities (MF1 MT458) and prompt neutron covariances (MF31). For the delayed neutron emission, as the correct physics is yet not included in TAFIS, a simple copy from existing libraries is done. For isotopes which are not included in other libraries, the delayed neutrons are simply copied from the nearest isotope. As for the MF35, a simple Monte Carlo variation of the model parameters is used to generate covariance files.

TARES, TAFIS and TANES provide everything which TALYS can not (yet) do. Note that all three codes come with complete covariance information and/or random sampling of parameters to produce probability distribution for all outputs.

Hence, central in the T6 software system are the above six codes. However, inspection of the entire T6 system reveals no less than 58 executable codes. We will explain, or at least shortly mention, most of them since that will elucidate how complicated the process still is. We want to stress here that a future clean up of T6 means getting rid of some of these codes, or merging some of them into one code. For sure, it is planned to have all 6 abovementioned core codes in TALYS-2.0, *i.e.*, in one and the same source code, usable by everyone. Further important software for TENDL production is:

- **autotalys**: a bash shell script that drives the entire T6 system. With autotalys, TENDL is produced, random files are made, TALYS parameters are optimized, *etc.* An isotope data file in TENDL is produced by one autotalys command, with several flags of course. Hence, TENDL-2017 is produced by 7 (projectiles) times about 2800 (target nuclides) = 19600 autotalys commands.
- **ENDFTABLES**: a FORTRAN code to transform an existing ENDF-6 formatted nuclear data file into a directory-structured x-y or x-y-dy database (if covariance matrices are available). Hence, all isotopic nuclear data files from the major world libraries are completely dismantled using ENDFTABLES and put into single files per reaction channel. This makes handling such data, for plotting, adoption into TENDL files *etc.* much more efficient and robust.
- **plot** : a plotting script which plots the cross sec-

tion for one particular nuclear reaction comparing all EXFOR data with TENDL-2017, ENDFB-VIII, JEFF-3.3, JENDL-4.0, CENDL-3.1, EAF-2010 and IRDF-1.05.

- **plotall**: a plotting script which runs the aforementioned 'plot' for all important reaction channels per target nuclide, thereby making a 'cross section book' for the nuclide under consideration.
- **autonorm**: A FORTRAN code to normalize TALYS against data from other nuclear data libraries. In the input file for autonorm, the reaction channels for which normalization to other libraries needs to take place are given. Next, the procedure is the following:
 - Run TALYS. This will produce for each reaction channel c , and incident energy E , the original TALYS cross section $\sigma_c^T(E)$.
 - We create a specific input file for autonorm for the normalization of the TALYS results to the cross sections of the nuclear data library, *e.g.*, IRDF-1.05 for some channels and ENDF/B-VIII for some other channels, in a certain energy range that we want to restrict the normalization to. This defines for a few channels the library cross sections $\sigma_c^L(E)$. Then, autonorm reads both the TALYS and the library cross sections and produce cross section ratios $R_c(E) = \sigma_c^L(E)/\sigma_c^T(E)$ and stores these in a so-called 'rescue' file (*i.e.*, a file to be used when anything else fails to get the perfect TALYS result).
 - Run TALYS for a second time, but now using 'rescue' keywords which make TALYS read in the rescue files with normalization factors. Hence, all channels for which normalization takes place now have their own 'rescue' keyword in the second TALYS input file. TALYS then multiplies the 'original' TALYS cross sections, $\sigma^{Tnew_c}(E) = R_c(E)\sigma_c^T(E)$, so that after the second TALYS run, the results for the specified channels will be exactly equal to that of the nuclear data library to which it was normalized. The difference $\sigma^{Tnew_c}(E) - \sigma_c^T(E)$ is added to, or subtracted from, the elastic cross section, which also means that this approach becomes dangerous if the original TALYS results are too far from the data one wants to normalize to. In a future version of autonorm, this redistribution will be made according to the cross-channel covariance matrix that is available from our calculations. This is physically better justified and also less risky than accounting for the difference in the elastic cross section.
- **driplist**: A code to produce the list of nuclides for TENDL. This can be the full TENDL range or

other ranges of nuclides. The code driplist may be called from autotalys.

- **mf1maker**: a bash shell script that produces a full MF1 documentation file. mf1maker can be steered by various flags and is called from the autotalys script.
- **extrema**: a very short FORTRAN program that determines the maximum and minimum of a cross section, for plotting purposes.
- **ZAres**: code to calculate the Z and A of the residual product given the MT number. This is needed for, and called from, 'plot'.
- **select**: bash script to randomize selected parts of an ENDF-6 file for sensitivity purposes, or to make covariance files during, instead of after, the random runs. This script is called from the TASMAN code.
- **run-plots**: script to run NJOY and produce plots from its ACER module, called from autotalys.
- **run-compa**: script to compare two ENDF files and compare the difference, makes use of PREPRO and NJOY, called from autotalys.
- **run-errorj**: script to run NJOY and produce covariance plots from NJOY, called from autotalys.

Various well-known nuclear data codes from other authors are included in T6

- BNL[50] checking codes for ENDF files (not all BNL codes are needed):
 - CHECKR: Format checks
 - FIZCON: Basic physics checks
 - PSYCHE: Advanced physics checks
 - INTER: Integral cross sections
- NJOY-12.99[51]: NJOY processing code
- njoycovx_ld: special version of NJOY for covariance data
- PREPRO[11]: suite of ENDF processing codes (not all PREPRO codes are needed)
 - recent: pointwise cross sections
 - sigma1: broadening cross sections
 - sixpak: transform MF6 into MF4 and MF5 (for testing only)
 - groupie: groupwise cross sections
 - evalhard: plot cross sections
 - evalplot: plot cross sections
 - activate: create MF10 out of MF3 and MF9
 - legend: transform Legendre coefficients into tables

- merger: combine evaluated data
- complot: comparison of cross sections
- comhard: comparison of cross sections
- dictin: sum rules for cross sections
- linear: linearize cross sections
- xcalendf[10]: CALENDF processing code
- fudge[52]: FUDGE toolkit for nuclear data management and processing

To run all the processing codes, scripts have been written which produce, for the ENDF file under consideration, an input file for these codes and then runs it. These bash shell script are:

- run.bnl
- run.prepro
- run.njoy
- run.fudge

Also, diagnosis scripts have been written which filter the warning and error messages out of the most important checking codes:

- diag.checkr
- diag.fizcon
- diag.psyche
- diag.prepro
- diag.njoy
- diag.fudge

Such diagnosis scripts are needed since TENDL contains about 20000 ENDF-6 formatted files which are to be tested by each of these codes, so a clever method to discover errors must be used.

2. Required Input for the TENDL Data Files

With the entire automated system ready to produce complete nuclear data libraries, all that is needed is nuclide-specific information (the actual 'evaluation'), which is available in input files for the various codes.

First of all, in the resonance parameter database the preferred resonance parameter set is flagged, such that the TARES code produces resonance information, in both the RRR and URR, for MF2, and the associated covariance data in MF32 or MF33. Similarly, for each target nuclide a so-called 'best' input file for TALYS may be available. Obtaining the optimal input parameter set for TALYS is an independent activity which takes place outside T6. Examples of such 'best' files are given in Section VB. It is done through trial and error and with expert

judgment, *i.e.*, in this respect is equal to more traditional nuclear data evaluation. The difference in the case of TENDL is of course that at the end of each year, when a new version of TENDL is produced, all these manually produced optimized TALYS input files are ready to be used as input in the automated production process.

The third set of input files for TENDL contains keywords for normalization to existing nuclear data evaluations. With the aforementioned code *autonorm* the TALYS calculation is automatically forced to fit exactly the data which we want to adopt from other libraries such as standards and dosimetry cross sections.

B. Optimized Input Parameters for TALYS 'Best' Input Files

The current TENDL-2017 includes recent results of a re-evaluation of neutron induced cross sections that was performed in the framework of the Fusion for Energy (F4E) and the CHANDA projects. This allowed to supply TALYS with a new set of improved input files with thoroughly optimized parameters for the generation of complete nuclear reaction excitation functions in the range of (0-60) MeV. The improvements have been performed for a list of nuclear reactions relevant for fusion technology applications as well as for fission products. In both cases the actions were targeted at getting a better cross section fit with respect to TENDL-2014, TENDL-2015, EAF, and JEFF-3.2 data libraries.

The optimization of parameters was done for a list of 154 fission products: ^{107}Ag , ^{109}Ag , ^{75}As , ^{130}Ba , ^{132}Ba , ^{134}Ba , ^{135}Ba , ^{136}Ba , ^{138}Ba , ^{79}Br , ^{81}Br , ^{106}Cd , ^{110}Cd , ^{111}Cd , ^{112}Cd , ^{113}Cd , ^{114}Cd , ^{115}Cd , ^{136}Ce , ^{140}Ce , ^{141}Ce , ^{142}Ce , ^{133}Cs , ^{134}Cs , ^{158}Dy , ^{161}Dy , ^{162}Dy , ^{163}Dy , ^{164}Dy , ^{154}Eu , ^{155}Eu , ^{69}Ga , ^{71}Ga , ^{72}Ge , ^{73}Ge , ^{74}Ge , ^{76}Ge , ^{152}Gd , ^{153}Gd , ^{154}Gd , ^{155}Gd , ^{156}Gd , ^{157}Gd , ^{158}Gd , ^{160}Gd , ^{127}I , ^{129}I , ^{131}I , ^{115}In , ^{162}Er , ^{164}Er , ^{166}Er , ^{167}Er , ^{168}Er , ^{170}Er , ^{163}Ho , ^{165}Ho , ^{80}Kr , ^{82}Kr , ^{83}Kr , ^{84}Kr , ^{85}Kr , ^{86}Kr , ^{139}La , ^{92}Mo , ^{94}Mo , ^{95}Mo , ^{96}Mo , ^{97}Mo , ^{98}Mo , ^{99}Mo , ^{100}Mo , ^{93}Nb , ^{94}Nb , ^{95}Nb , ^{142}Nd , ^{146}Nd , ^{148}Nd , ^{150}Nd , ^{102}Pd , ^{104}Pd , ^{105}Pd , ^{106}Pd , ^{108}Pd , ^{110}Pd , ^{147}Pm , ^{148}Pm , ^{149}Pm , ^{141}Pr , ^{143}Pr , ^{85}Rb , ^{86}Rb , ^{87}Rb , ^{103}Rh , ^{96}Ru , ^{98}Ru , ^{100}Ru , ^{101}Ru , ^{102}Ru , ^{104}Ru , ^{121}Sb , ^{123}Sb , ^{74}Se , ^{76}Se , ^{77}Se , ^{78}Se , ^{79}Se , ^{80}Se , ^{82}Se , ^{144}Sm , ^{148}Sm , ^{150}Sm , ^{151}Sm , ^{152}Sm , ^{153}Sm , ^{114}Sn , ^{115}Sn , ^{116}Sn , ^{117}Sn , ^{118}Sn , ^{119}Sn , ^{120}Sn , ^{121}Sn , ^{125}Sn , ^{126}Sn , ^{84}Sr , ^{86}Sr , ^{87}Sr , ^{88}Sr , ^{99}Tc , ^{159}Tb , ^{160}Tb , ^{120}Te , ^{123}Te , ^{124}Te , ^{126}Te , ^{128}Te , ^{130}Te , ^{132}Te , ^{126}Xe , ^{128}Xe , ^{130}Xe , ^{131}Xe , ^{132}Xe , ^{134}Xe , ^{136}Xe , ^{89}Y , ^{176}Yb , ^{90}Zr , ^{91}Zr , ^{92}Zr , ^{94}Zr , ^{95}Zr , ^{96}Zr . In total 285 nuclear reaction channels have been considered and improved by normalizing to high quality experimental data.

The list of elements that was considered under the F4E project accounted for 70 elements: ^{27}Al , ^{130}Ba , ^{138}Ba , ^{140}Ba , ^{36}Cl , ^{37}Cl , ^{41}K , ^{44}Ca , ^{46}Ca , ^{48}Ca , ^{106}Cd , ^{140}Ce , ^{59}Co , ^{50}Cr , ^{52}Cr , ^{53}Cr , ^{54}Cr , ^{63}Cu , ^{65}Cu , ^{72}Ge , ^{74}Ge , ^{164}Er , ^{166}Er , ^{167}Er , ^{152}Gd , ^{54}Fe , ^{58}Fe , ^{180}Hf , ^{163}Ho , ^{86}Kr , ^{24}Mg , ^{92}Mo , ^{94}Mo , ^{95}Mo , ^{54}Mn , ^{55}Mn , ^{142}Nd , ^{58}Ni , ^{60}Ni ,

^{22}Ne , ^{23}Na , ^{28}Si , ^{30}Si , ^{32}S , ^{34}S , ^{36}S , ^{82}Se , ^{144}Sm , ^{114}Sn , ^{116}Sn , ^{117}Sn , ^{120}Sn , ^{123}Sb , ^{88}Sr , ^{181}Ta , ^{46}Ti , ^{48}Ti , ^{50}Ti , ^{171}Tm , ^{187}Re , ^{205}Tl , ^{205}Pb , ^{207}Pb , ^{51}V , ^{180}W , ^{183}W , ^{186}W , ^{67}Zn , ^{90}Zr , ^{96}Zr . In total 97 nuclear reactions relevant for fusion were improved by means of nuclear model parameter adjustment.

The procedure of cross section evaluation with T6 is a complex action that accounts for all energetically open reaction channels for specific target nuclides in a consistent way. For each element there is an individual optimized input file that is valid for one nuclide and may imply changes in several reaction channels of interest. One single TALYS run includes a set of parameters by default (general file) and a so called “best” file (see Listing 1) that can be found in the code’s structure directory (talys/structure/best). The parameters by default are basically the same for all elements but “best” files include adjusted values to guarantee the best agreement with experimental data after differential and integral data analysis. Mainly those parameters were related to a change of: radius and diffuseness in optical potential (rvadjust, avadjust), choice of level density model (ldmodel 1-5), densities of exciton model constituents (gpadjust, gnadjust), pre-equilibrium gamma emission (rgamma), branching ratios for isomeric states, formation of $\alpha/d/t$ in exit channel (cstrip, cknock). The magnitude of those parameters was varied for different reactions and was fixed for certain residual nuclides. It should be emphasized that keeping a reasonable balance between potentially related channels is a crucial issue. The majority of TALYS parameters affects the excitation function overall but not in a local small area. Only several parameters similar to “rvadjustF” do affect the excitation function locally in the narrow energy range specified by the user. This is a very efficient way to make the fine tuning of *e.g.*, the (n,α) reaction. The adjustment was aimed at achieving the best agreement between the latest experimental data, taken from the EXFOR database, and presently calculated TALYS curves. Also it was important to control the value of the total cross section and the shape of excitation functions, and to adjust parameters within acceptable physical limits. The applicability margins of all parameters are given in the TALYS manual. In addition it is important to be careful at the energies around threshold, specially, for reactions like (n,d) or (n,t) , since the uncontrolled increase of cross section at energies around 8 MeV may easily cause a rapid increase of cross section at energies of 20 MeV or higher. In Listing 1 there is an example of an input file used for calculating the cross sections for ^{90}Zr . This file consists of three clear parts. For the case of reactions with formation of reaction products in isomeric and ground states there is also a “best.branch” file that contains information on the level structure of the final nucleus and probability of transitions. In the sample case of Listing 1 the assigned branchings are included in the input file itself. The experimental data regarding the level structure is taken from ENSDF but in those cases when a transition is unmeasured and

data is lacking then there is a chance to fit isomeric cross sections by assuming the probability distribution within a specific transition branch.

Listing 1. Example TALYS input file for ^{90}Zr , using optimised parameters.

```
# TALYS input file generated by Autotalys
projectile n
element Zr
mass 090
Ltarget 0
energy energies
# Use best parameters from database
ldmodel 2
best y
# Output of extra channels
channels y
filechannels y
integral y
resonance y
# Reduce output for activation-only calculation
outspectra n
outangle n
ddxmode 0
outdiscrete n
integral xs200000.tot fns-7hour 7.110000e-01
integral xs200000.tot cf252-flux-1 2.670000e-04
integral xs200000.L01 fns-5min 1.160000e-01
integral xs010000.L01 fng-heat 9.830000e-03
integral xs000100.tot d-Be 5.100000e-02&
# (n,tot), (n,el), (n,inl)
rvadjust n 1.0 4. 8. 6. 0.99
rvadjust n 1.0 12. 16. 14. 0.995
# (n,p), (n,2n), (n,np)
rvadjust p 0.69
rvadjustF p 12 25 -80 4.0
gpadjust 40 91 1.11
aadjust 39 90 1.15
gpadjust 39 90 1.15
# (n, alpha)
alphaomp 6
rvadjust a 0.98
cstrip a 1.5
rvadjustF a 12 28 -53 4.
rvadjustF a 12 28 -53 4.
# (n, gamma)
gamgamadjust 40 91 0.65 0.10
# Other: Isomers, (n,d), (n,t), (n,h) {\it etc.}
rvadjust d 1.21
avadjust d 1.21
cstrip d 0.8
cknock d 0.8 & branch 40 89 15 2 2 0.1 0 0.9
branch 40 89 18 2 3 0.9 1 0.1
branch 40 89 26 1 4 1.0
branch 40 89 27 1 4 1.0
branch 40 89 31 1 4 1.0
branch 39 90 2 2 0 0.99 1 0.01
branch 39 90 11 2 4 0.01 0 0.99
branch 39 90 18 2 3 0.99 1 0.01
branch 39 90 21 2 3 0.99 1 0.01
branch 39 90 26 2 4 0.1 0 0.9
```

C. TENDL Neutron Data Library

In Table II, a comparison of the contents of TENDL with the other major world libraries is given. There are,

according to the ENSDF-based discrete level database of RIPL, 2813 target nuclides, in either ground state or isomeric state, which are either stable or have a half life beyond 1 second, and these are all included in TENDL. The nuclides range from ^1H to ^{289}Fl . Of these 2813 nuclides, 2808 can in principle be provided by TALYS, which does not accept H and He isotopes as targets. These cover all of the nuclides shown in Fig. 15, including 543 isomer targets. For comparison, the most complete alternative activation library besides TENDL, EAF-2010, considers only 816 targets. However, as Table II shows, all important stable light nuclides and the major actinides have been adopted from ENDF/B-VIII, which make integral testing of TENDL-2017 practically an integral test for all other nuclides. With the exception of these adopted files from ENDF/B-VIII, the evaluation method and ENDF-6 structure of all isotopic files in TENDL are the same. The entire structure of such a TENDL file has already been extensively outlined in Ref.[53] and will not be repeated here. We note that the TENDL neutron library comes with a full set of covariance data, *i.e.*, MF31-35,40 are generally filled with covariance data. Although technically possible, we have not included cross-isotope correlations.

TABLE II. Neutron nuclear data libraries considered for TENDL for adoption and comparison.

| Library | #nuc | Comment |
|------------|------|--|
| TENDL-2017 | 2813 | $^1,2,3\text{H}$, $^3,4\text{He}$, $^6,7\text{Li}$, ^9Be , $^{10,11}\text{B}$, ^{12}C , $^{14,15}\text{N}$, ^{16}O , ^{19}F , ^{232}Th , $^{233,235,238}\text{U}$, ^{239}Pu from ENDF/B-VIII |
| CENDL-3.1 | 240 | [54] |
| ENDFB/VIII | 556 | [4] |
| JEFF-3.3 | 562 | [55] |
| JENDL-4.0 | 405 | [56] |
| IRDFF-1.05 | 56 | [57] Dosimetry library |
| EAF-2010 | 816 | [58] Activation library |

D. TENDL Photonuclear Data Library

The photonuclear library is, next to the neutron library obviously, the only TENDL-2017 sublibrary which is no longer produced using global TALYS parameters. For TENDL-2017, in contrast to earlier versions of TENDL, an effort has been made to adjust nuclear model parameters such that TALYS predictions match as good as possible experimental (γ, n) , $(\gamma, 2n)$ etc data. In almost all cases, this concerns minor adjustment of the Giant-Dipole Resonance parameters, which are available in the RIPL database as Generalized Lorentzian parameters for the photon strength function. In some cases, also the radius of the real volume optical potential and the level density for the final nucleus were adjusted, especially to fine-tune

the ratio between (γ, n) and $(\gamma, 2n)$. Fig. 16 shows an example of TENDL photonuclear cross sections compared with other nuclear data libraries. All photonuclear data files of TENDL contain covariance information. Table III shows the nuclear data libraries we considered.

TABLE III. Photonuclear nuclear data libraries considered in TENDL for adoption and comparison.

| Library | #nuc | Comment |
|---------------|------|-------------------------------|
| TENDL-2017 | 2809 | ^2H from ENDF/B-VIII |
| ENDFB/VIII | 164 | [4] Adopts IAEA |
| JEFF-3.3 | 2809 | [55] Adopts TENDL-2017 |
| JENDL-2016/PD | 2681 | [59] |
| IAEA | 164 | [60] Result of IAEA CRP |

E. TENDL Charged Particle Data Libraries

For the TENDL charged particle libraries all calculations are performed with default parameters, even though we are well aware that better fits to experimental data can be obtained for several nuclides. These data libraries can thus be seen as an alternative to the intranuclear cascade codes used at energies up to 200 MeV, in which also no adjustment to experimental data takes place. There is still no efficient method to collect experimental data for charged particle-induced reactions, and to adjust TALYS input parameters to obtain the optimal description for each isotope. The semi-automatic method of TALYS parameter adjustment for the neutron library has not been applied to the charged particle library, simply because there is little guidance to what level of quality charged particle libraries should be evaluated for each material. Also, sensitivity analyses for charged particle applications such as accelerator shielding and medical isotope production are to our knowledge non-existent and do not translate in real evaluation needs (though there are modelling and experimental needs in that community). In short, they are considered less important than neutron libraries, which holds to an even larger extent for other incident charged particles. Fortunately, it is our experience that the difference between a global and a parameter-adjusted evaluation is larger for neutrons than for charged particles, *i.e.*, for charged particles there is less to be gained, and libraries produced by default TALYS calculations already perform reasonably well. We note that due to restricted computer power, only the proton nuclear data libraries of TENDL contain covariance data. For the other charged particles this will be included when a real need is expressed.

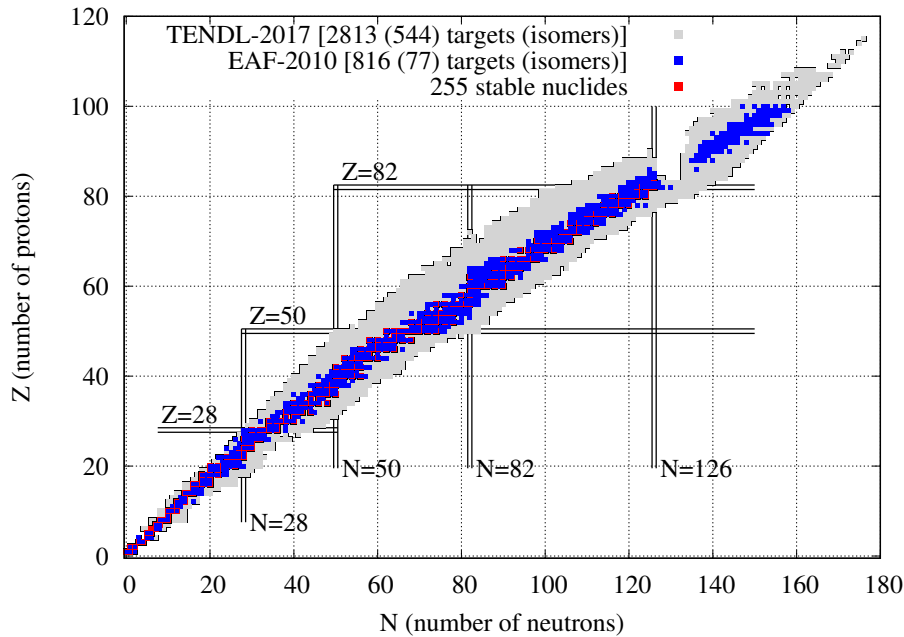


FIG. 15. (Color online) Chart of the nuclides showing the targets include in the TENDL-2017 and EAF-2010 neutron-induced reaction libraries. Note that TENDL includes all isomeric states with half life above 1 second, amounting to 544 of the 2813 files.

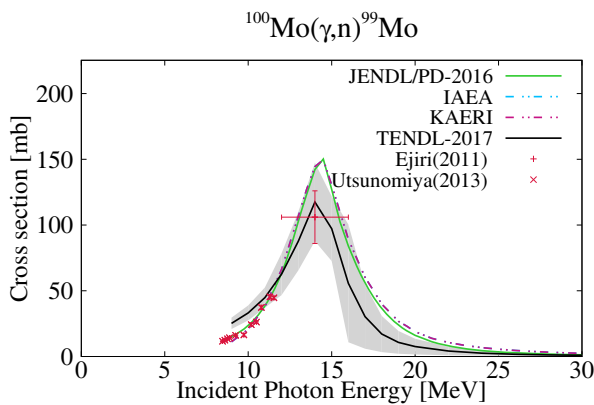


FIG. 16. (Color online) Comparison of photonuclear data libraries and EXFOR data for the $^{100}\text{Mo}(\gamma,n)^{99}\text{Mo}$ reaction.

1. Proton Sublibrary

For incident protons, the most important, and most measured, observables are elastic scattering angular distributions, total non-elastic cross sections, double-differential particle emission spectra and residual production cross sections. The general quality of TENDL for these reactions is directly related to the quality of the optical proton models of Ref. [21], and pre-equilibrium

exciton model of Ref. [34]. As can be inferred from these two papers, a rather good description can already be obtained without nuclide-by-nuclide adjustment. Fig. 17 shows an example of TENDL proton cross sections compared with other nuclear data libraries.

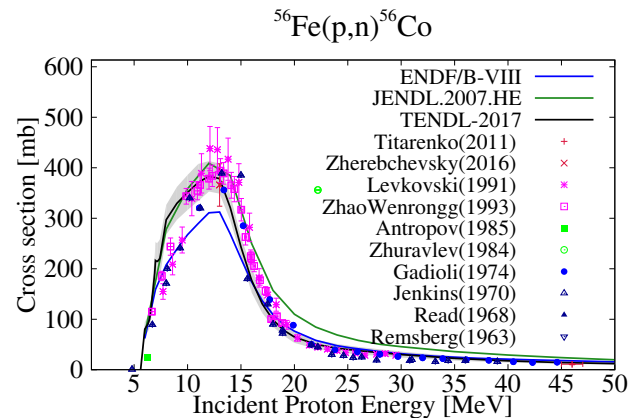


FIG. 17. (Color online) Comparison of proton data libraries and EXFOR data for the $^{56}\text{Fe}(p,n)^{56}\text{Co}$ reaction.

An extensive description of the ENDF-6 procedures used to build a proton library has been given in [8]. The TENDL-2017 proton libraries differs in two aspects from

that. First, similar to neutrons, we use explicit MT numbers for all reactions up to 30 MeV, while shifting to a MF6/MT5 description at higher energies. Also, covariance data are included, for cross sections in MF33 and isomeric cross sections in MF40. These include the full range of residual nuclides, as seen in Fig. 18 for ^{120}Sn . This allows accurate study of the activation-transmutation effects in systems with incident particle energies up to 200 MeV. Note that corresponding fission yield data is required for those with open channels.

In [8], a global comparison between TENDL-2011 and various intranuclear cascade models, as implemented in MCNPX, turned out favorably for TENDL-2011. Since then, the default parameters sets of TALYS have improved and it is expected that the TENDL-2017 performance is therefore at least as good. This an assumption, as global data validation for proton data libraries and other models has not been approached as thoroughly as for incident neutrons. Table IV gives a comparison with other existing libraries.

TABLE IV. Proton nuclear data libraries considered in TENDL for adoption and comparison.

| Library | #nuc | Comment |
|---------------|------|---|
| TENDL-2017 | 2812 | $^1,^2,^3\text{H}$, ^3He from ENDF/B-VIII |
| ENDFB/VIII | 48 | [4] |
| JEFF-3.3 | 2812 | [55] Adopts TENDL-2017 |
| JENDL-2007/HE | 106 | [61] |
| IBANDL | 14 | [62] Ion Beam Analysis library |
| IAEA | 34 | [63] Medical isotope library |
| HEIR-0.1 | 2094 | [64] MF10/MT5, 30-1000 MeV |

2. Deuteron Sublibrary

Compared to the last general publication about TENDL [8], there have been some significant improvements in the TALYS prediction for incident deuteron, triton, Helium-3, and alpha data, which is naturally reflected in the quality of the libraries. The major contribution to this improvement comes from the latest break-up model published by Kalbach [65], which provide a better description of *e.g.*, (d,p) and (d,n) reaction channels and thereby automatically also the competing reaction channels. This model is used in combination with her pick-up and stripping models [66] for all combinations of projectiles and ejectiles. The TENDL deuteron libraries find their application in various fields, most notably medical isotope production, and shielding and activation of deuteron accelerators for the IFMIF project, which simulates fusion neutron spectra. A global comparison with other libraries is given in Table V. At the moment, no channel-by-channel data are adopted from other libraries. In other words, with exception of the 5 isotopic data files adopted in their entirety from ENDF/B-VIII, all data

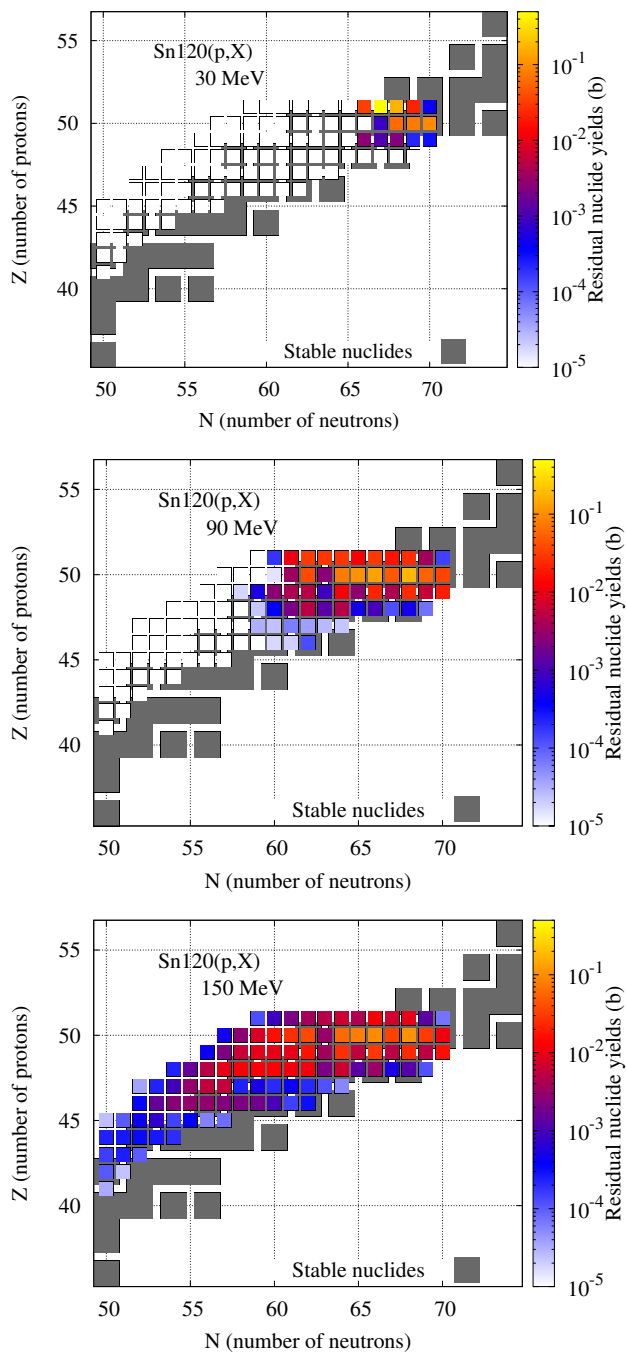


FIG. 18. (Color online) Cross sections for all residual isotopes in proton irradiation of ^{120}Sn , as extracted from the full MF6/MT5 data set of TENDL-2017.

come from default TALYS calculations. Fig. 19 shows an example of TENDL deuteron cross sections.

4. Helium-3 Sublibrary

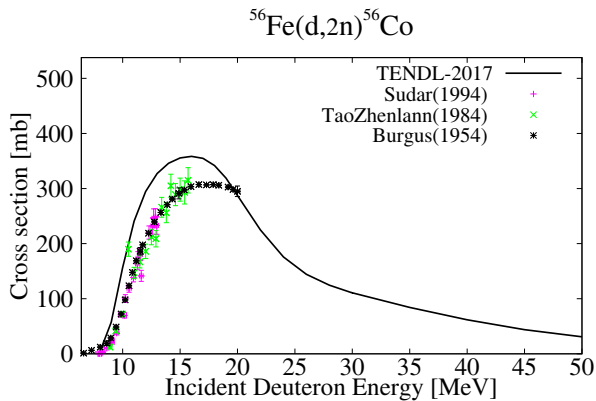


FIG. 19. (Color online) Comparison of TENDL deuteron data library and EXFOR data for the $^{56}\text{Fe}(d,2n)^{56}\text{Co}$ reaction.

TABLE V. Deuteron nuclear data libraries considered in TENDL for adoption and comparison.

| Library | #nuc | Comment |
|------------|------|---|
| TENDL-2017 | 2811 | $^2,^3\text{H}$, ^3He , $^6,^7\text{Li}$ from ENDF/B-VIII |
| ENDFB/VIII | 5 | [4] Only very light targets |
| JEFF-3.3 | 2811 | [55] Adopts TENDL-2017 |
| IBANDL | 2 | [62] Ion Beam Analysis library |
| IAEA | 15 | [63] Medical isotope library |

3. Triton Sublibrary

Of all the charged-particle libraries, the triton library is probably the least used, if at all. There is obviously an application in fusion reactor design for light targets, but TALYS does not handle those, while for medium and heavy nuclides there is almost no EXFOR data, and we are also not aware of any technological application of the TENDL library for tritons. Table VI shows what is available.

TABLE VI. Triton nuclear data libraries considered in TENDL for adoption and comparison.

| Library | #nuc | Comment |
|------------|------|---|
| TENDL-2017 | 2810 | ^3H , ^3He , ^6Li from ENDF/B-VIII |
| ENDFB/VIII | 3 | [4] Only very light targets |
| JEFF-3.3 | 2809 | [55] Adopts TENDL-2017 |

The Helium-3 library is, like the triton library, also seldom used, although TENDL has been used in several occasions for the estimation of medical isotope production using incident Helium-3 particle beams. Table VII shows the available nuclear data libraries.

TABLE VII. Helium-3 nuclear data libraries considered in TENDL for adoption and comparison.

| Library | #nuc | Comment |
|------------|------|--|
| TENDL-2017 | 2809 | ^3He , ^6Li from ENDF/B-VIII |
| ENDFB/VIII | 3 | [4] Only very light targets |
| JEFF-3.3 | 2809 | [55] Adopts TENDL-2017 |
| IAEA | 15 | [63] Medical isotope library |

5. Alpha Sublibrary

Besides TENDL, there are only a few nuclear data libraries for alpha particles available, see Table VIII. There are a few relevant reactions which have been evaluated for ion beam analyses and medical isotope production. Perhaps the best known nuclear energy related application for alpha libraries is the (α, n) reaction in spent fuel. This has several important aspects for safeguards [67], and for this reason important data sets have been evaluated for the JENDL-2005/AN library. One of the future actions for TENDL is to adopt the evaluated reactions from JENDL-2005/AN channel by channel, thus keeping the original evaluation, and/or to do an authentic re-evaluation of the data. In both case, the TENDL structure, and its applicability in various application codes, remains intact. In the last few releases of TENDL, the alpha optical model potential by Avrigeanu [28] has been used as default, improving the comparison of TENDL with experimental data for both alpha-induced reactions as reactions with alpha particles as ejectiles. Fig. 20 shows an example of TENDL alpha cross sections.

TABLE VIII. Alpha nuclear data libraries considered in TENDL for adoption and comparison.

| Library | #nuc | Comment |
|---------------|------|--------------------------------|
| TENDL-2017 | 2808 | |
| JEFF-3.3 | 2808 | [55] Adopts TENDL-2017 |
| JENDL-2005/AN | 17 | [68] |
| IBANDL | 4 | [62] Ion Beam Analysis library |
| IAEA | 4 | [63] Medical isotope library |

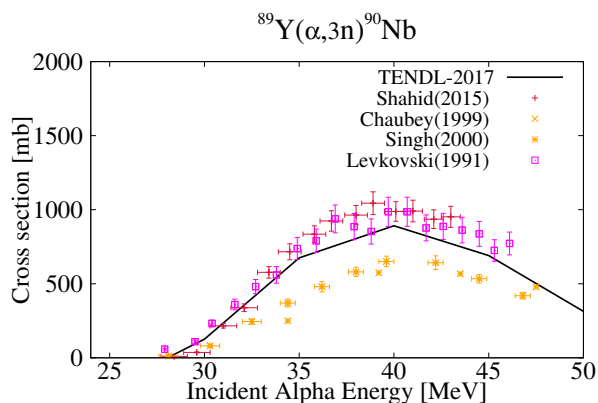


FIG. 20. (Color online) Comparison of TENDL alpha data library and EXFOR data for the $^{89}\text{Y}(\alpha,3n)^{90}\text{Nb}$ reaction.

F. Differential Validation with EXFOR

In order to assure the reliability of an evaluation it is essential to validate the cross section fits at differential and integral levels. Differential validation means a comparison of the evaluated data taken from TENDL-2017 to currently available experimental data. For this reason the experimental data for neutron cross sections were taken from the entire EXFOR database as well as the curves from other evaluated neutron data libraries namely JEFF-3.2, JENDL-4.0, EAF-2010, and TENDL-2015. Unfortunately the experimental data is mainly available in the range of 0 MeV to 20 MeV, which is linked to the amount of neutron sources used for measurement techniques. The fitting procedure was performed in a way that the TALYS curve is in good agreement with the recent experimental data points. Every time when there was a change in the set of nuclear model parameters the final plot was examined until the agreement was at a required level. Figs. 21-24 show several comparisons for different nuclear reaction channels. TENDL-2017 is represented by solid black line labelled ‘TALYS’. The visual analysis is a prompt way of judging the achieved level of agreement. The experimental points that are out of the general trend were not taken into account. In some cases the agreement is good but still some deviations are observed and that is explained by the fact that there is a connection between calculated channels and, for instance, a large variation of $(n,2n)$ may cause the increased disagreement to the other ones. Therefore it is important to keep a balance between all channels in order to stay within physical limits.

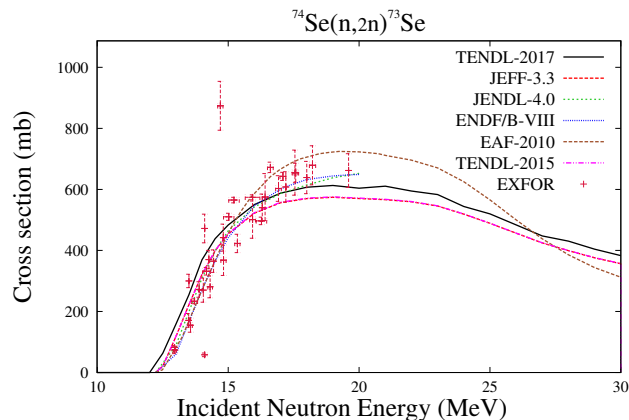


FIG. 21. (Color online) Excitation function for the $^{74}\text{Se}(n,2n)^{73}\text{Se}$ reaction.

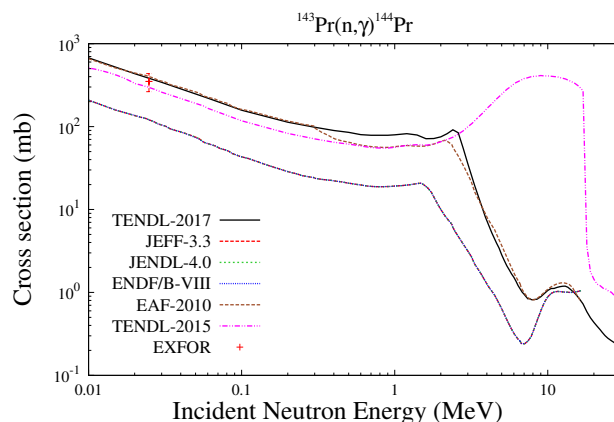


FIG. 22. (Color online) Excitation function for the $^{143}\text{Pr}(n,\gamma)^{144}\text{Pr}$ reaction.

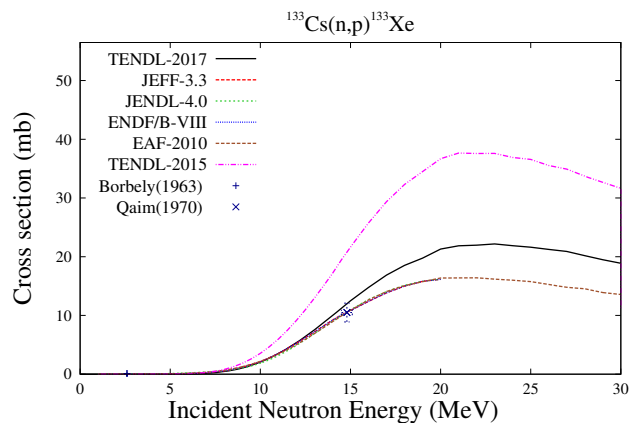


FIG. 23. (Color online) Excitation function for the $^{133}\text{Cs}(n,p)^{133}\text{Xe}$ reaction.

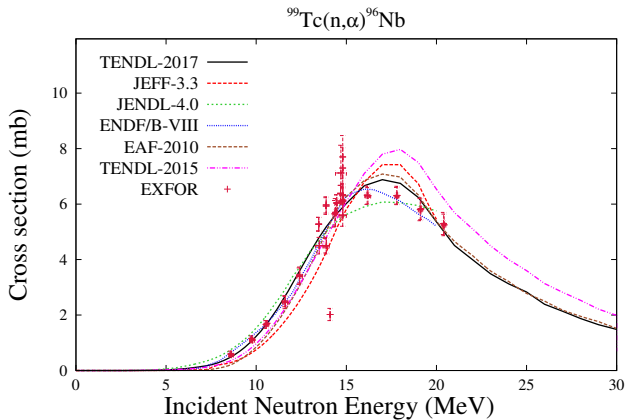


FIG. 24. (Color online) Excitation function for the $^{99}\text{Tc}(n,\alpha)^{96}\text{Nb}$ reaction.

Special attention was paid to fitting the isomeric cross sections. Data on cross sections for formation of short and long-lived nuclear metastable states are relevant because these values can be used for determining decay constants and internuclear transitions. In case of isomeric cross sections, first of all there was a need to analyze the level structure of the final nucleus in detail and to vary the probability of transitions between isomer and ground states. Where the information on that transition probability was not given in experimental data tables (incorporated into the TALYS system) the values could be estimated. In order to introduce this option it is needed, first of all, to set `bestbranch n` in the general TALYS input file and next to add additional input with the transition probabilities between the considered levels of the final nucleus. The fitting procedure includes fixing the total cross section first, and next with the variation of the transition probabilities, the fitting was focused at metastable and ground states separately. In Fig. 25 there is the example of the $^{95}\text{Mo}(n,p)^{95}\text{Nb}$, $^{95}\text{Mo}(n,p)^{95m}\text{Nb}$, and $^{95}\text{Mo}(n,p)^{95g}\text{Nb}$ nuclear reactions. One of the most important steps of the evaluation procedure is a decision on which experimental set is the most credible for fitting and should be taken for evaluation. Unfortunately it is hard to analyze all experimental data but in some cases when there were several discrepant experimental values, there was an attempt to find a reason. The study of the publications related to measurements supported to understand why some points are outliers as compared to the general trends. The difficulty to judge those measurements can be explained by lacking as well as insufficient descriptions of the experiments. The most common problems are based on using wrong time information or technique with measurements of β -spectra which is less selective than γ -spectroscopy. During the preparation of TENDL-2017 some effort was applied in order to find out the arguments of outliers in support of the current evaluation. For example, for the $^{170}\text{Er}(n,p)^{170}\text{Ho}$ reaction there are experimental data measured for formation of

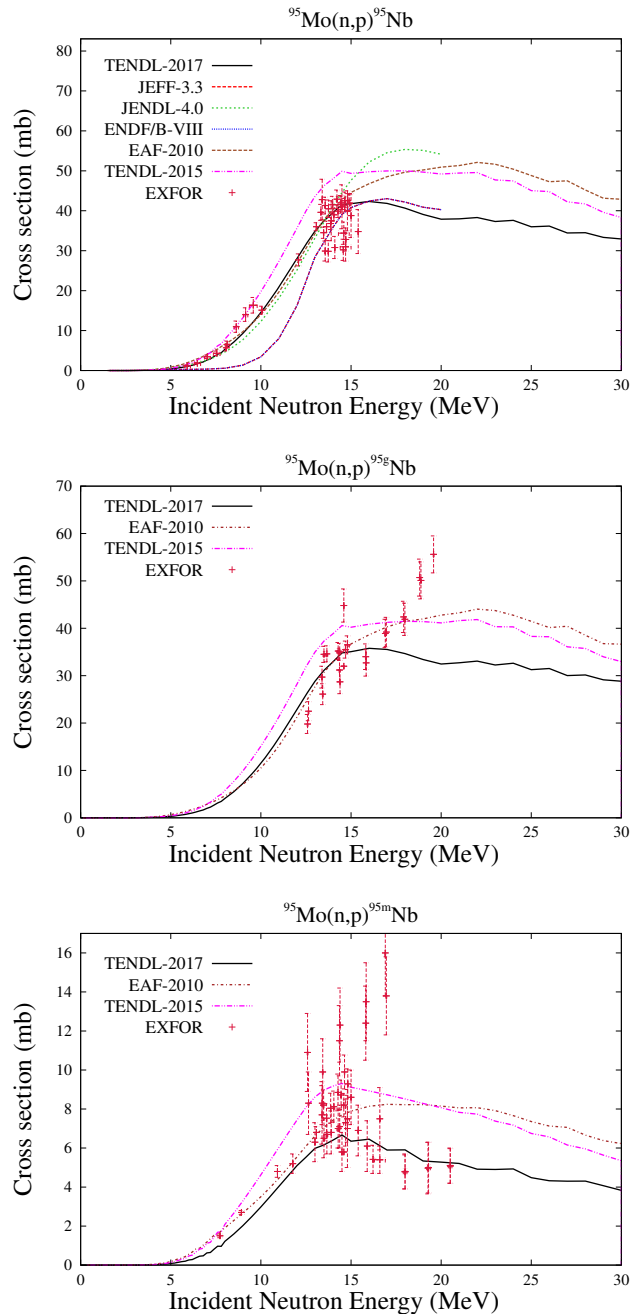


FIG. 25. (Color online) Excitation function for the $^{95}\text{Mo}(n,p)^{95}\text{Nb}$ reaction.

isomeric and ground states. In case of $^{170}\text{Er}(n,p)^{170g}\text{Ho}$ a difference of one order of magnitude was observed between data of Luo [69] comparing to measured by Dzyziuk [70] (Fig. 26). The most evident explanation of such a difference is that Luo did not account for an interfering reaction, namely $^{162}\text{Er}(n,2n)^{161}\text{Er}$. They claimed their use of the 931.4-keV γ -line from ^{170g}Ho decay for determination of this cross section, but for an interfering

reaction $^{162}\text{Er}(n,2n)^{161}\text{Er}$ the decay of ^{161}Er is accompanied by the emission of a 931.7 keV from ^{161}Ho . Due to the high value of the $^{162}\text{Er}(n,2n)^{161}\text{Er}$ reaction cross section with respect to (n,p) reactions for the considered energy range, an essential increase in the cross section of interest $^{170}\text{Er}(n,p)^{170\text{m}}\text{Ho}$ might be observed. As could be seen in Fig. 6 the JEFF curve is in agreement with the upper experimental point and we would recommend to reconsider that. The current evaluation (TALYS black curve) is more reliable. For the $^{100}\text{Mo}(n,p)^{100}\text{Nb}$ reaction

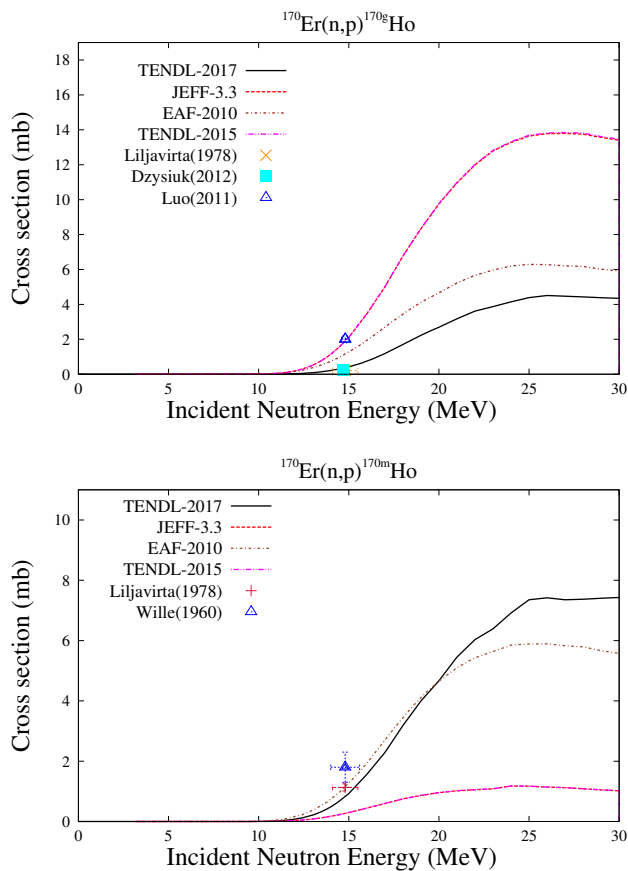


FIG. 26. (Color online) Excitation function for the $^{170}\text{Er}(n,p)^{170\text{m}}\text{Ho}$ reaction.

there are also only two experimental data points. After analysis of the measurements, the decision to include the Amemiya [71] data into the evaluation was made. The data of Cuzzocrea [72] was not taken into consideration as the authors used the wrong information for the $T_{1/2}$ of the reaction product. The actual half-life of ground state of ^{100}Nb is 1.5 s (Fig. 27) but in the paper there is a description of the measurement that resulted in a half-life of about 3 min. That most possibly caused an overestimation of the cross section value.

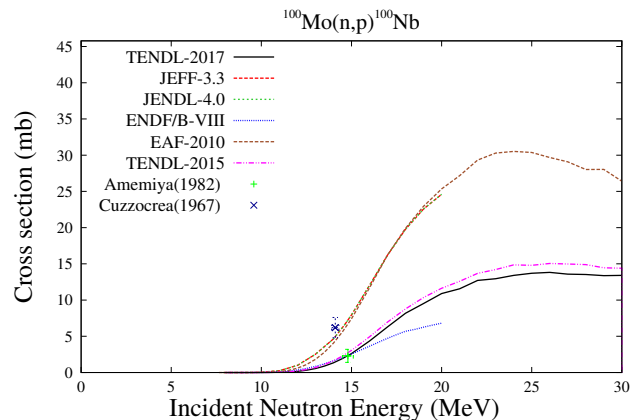


FIG. 27. (Color online) Excitation function for the $^{100}\text{Mo}(n,p)^{100}\text{Nb}$ reaction.

Differential validation is a very efficient and practical approach to analyze each reaction channel individually and it helps to increase the total accuracy of evaluation. However a fully comprehensive validation can not be accomplished due to the limitation of available differential as well as integral nuclear reaction cross section measurements at the considered energy range (0-30 MeV). For that reason it is relevant to prioritize the experimental needs on appropriate lists, such as the High Priority Request List, which can then be combined with modelling efforts.

G. Validation with Compiled Experimental Data Sets

1. Thermal Cross Sections

Cross sections for thermal Maxwellian spectra or differential measurements are the subject of many experimental measurements and these data have been compiled into databases such as the *Atlas of Neutron Resonances* [12] and the *CRC Handbook* [73]. A review of these data, with a cross-comparison using EXFOR, was performed at the UKAEA, producing an amalgamated database of thermal cross sections [74]. In a few cases, discrepancies between these databases were dealt with by direct interrogation of the cited publications, or review of the most recent data in EXFOR.

The ratio of calculated (TENDL-2017) to experimental cross sections in this thermal cross section database are shown in Fig. 28. The distribution is very closely centred around perfect agreement at 1.0, although some few errors are present. Notably, some reaction channels are absent in the adopted files from ENDF/B-VIII.0, such as the $^{233}\text{U}(n,\alpha)$ channel. The majority of all values that are not in perfect agreement are due to partial, isomeric production cross sections. A system to handle isomeric production is in development for future versions.

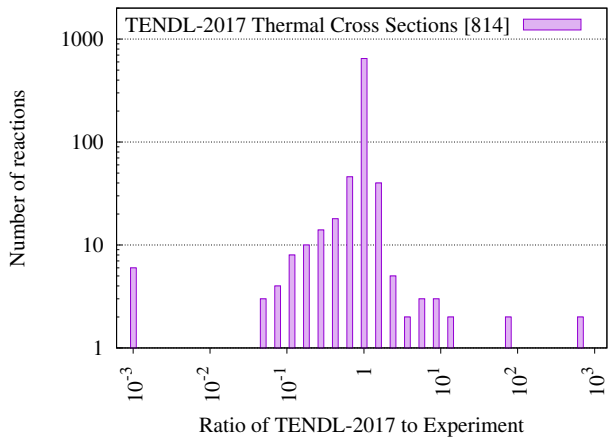


FIG. 28. Distribution of TENDL-2017 thermal cross section to experimental cross section ratio (C/E) using the UKAEA thermal cross section database.

2. Resonance Integrals

Resonance integrals provide a standard, simple method for comparing reaction probabilities in the resonance range, which are due to potentially many hundreds or thousands of parameters. The standard integral is calculated in the slowing $1/E$ spectrum, as

$$RI = \int_{E_1}^{E_2} \frac{\sigma(E)}{E} dE, \quad (23)$$

where the integration limits are subject to modification for each experimental measurement. Typically values are $E_1 = 0.5$ eV and $E_2 = 100$ keV. The reference set for these data is the *Atlas of Neutron Resonances*. The data in the *Atlas* includes two options, the calculated data based on the resonance parameters provided in that text, or experimental data. In the cases where these are in disagreement, such as the $^{196}\text{Pt}(n,\gamma)$, experimental values are selected.

The distribution of TENDL-2017 calculated resonance integrals to reference resonance integrals is shown in Fig. 29. These are helpful, integral quantities to complement evaluation of resonance parameters and provide a verification check. As the majority of the resonance integral for measured nuclides are due to resonances with evaluated parameters, this effectively provides a test for the TARES resonance parameter database. It also provides a verification check for the High-Fidelity Resonance generation (see Section II B), where these resonances are a significant contribution of the total integral.

3. MACS and the KADoNiS Database

The importance of neutron capture to stellar astrophysics, through the nucleosynthesis s -process, has led to

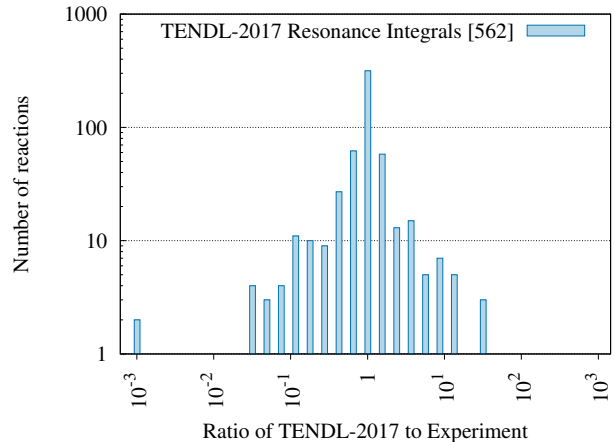


FIG. 29. Distribution of TENDL-2017 resonance integral cross section to experimental cross section ratio (C/E) using the UKAEA resonance integral cross section database.

considerable efforts to evaluate the integral cross sections of Maxwellian neutron energy spectra with kT between 1 and 100 keV. This data was assembled in the work by Bao *et al.* [75] before being compiled in the on-line format of the Karlsruhe Astrophysical Database of Nucleosynthesis in Stars (KADoNiS) [76]. This database provides a range of Maxwellian-averaged cross sections, as well as an uncertainty for the 30 keV value, which is broadly representative of the uncertainty over the whole energy range. It must be noted that the data for 80 of the 357 isotopes (22%) are taken from statistical model calculations and are not experimental. These are instead code to code comparisons, although they provide a verification check for nuclear data libraries.

For TENDL-2017, the capture cross sections are provided with full MF=33 covariance data. In the unresolved resonance range, this data comes from Bayesian Monte-Carlo TALYS evaluations and within the resonance range a novel approach using SAMMY has been employed. For more details, see Section IV and Section IV B, respectively. These covariances can be used to calculate the uncertainty in the spectrum-averaged cross sections, as shown in Fig. 30, as a continuous plot over the temperature-dependent averaged cross sections.

The overall performance of the TENDL-2017 library, as compared with the full KADoNiS database, is shown in Fig. 31. Most of the well-known nuclear data libraries exclude several of the KADoNiS isotopes, resulting in the '<1/10' peaks on the left-hand side. That TENDL contains complete nuclear data to cover all of these isotopes is well-known, but TENDL contains resonance evaluations that best match these MACS measurements and combines this with covariance evaluations that cover all incident neutron energies. KADoNiS contains several datasets that are not experimentally determined, but approximately 22% are derived from some statistical model calculations, including values obtained from the

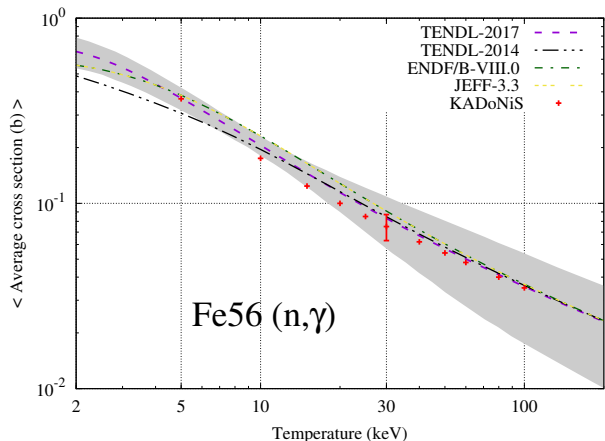


FIG. 30. (Color online) Temperature-dependent MACS for Fe55, including temperature-dependent, full covariance uncertainties calculated using TENDL-2017 and FISPACT-II.

NON-SMOKER code [77]. The agreement found in this case does not provide direct validation with experimental data, yet the cross-validation with different model calculations provides a measure of verification in the absence of experiment.

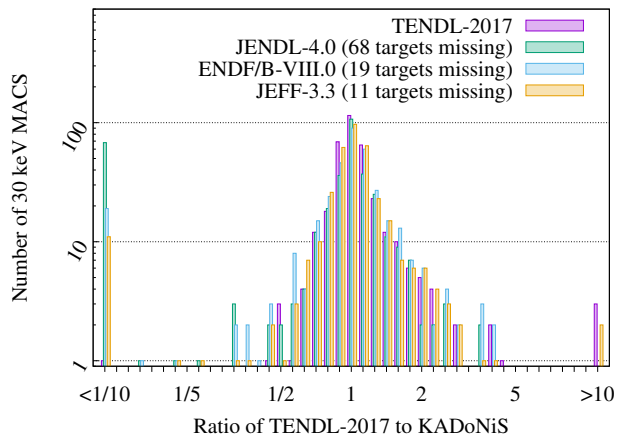


FIG. 31. (Color online) Comparison of C/E distributions for all 357 KADoNiS 30 keV cross sections with TENDL-2017, JENDL-4.0 and ENDF/B-VIII.0 values calculated with maxwav. C/E values for missing nuclides in JENDL-4.0 and ENDF/B-VIII.0 are tallied in the $<1/10$ bin.

VI. ADJUSTMENT

The adjustment of the calculated nuclear data is a necessary step for many libraries. In a usual evaluation scheme, the evaluators will spend a large amount of time in finding the right model parameters to reproduce differential data, often from the EXFOR database [1].

Once this is done, there might still be discrepancies between calculated cross sections and the measured ones. The next step would then be to change the calculated values to be more in agreement with the desired values. Such changes can be done by hand, or using some more advanced methods (*e.g.* Kalman filter [78], GLLS [79], Bayesian [80, 81]). In the next section, this step is described under the adjustment *via* differential data. Once since step is performed, a true general purpose nuclear data library is obtained, meaning that it has not been targeted, or adjusted to specific particular applications. This was up to TENDL-2015 the general adopted approach in TENDL.

An additional step of adjustment is generally taken for almost all libraries, *i.e.*, final modifications to obtain good performances for a selection of integral benchmarks. Historically, these benchmarks have been a selection of critical experiments, most often restricted to the calculation of k_{eff} . There are many reasons for these choices, but the most obvious one is the availability of these benchmarks in terms of simulation inputs and the relatively ease to use them. It can be noted that this is slowly changing: not only k_{eff} are being analyzed, but also spectral indexes. Additionally, other types of benchmarks are now used: shielding and reactor benchmarks. This second step of adjustment is making sure that a library is also performing well with this selection of integral benchmarks. This being done, the updated files are no longer *as general as before*, but they are still claimed to be of general application. In the case of the TENDL library, this approach was taken for TENDL-2017, where the major actinides and light elements were adopted from ENDF/B-VIII.0.

There is another advantage of using integral benchmarks during the evaluation procedure: the reduction of calculated uncertainties. By using some well selected benchmarks, cross-correlations between certain reactions and isotopes appear, together with a reduction of uncertainties for specific channels (see for instance Refs. [82, 83]).

In the following, a practical example will be presented with ^{56}Fe with a few steps adjustment, for future releases of TENDL versions. The steps to be undertaken will be the following:

1. Produce prior based on model knowledge,
2. Based on the prior, update with differential data,
3. A second adjustment step is done with integral data.

This simple description has the advantage to clearly separate the differential and the integral adjustments. Such approach is also currently under discussion for the preparation of the JEFF-4.0 library, where one possibility will be to produce two sets of files, A and B, the first one would correspond to the EXFOR adjustment, the second one to EXFOR plus integral data.

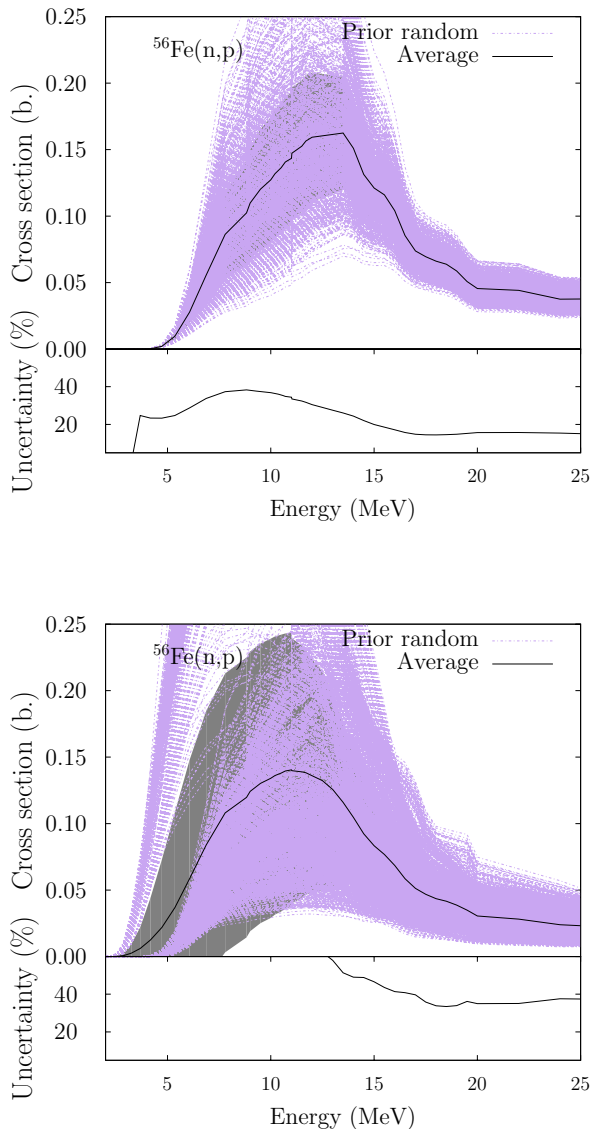


FIG. 32. (Color online) Example of random $^{56}\text{Fe}(n,p)$ cross sections based on the variations of model parameters (top) and on the variations of model parameters and of models (bottom).

A. Prior Nuclear Data

As explained above, the prior nuclear data can be produced in TENDL based on the “T6” code package. The output of such calculation is one single ENDF file (for instance for ^{56}Fe), solely based on the knowledge included in the T6 models, and on the global (and sometimes local) adjustment of model parameters. An example for $^{56}\text{Fe}(n,p)$ is presented in Fig. 32 (top). Such random curves are obtained by varying in a random way all model parameters (optical model, pre-equilibrium, level densi-

ties, *etc.*) but the model themselves are fixed. The results for the (n,p) reactions are representative of the other channels. As observed such spread of curves have a limited degree of freedom: they are more or less parallel and do not cross each other.

To increase the variability of the random curves, one can also change the models together with the parameters: optical model, level densities, mass models, *etc.* Table IX presents the list of the models which are varied to increase the dispersion of the prior. For details on these

TABLE IX. Example of the models which are randomly changed in the TALYS calculations to create a large spread in the prior calculations. This example represents the ^{56}Fe calculations presented in the following. OM means optical model.

| Models | TALYS keywords | Range |
|--------------------------------|----------------|-------|
| Level density | ldmodel | 1-5 |
| Constant Temperature Model | ctmglobal | n-y |
| Spin cut-off parameter | spincutmodel | 1-2 |
| Shell effects | gshell | n-y |
| Gamma-strength function | strength | 1-8 |
| M1 gamma-ray strength function | strengthM1 | 1-2 |
| Excited state in OM | statepot | n-y |
| Spherical OM | spherical | n-y |
| microscopic OM | jlomp | n-y |
| Radial matter densities | radialmodel | 1-2 |
| Liquid drop expression | shellmodel | 1-2 |
| Vibrational enhancement | kvibmodel | 1-2 |
| Pre-equilibrium model (PE) | preeqmode | 1-4 |
| Spin distribution (PE) | preeqspin | 1-3 |
| Surface corrections (PE) | preeqsurface | n-y |
| Kalbach model (pickup) | preeqcomplex | n-y |
| Component exciton model | twocomponent | n-y |
| Pairing correction (PE) | pairmodel | 1-2 |
| Experimental masses | expmass | n-y |
| Mass model | massmodel | 0-3 |
| Width fluctuation | widthmode | 0-3 |

models, see Refs. [8] and the TALYS manual. The combination of some of these keywords has also to be done in a proper way, otherwise some of them will have no effect. In Fig. 32, one can see two groups of calculations in the case of the variation of models. The main difference between these two groups is the change of the mass model: the highest cross sections near the threshold are obtained with theoretical masses based on the Gogny force (keyword *massmodel* equal to 3).

The results are presented in Fig. 32 (bottom): the spread is indeed larger (larger uncertainties and some of the random curves are crossing each other). To also vary models is not usually done when creating prior curves, but it certainly leads to a better coverage of possibilities. One can say that such model variations are similar in the experimental side to considering different types of measurements for a specific reaction.

The variation of models for the prior also have consequences for the prior correlation matrices. Similar to Fig. 32, the (n,p) correlations are presented in Fig. 33.

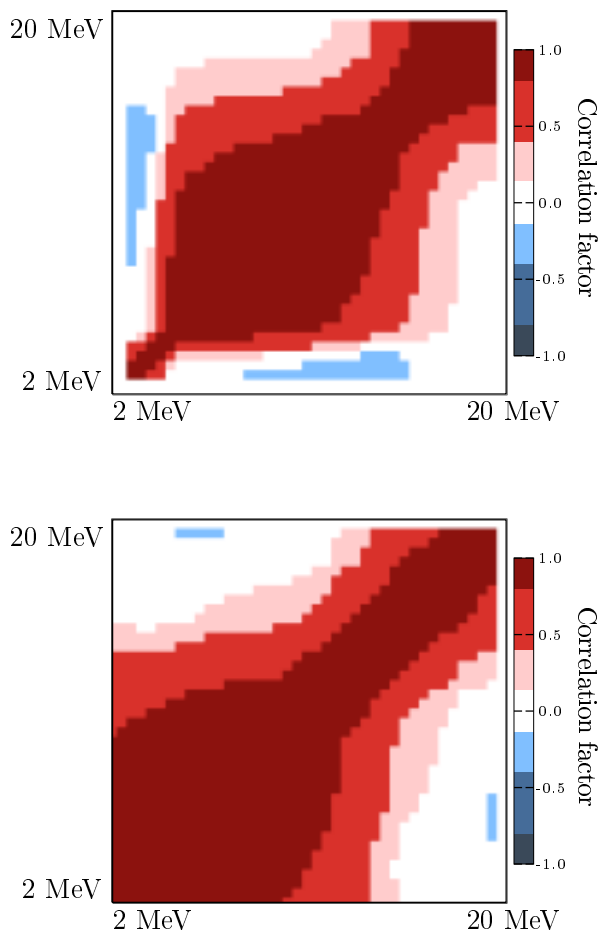


FIG. 33. (Color online) Example of $^{56}\text{Fe}(n,p)$ correlations based on the variations of model parameters (top) and on the variations of model parameters and of models (bottom). The x and y axis are from 1 to 20 MeV.

As expected, correlation matrices are different, due to the use of different models. This is emphasizing again that covariance matrices are coming from the assumptions made during the calculation procedure. They do not represent absolute *truth*. By repeating this for all important channels, one can generate prior realizations which cover a large part of the possibilities. Naturally, the next step will be to compare such prior cross sections with differential data.

B. Inference via Differential Data and Monte Carlo

Based on the above curves, one can make a selection of EXFOR data and compare them with the prior calculations. Of course this is only the first step towards producing an adjusted library, and users may not want

to deal with hundreds of such cross sections for one isotope. There are at least two convenient ways to produce a posterior, once the EXFOR selection is made.

The first one was presented in Refs. [84, 85] and was subsequently called the Petten method. It simply consists in comparing the random curves with the differential (or integral) data and to select the random ENDF file which is in best agreement with EXFOR. This is equivalent to calculate a simplified or generalized χ^2 for each random file, and to select the one with the smallest χ^2 . Such method is extremely simple but has the disadvantage to not providing covariance data. One could still, based on the best ENDF file and its T6 input parameters, calculate a covariance file by sampling the parameters used to produce this best file.

A second approach is based on Bayesian updating. It was presented in a few papers, with its origin Bayesian Monte Carlo (BMC) definition [36, 81, 86], or with practical changes within the Backward-Forward Monte Carlo [87] (BFMC). Such methods consist in calculating (again) χ^2 values for each random file and to derive weights for these files. As explained in Section IV, in the BMC method, the weight w_i for a random file i is calculated by

$$w_i = \exp(-\chi_i^2/2), \quad (24)$$

while in BFMC, the weight w is

$$w_i = \exp(-(\chi_i^2/\chi_{\min}^2)^2). \quad (25)$$

The second definition avoids having a very large spread of χ^2 values due to good, bad and very bad agreement between differential data and random files. The definition of the χ^2 is not of prime importance for the following, but one can consider the simplified χ^2 (without experimental correlations) or the generalized χ^2 (with experimental correlation). These experimental correlations are difficult to obtain and require a precise study of all experimental set-up. In this case, and considering that the underlying reaction models are correct, the BMC method is the most appropriate choice. Otherwise, in order to compensate for missing (experimental) correlations and defaults in the reaction models, the BFMC method offers a practical solution. By normalizing with the minimum χ^2 (called χ_{\min}^2), the distribution of weights is not as widely spread as in BMC. Based on these weights (one for each random ENDF file), one can calculate cross section weighted average, standard deviations and correlations, as in Eqs. (15)-(15).

Examples for the $^{56}\text{Fe}(n,p)$ cross section are presented below in the case of the BMC and BFMC approaches: Figs. 34 for the cross sections and uncertainties and 35 for the correlation matrices. As expected, the prior provides a large range of possibilities, as in the case of the (n,2n) cross section. Because of the spread from the models, the average prior is also relatively away from the experimental data. One should notice that the prior spread is much larger than in the conventional TENDL approach

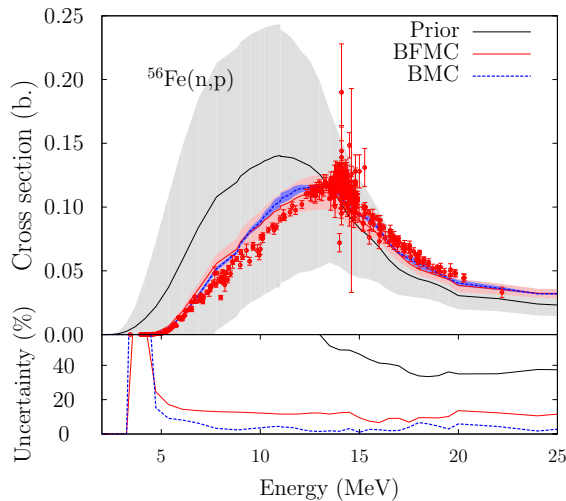


FIG. 34. (Color online) Example of posterior $^{56}\text{Fe}(n,p)$ cross sections and uncertainties based on BMC and BFMC. The grey band represents the prior uncertainty.

where only the model parameters are varied. It was nevertheless repeatedly noticed that by selected only one set of models, a number of experimental data could not be represented by random calculations; such deficiencies is up-to-now compensated by so-called model defects, with the use of Gaussian processes [41, 87, 88]. As presented in Figs. 32 and 34, another advantage to vary models (such as mass models) is to allow the threshold of the reactions to increase or decrease. Additionally, the changes from the pre-equilibrium models also helps to obtain a better agreement at the threshold or reactions such as $(n,2n)$ and (n,p) . In Fig. 34, it is clear that the flexibility from the prior random cross sections helps to obtain a posterior in better agreement close to the (n,p) threshold.

As expected, the posterior cross sections and uncertainties, taking into account differential data, are quite different than the prior. The average cross sections (for both BMC and BFMC) are in closer agreement with the experimental data, and the uncertainties are strongly reduced. As observed, the BMC method leads to smaller uncertainties than the BFMC method (as also observed in Ref. [47]). Small differences appear for the posterior averages, which are still within the 1-sigma uncertainty bands represented in the figure. In the present case, both BMC and BFMC are very effective to produce posterior distributions (being in fact simply prior random calculations with specific weights) in agreement with the experimental data. In a similar way, the posterior correlation matrices can be produced and are presented in Fig. 35. Both of these correlation matrices are relatively different and one can also notice that the prior correlations are hardly subsisting.

One can still notice in Fig. 34 that some experimen-

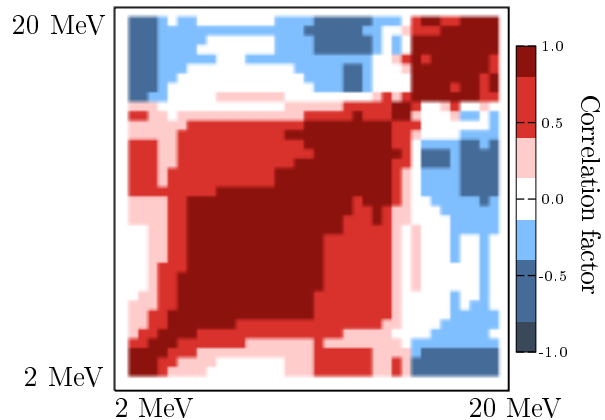
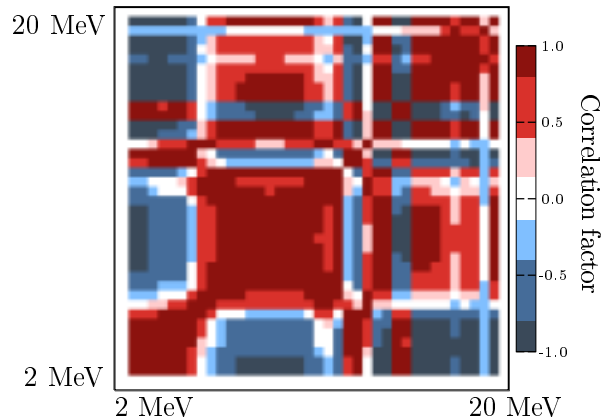


FIG. 35. (Color online) Example of posterior $^{56}\text{Fe}(n,p)$ cross section correlations based on BMC (top) and BFMC (bottom).

tal data cannot be fitted, especially below 15 MeV. This means that the variations allowed by the set of selected models does not provide enough flexibility to lead to an agreement with these data. One solution which is currently being explored is also to sample models as well, and not only model parameters. This will certainly enlarge the possibility space and provide a better match with experimental data. But such work is not yet at the stage to be included in a library.

For a full evaluation as performed in the TENDL libraries, many channels are considered together. Also, different isotopes of the same element can be analyzed together, for instance including experimental data on natural targets. The use of natural differential data will have a similar effect compared to using integral benchmarks: it is leading to the creation of cross-isotope correlations for specific reactions.

C. Inference via Integral Benchmarks and Monte Carlo

The use of integral benchmark in nuclear data evaluation is still a debated question. As explained in Ref. [47], the main drawback in avoiding integral experiments in the evaluation process is that the calculated uncertainties for these benchmarks, taking into account differential data solely, are larger than the reported integral benchmark uncertainty. This is not a fundamental problem *per se*, but nuclear data users from large-scale facilities do not always appreciate the origin of such differences. One reason for this difference may be the omission of correlation between important data which is not available from measurements. Another drawback in not clearly including some integral benchmarks in the evaluation process is that it is done anyway, but without explicitly stating it. Unfortunately, when an adjusted library is produced by other experienced people (see for instance Refs. [79, 89]), some benchmarks are therefore used again in the adjustment process, therefore biasing the results towards specific benchmarks.

There are also possible drawbacks in including integral benchmarks in the evaluation process. The selection of such benchmarks cannot be done blindly and needs to be representative of a large variety of applications. It should not be restricted to criticality benchmarks only, and at least makes use of spectral indexes, shielding benchmarks, and possibly reactor experiments. The main difficulties in using a variety of integral systems are the availability of computer models, the possibility to run them in a reasonable amount of time, and a convenient way to compare calculated and measured values. For these reasons, the nuclear data community has for a long time restricted itself to k_{eff} calculations for systems defined in the ICSBEP database [90].

The TENDL libraries were up to 2015 free of integral adjustments. This was achieved by only considering differential experiments, with or without Bayesian adjustments. As observed, this has led to good agreement with EXFOR data, but to a limited one with criticality benchmarks. Additionally, the calculated uncertainties with TENDL were in general larger than the ones coming from other libraries. Even if this can present some advantages, the TENDL-2017 release (and probably the future ones) did not follow this approach for some isotopes, and a limited number of evaluations were adopted from ENDF/B-VIII.0 (*e.g.*, $^{235,238}\text{U}$ and ^{239}Pu). The consequence is a stronger agreement with ICSBEP benchmarks.

The ^{56}Fe evaluation was not adopted from another library in any TENDL release, except for the elastic angular distributions (MF4 MT2) which was directly taken from JENDL-4.0 [56]. In the following, a simple example of the use of k_{eff} integral benchmarks is presented, with the BFMC method in order to rank random ^{56}Fe realizations. The first step was presented in the previous section: producing a large amount of random ^{56}Fe files; the second step is to use these random files with a selection

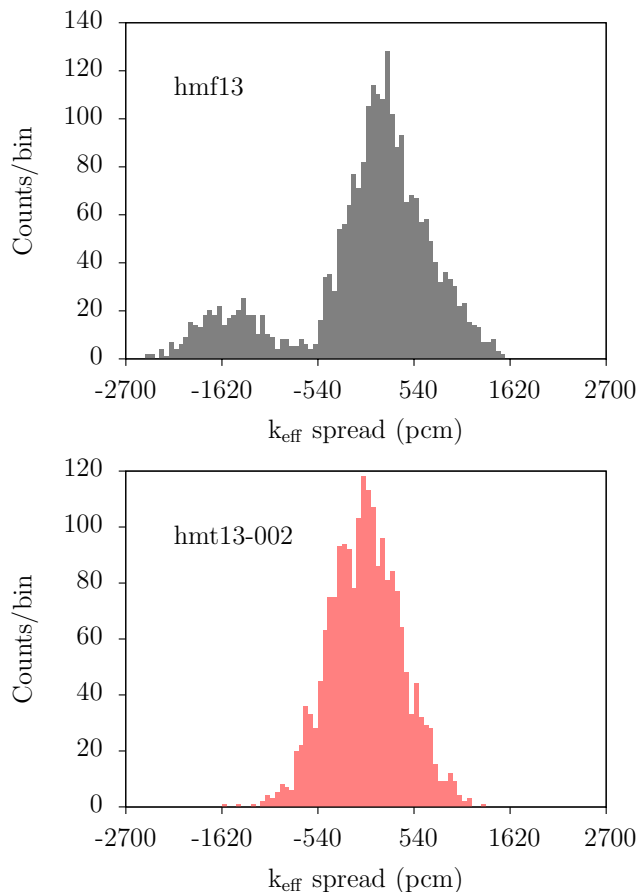


FIG. 36. Examples of the calculated k_{eff} spread for two benchmarks highly sensitive to iron. All nuclear data of ^{56}Fe are varied, using about 2400 random files, with different models and model parameters.

of benchmarks. Here, only two criticality benchmarks are selected, highly sensitive to iron: the hmf13 and hmt13-002. The first one is a sphere of highly enriched uranium reflected by steel and the second one is a highly enriched uranium system including an iron plate and moderated by polyethylene. Examples of the spread of the calculated k_{eff} are presented in Fig. 36, where the spread is calculated around the mean k_{eff} values.

One can see that the variation of the ^{56}Fe nuclear data has a large effect on the k_{eff} of these two benchmarks. For the thermal benchmark, the standard deviation is about 400 pcm, which is not negligible, and in the case of the fast benchmark, the effect is much larger, with a standard deviation of 770 pcm. What is more striking for the fast benchmark is the double-hump distribution of the k_{eff} , due to the use of very different optical models in the fast neutron range. Such results come from the method presented above, and such approach unfortunately leads to average k_{eff} values which are not in agreement with the benchmark values, as presented in Table X. The benchmark k_{eff} values are 0.99900 ± 0.00150 and 1.00060 ± 0.00220 for hmf13 and hmt13-2, respectively. The cal-

TABLE X. Characteristics of the probability density functions for both benchmarks, varying the ^{56}Fe nuclear data. “All random MF” means that the full ^{56}Fe ENDF files are random from one calculation to another. Other isotopes come from the JEFF-3.3 library.

| | All random MF | | | Fixed MF4 | | |
|---------|------------------------------------|--------------|-----------------|------------------------------------|--------------|-----------------|
| | $\overline{k_{\text{eff}}}$ (-) | Std (pcm) | skewness (-) | $\overline{k_{\text{eff}}}$ (-) | Std (pcm) | skewness (-) |
| hmf13 | 1.01998 | 770 | 1.02 | 1.01096 | 450 | 0.46 |
| hmt13-2 | 1.01166 | 410 | 0.02 | 1.01031 | 390 | 0.03 |

culated values are not in agreement with the benchmark values, and possibly not only because the ^{56}Fe nuclear data are not correct. Still, the calculated uncertainties point to a possible room for improvements.

A simple way to check the origin of these uncertainties is to repeat the above calculations, this time fixing some nuclear data. This was done by producing random ^{56}Fe nuclear data files with non-random angular distributions (MF4). The MF4 was taken from the JENDL-4.0 library. The results of such new calculations are also presented in Table X and in Fig. 37. As observed, the average k_{eff} value for the fast benchmark is closer to the benchmark values, and the uncertainties are sensibly reduced (especially for hmf13), indicating that the elastic and inelastic angular distributions have a relatively important impact. Note that the double hump for the hmf13 benchmark has disappeared. Such double-hump distribution is simply the reflection of the large variations of the prior nuclear data distribution. The main information that we can extract is an indication that the angular distributions play an important role for this criticality benchmark; this can be related to the similar expected sensitivity in the case of shielding benchmarks (for instance the ASPIS benchmark), pointing out at the necessity of a dedicated effort towards better evaluated angular distributions (mainly through better modeling).

If we consider that the prior ^{56}Fe random nuclear data files were covering a large part of the likelihood, and that other nuclear data important for these benchmarks are well known, it can be proposed that the current theoretical knowledge for ^{56}Fe (including its angular distribution) is not adequate. In this case, the compensation of calculated nuclear data with specific approaches using model defects can be very useful.

VII. PROCESSING ROUTES

An important aspect of the quality and usefulness of any evaluated file resides in its ability to be properly parsed through processing codes prior to being used. This could take many forms - use in solvers for transport (Boltzmann) or Bateman equations or simply to be displayed to a human eye and compared with experimental data. It is necessary to demonstrate the ability

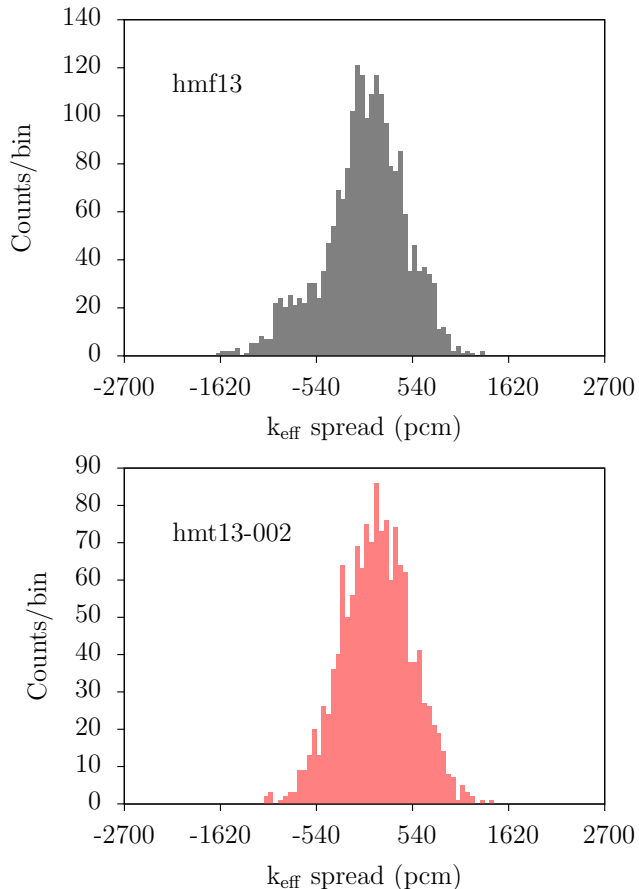


FIG. 37. Same as Fig. 36, but keeping MF4 fixed (no variation of the angular distributions).

to successfully convert evaluations into formats useful for the many applications that need them.

Depending on the applications, the data formats have quantitative and qualitative requirements that are not alike or even always compatible. The cross section reconstruction accuracy criteria, for example, are different for simple display and for pointwise cross sections used in Monte Carlo transport. The strength behind a uniform data structure format for all evaluations is that it allows the use of single script that contains all necessary input sequences to process an entire library. This uniqueness in processing also allows one to compare the data on an equal footing. The general processing workflow used with TENDL is shown in Fig 38.

A. PREPRO

The PREPRO suite contains several codes that provide data pre-processing functions to transform the raw ENDF-6 data into different data and formats that may be used by some application codes. Each code performs

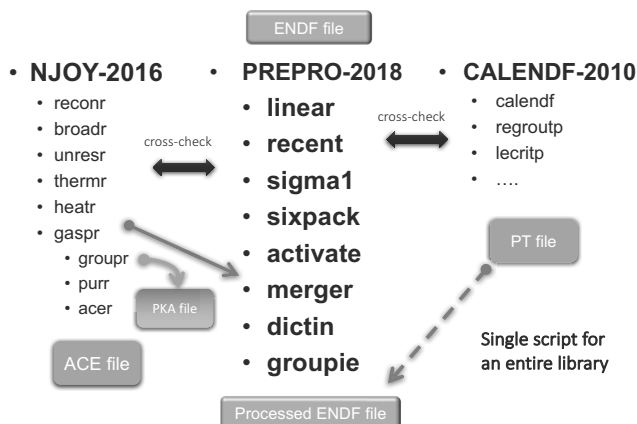


FIG. 38. Enhanced processing steps, three codes NJOY, PREPRO and CALENDF [10, 11, 91].

one or more independent operations on the data while reading and writing structured data formats respecting the ENDF-6 format frame at any stage.

The high-energy (> 30 MeV) part of the file stored as MF-3/MT-5*MF-6 is parsed by the sixpack module that extracts the production cross sections before embedding them as an MF-10 MT5. Furthermore, gas production, kerma and dpa information uniquely produced by NJOY from the same original data file are also carefully stacked into the ENDF-6 formatted file before the relevant data formats, the cross sections and other derived quantities, are group averaged by the groupie module.

1. Data Formats for Applications

One important aspect of nuclear data has been the format and structure in which basic physics information could be stored, distributed and used in applications. These basic physics data must be stored in evaluated files and then processed into engineered applied data sets. The TENDL formats are multiple but coherent, originating from the same technological setup. They serve many different research fields ranging from astrophysics to medical; earth to life sciences; fusion and accelerator-based systems. Those formats can be categorized as:

- physic tables, X-Y format for cross-sections, emitted spectra and angular distributions;
- S_0 ENDF-6 formats, single reaction channel: MF-3/MT-5*MF-6 to 200 MeV;
- S_{30} ENDF-6 formats, multiple reaction channels: MF-3/MT-1 to 891*MF-4/MF-5/MF-6 to 30 MeV, then as S_0 afterwards; and
- model based variance-covariance information, ENDF-6 formats MF-32, -33, -34, -40 and -31, -35 for the actinides.

Most of the above exist for α , γ , ^3He , triton, proton and neutron incident and would need to be manipulated and/or processed to be used in publications or applications. The applications are wide ranging but when fed into a modern simulation platform such as FISPACT-II [92, 93], MCNP [94], SERPENT [95], and TRIPOLI [96], those enhanced, complete data formats enable detailed and probing study of nuclear phenomena. This allows a more reliable and safe study of scenarios that are less well studied – particularly those beyond the legacy systems already commissioned. This is most valuable when no experimental information exists to pave the way.

The applications formats can be described as:

- pointwise or groupwise temperature-dependent cross section;
- background, dilution cross section;
- double differential cross section;
- total or partial channel cross section, macro-partial;
- coherent, incoherent, elastic, inelastic, bound cross section;
- cross section for production of radioactive nuclide;
- isomeric branching ratio;
- tabulated and/or legendre polynomial angular distribution;
- function based and/or tabulated particles and recoil emitted spectra;
- primary and secondary, prompt and delayed data;
- resonance parameter;
- probability distribution function;
- Bondarenko, probability table self-shielding factor;
- damage energy metrics, particles heating;
- $A < 4$ particles plus residual production matrix (yield-energy,angle); and
- covariance-related quantities for many of the above.

B. NJOY Processing

The nuclear data evaluations are physics representations of the data encoded in the unified, computer-readable format structure. They need to be converted into suitable data formats for applications, such as transport, activation-transmutation, criticality or shielding simulations using either pointwise or multi-group representations. The NJOY12 [42] or NJOY2016 [91] codes

have been designed and maintained over decades to handle the unified format and so feed the many nuclear codes that rely on nuclear data. These include various modules to produce different outputs for these applications, such as HEATR, LEAPR, THERMR, and GROUPE.

With the full residual emitted particle spectra from TALYS stored in the TENDL data files, NJOY may be used to extract this information, as shown in Fig. 39. When coupled with codes such as SPECTRA-PKA [97], this uniquely allows users to extract the full primary knock-on atom spectra for materials damage studies. An example for aluminum is given in Fig. 40.

The different NJOY modules can be sequenced to output nearly all the necessary information required for many modern codes used in R&D, but also the legacy ones deployed by the nuclear industry worldwide. Its most useful and unique formats are the thermal S(a,b) or free gas, heating and displacement energy, primary knock on atoms spectra, matrices of emitted particle and recoil, probability tables for the URR and ACE (A Compact ENDF) that serve several Monte Carlo simulation codes.

C. CALENDF Processing

The CALENDF [10] nuclear data processing system is used to convert the evaluation defining the cross-sections in ENDF-6 format (*i.e.*, the point-wise cross-sections and the resolved and/or unresolved resonance parameters) into formats useful for applications. Those formats used to describe the neutron cross-section fluctuations or resonances correspond to cross-section probability tables based on Gauss quadratures and effective cross-sections.

CALENDF accesses the data stored in MF-2 (resonance parameters) and MF-3 (point wise cross-sections) of the ENDF-6 data file provided as input, ignoring all other MFs. ‘Ladders’ of resonance parameters are generated into defined energy ‘zones in the unresolved range, which are then treated in the same way as the resolved range. The random ladders of resonances are generated with energies extracted from a table of 1185 values that are the eigenvalues of a random matrix (Dyson and Mehta) and with resonance widths chosen from a distribution laws with stratified and antithetic sampling. Additional resonances are added below and above the range of the energy zone to properly handle edge effects. Checks of the consistency of the evaluated MF-2 resonance parameters are performed and messages emitted when necessary.

Within the resonance range the cross-sections are calculated from the resonance parameters described in the ENDF file using different formalisms. All the different formalisms can be handled, but when judged necessary, a slightly modified multi-level Breit and Wigner formalism (Multi Niveau Breit and Wigner MNBW \neq MLBW) is applied by CALENDF in this energy range allowing the pointwise cross-sections to be reconstructed with psi-

chi Doppler broadening. There are no normalizations done except for the cases with LSSF=1. The moments of these cross-sections are computed, and the probability tables deduced from them. The table orders will mainly depend on the required accuracy, with a maximum of 11. The probability tables for all zones and ladders are then merged to get the final table in each energy group. The Gauss-quadrature mathematical principle gives those probability tables their sturdiness, allowing many utilitarian operations such as table condensation, isotope mixing, or interpolation to be performed. In the URR range CALENDF applies the “statistical hypothesis” based on the fact that the resonances can only be statistically described.

VIII. BENCHMARKING

A. ICSBEP

The neutron library can be tested by making use of the criticality safety benchmarks available in the International Handbook of Evaluated Criticality Safety Benchmark Experiments, a product of the International Criticality Safety Evaluation Project (ICSBEP) [100]. This was done for the recently released library versions ENDF/B-VIII.0 [4] and JEFF-3.3 [55], and is repeated here for TENDL-2017. All benchmark runs were performed using MCNP version 6.1.1 [94].

The number of benchmark cases used was 2528, which is why the results are not all listed individually here. Instead the average results for all these calculations are summarized in Tables XI–XII, for each main category of ICSBEP.

Based on a close inspection of the results for the individual benchmark cases, the following can be said.

- The average performance of the library is good. This is mainly due to the fact that the evaluations for the major isotopes were adopted from ENDF/B-VIII.0.
- There are many cases where the results are also strongly influenced by isotopes other than the majors, such as Fe isotopes, or Gd isotopes. In most of those cases, the results are good. For some elements, it can be observed that the TENDL-2017 evaluation influences the criticality safety results negatively. These elements are nickel, copper, lead, and thorium.
- When the evaluations for Ni isotopes are replaced by ENDF/B-VIII.0, the criticality results are lower, on average, by 1200 pcm. This average is based on the benchmarks PU-MET-FAST-014 (simple case), PU-MET-FAST-045 (detailed cases 1–7), and HEU-MET-FAST-003 (case 12).
- When the evaluations for Cu isotopes are replaced by ENDF/B-VIII.0, the criticality results are lower,

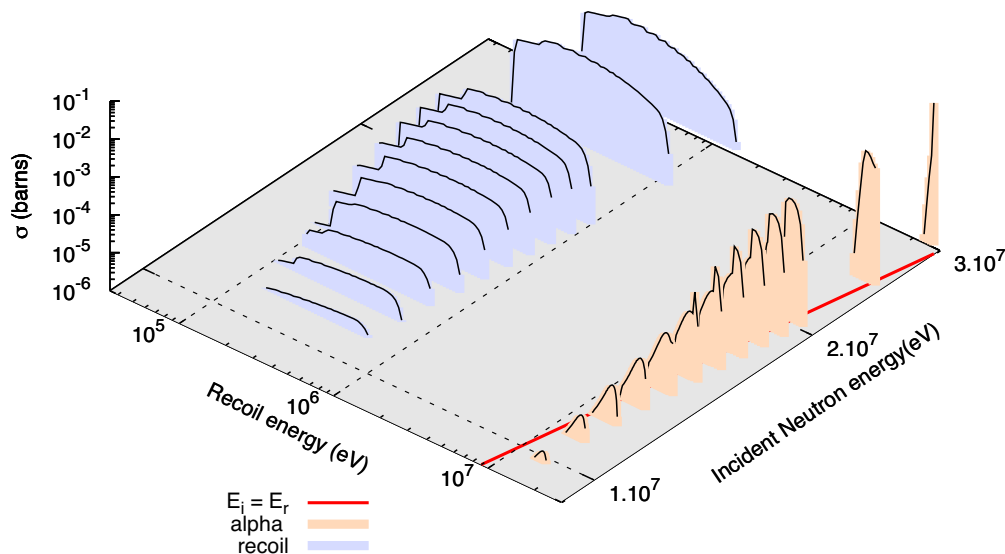


FIG. 39. (Color online) Q positive (7.3 MeV) (n, α) ^{184}W , residual ^{181}Hf (blue), emitted ^4He (beige) energy spectra [98], neutron incident energy in red, note the alpha energy superior to the neutron incident one, the spectra truncation above the 30 MeV upper energy. Figure taken from Ref. [92].

TABLE XI. The average value of $C/E - 1$ in pcm (100 pcm=0.1%) for TENDL-2017 per main ICSBEP category for compound (COMP) and metal (MET) systems. Also listed is the standard deviation of the $C/E - 1$ values per main ICSBEP category, except for the categories with only benchmark case. Shown in *italics* is the number of benchmarks in that category.

| | COMP | | | | MET | | | |
|------------------|--------------------------|------------------------|-----------------------|------------------------|--------------------------|----------------------|------------------------|-----------------------|
| | therm | inter | fast | mixed | therm | inter | fast | mixed |
| LEU | -116 ± 500 (462) | | | | -2476 ± 1594 (31) | | | |
| IEU | -562 ± 666 (33) | -412 ± 1452 (4) | -36 ± 28 (2) | | | | 58 ± 334 (28) | |
| HEU | 638 ± 727 (154) | 1865 ± 4104 (6) | -244 ± 212 (6) | -915 ± 478 (8) | 102 ± 703 (51) | 751 ± 413 (5) | -98 ± 483 (294) | -367 ± 702 (6) |
| MIX | -304 ± 1058 (100) | | 13 ± 255 (9) | | | | 282 ± 255 (33) | |
| PU | | 835 (1) | | 1961 ± 979 (34) | | 27 ± 1350 (5) | 352 ± 735 (100) | 102 ± 645 (6) |
| ^{233}U | 184 ± 147 (8) | | | | -3174 (1) | | -135 ± 167 (10) | |

on average, by 660 pcm. This average is based on the benchmarks HEU-MET-FAST-072, HEU-MET-FAST-073, and HEU-MET-INTER-006 (cases 1–4).

- When the evaluations for Pb isotopes are replaced by ENDF/B-VIII.0, the criticality results are lower, on average, by 630 pcm. This average is based on the benchmarks HET-MET-FAST-027, HET-MET-FAST-057 (cases 1–6), and HET-MET-FAST-064 (cases 1–3).

An attempt was also made to analyze the data in a dif-

ferent way, to obtain information per element. The tool DICE, which comes with the ICSBEP package, was used to find benchmarks that are sensitive to specific elements. The focus was on the elements from Na through Th, since the evaluations for elements H through F were adopted from ENDF/B-VIII.0. In first instance the minimum for the sensitivity was set low, which led to too many benchmarks per element. In this situation one can only analyze the average of those benchmarks, which does not reveal anything new. However when the minimum sensitivity was set higher, the number quickly reduced to zero for

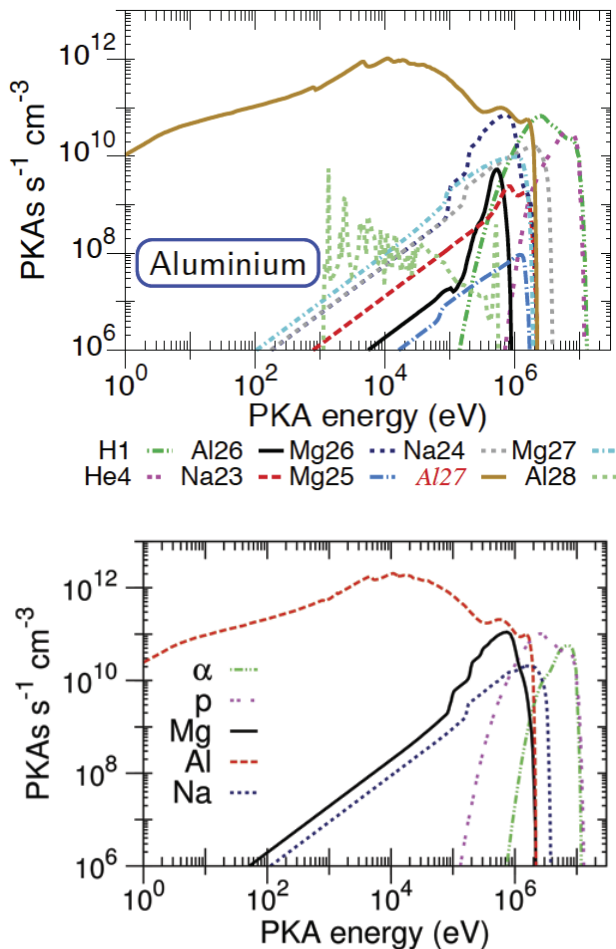


FIG. 40. (Color online) Isotopic and elemental residual Primary Knock on Atoms energy, n-induced on aluminum, extended during processing at low energy for non-elastic events [99]. Figure taken from Ref. [92].

TABLE XII. The average value of $C/E - 1$ in pcm (100 pcm=0.1%) for TENDL-2017 per main ICSBEP category for solution (SOL) and miscellaneous (MISC) systems. Shown in *italics* is the number of benchmarks in that category.

| | SOL | | MISC | |
|------------------|--------------------|---------------------|------------------|--------------------|
| | therm | inter | therm | fast |
| LEU | 125 ± 285 (67) | | | |
| IEU | 94 ± 505 (60) | | | |
| HEU | 14 ± 878 (402) | | | |
| MIX | -550 ± 360 (53) | | 56 ± 600 (60) | -402 ± 256 (11) |
| PU | -7 ± 540 (385) | | | |
| ²³³ U | 278 ± 719 (60) | -1813 ± 812 (33) | | |

many elements. It has proven difficult to find a useful setting for the minimum sensitivity, not least because this setting needs to be different per element: for a strong absorber such as B or Gd, the sensitivity is much higher than for an element with low cross section such as Al, even though Al may be present in high amounts in the experimental setup. More time is needed to retrieve element specific information from the benchmark results in this way.

Another way to summarize all criticality safety benchmark results is shown in Fig. 41. For this figure, a histogram was made of all the $C/E - 1$ results (expressed in units of a standard deviation) of benchmark cases with *e.g.*, a thermal spectrum. Subsequently a normal distribution was fitted to this histogram. If the nuclear data were perfect (and the benchmark evaluations were perfect), the distribution of $C/E - 1$ would be the normal distribution with average zero (0) and standard deviation one (1). The figure shows that for thermal spectrum cases, the performance of TENDL-2017 is close to that of JEFF-3.3 and ENDF/B-VIII.0. For the fast spectrum cases, the performance of TENDL-2017 is close to that of JEFF-3.3, and only marginally less than that of ENDF/B-VIII.0. For the intermediate and mixed spectrum cases there are not enough benchmark cases to draw firm conclusions, but the bias in k_{eff} calculations is roughly the same for TENDL-2017 as for the other libraries.

In sum, Fig. 41 can be regarded as a challenge for statistically consistent predictions from nuclear data; improvement in criticality estimation is represented by smaller deviations from the exact Gaussian distributions.

B. Shielding

A number of shielding benchmarks were used to test TENDL-2017. The benchmarks used were FNS [101, 102], Oktavian [101, 103], and the LLNL Pulsed Spheres [104], all of which start from a fusion neutron source. For the Oktavian benchmark, for each element the neutron leakage spectrum was measured for a single case of material thickness. For the LLNL Pulsed Sphere benchmark, the neutron time of flight was measured for, with most elements, two or three thicknesses of shielding material. For the FNS benchmark, several thicknesses were used, as well as five different angles.

The elements for which benchmark calculations were performed are Be (FNS, LLNL), Li (LLNL), C (FNS, LLNL), N (FNS, LLNL), O (FNS, LLNL), Mg (LLNL), Al (Oktavian, LLNL), Si (Oktavian), Ti (LLNL, Oktavian), Cr (Oktavian), Mn (Oktavian), Co (Oktavian), Cu (Oktavian), Zr (Oktavian), Mo (Oktavian), Fe (FNS, LLNL), W (Oktavian), Pb (FNS, LLNL, Oktavian). The materials for which benchmark calculations were performed are H₂O (LLNL), D₂O (LLNL), polyethylene (LLNL), teflon (LLNL), LiF (Oktavian), concrete (LLNL).

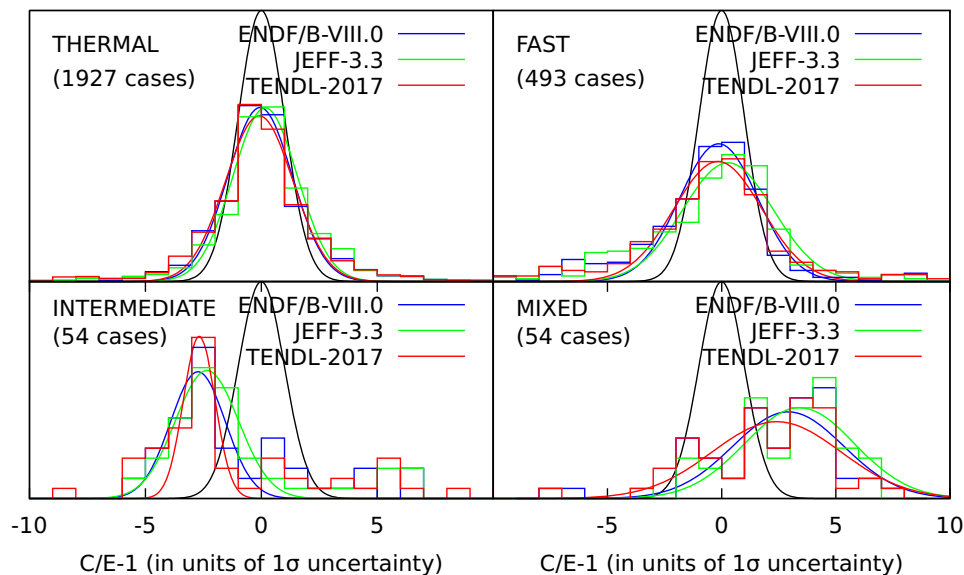


FIG. 41. (Color online) The distribution of C/E for criticality safety benchmarks, in units of the combined benchmark and statistical uncertainty. The normal distribution (in black) would be the perfect situation.

The results of all these calculations were compared with results based on ENDF/B-VIII.0 and JEFF-3.3. In almost all cases the differences were small. Noticeable differences occurred for only two elements, viz. Mg and Fe, as shown in Figs. 42 and 43.

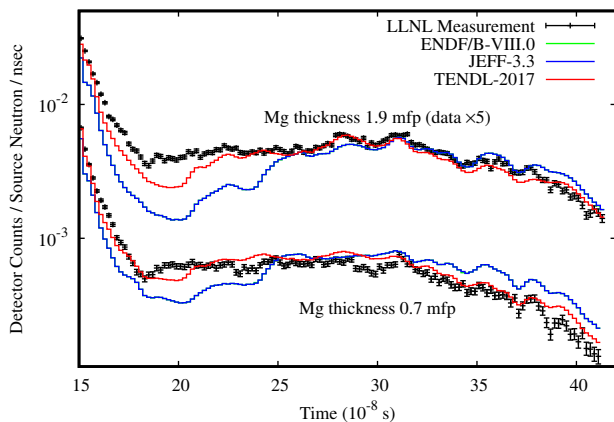


FIG. 42. (Color online) The results for the LLNL Pulsed Sphere benchmark for magnesium. The results for Mg thicknesses of 0.7 mean free path (mfp) and 1.9 mfp are shown. All results for 1.9 mfp are multiplied by 5, for visibility. The results based on ENDF/B-VIII.0 are hardly visible, because they are almost identical to the results based on JEFF-3.3.

The results for Mg shielding based on TENDL-2017 are closer to the benchmark data than the results based on either ENDF/B-VIII.0 or JEFF-3.3. For Fe shielding, the situation is the other way around. For all other materials used here in the shielding benchmark calculations, the differences between the results on the various data libraries are of less importance.

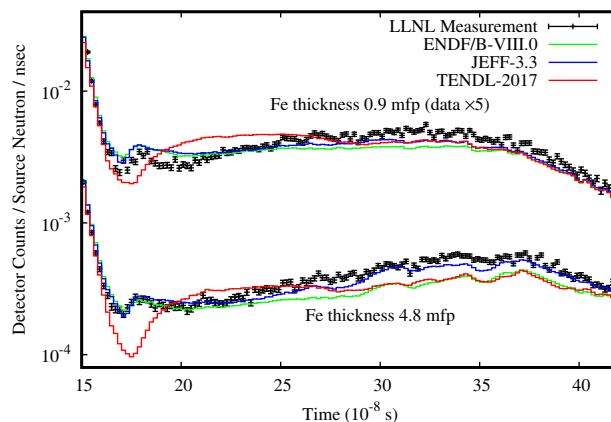


FIG. 43. (Color online) The results for the LLNL Pulsed Sphere benchmark for iron. The results for Fe thicknesses of 0.9 mean free path (mfp) and 4.8 mfp are shown. All results for 0.9 mfp are multiplied by 5, for visibility.

C. Delayed Neutron Data Testing

The TENDL-2017 data have also been tested against measurements of effective delayed neutron fraction β_{eff} in critical configurations. For β_{eff} only a handful of measurements have been reported in open literature with sufficiently detailed information. Here we use 21 measurements of β_{eff} and 10 measurements of Rossi- α , which is closely related to β_{eff} through the prompt neutron generation life time. These measurement data were also used for testing among others ENDF/B-VIII.0 [4] and JEFF-3.3 [55]. The results based on TENDL-2017 are given in Tables XIII and XIV. The results for TENDL-2017 are

TABLE XIII. The values for $C/E - 1$ for the β_{eff} calculations. The uncertainty quoted for $C/E - 1$ includes only the statistical uncertainty of the calculation. All the cases have a fast spectrum, except for TCA and IPEN/MB01.

| | Experiment | | TENDL |
|---------------|----------------------|--------|---------------|
| | β_{eff} | | 2017 |
| | (pcm) | | $C/E - 1$ (%) |
| TCA | 771 | (2.2%) | 0.4±0.8 |
| IPEN/MB01 | 742 | (0.9%) | 0.8±0.9 |
| Masurca/R2 | 721 | (1.5%) | 2.6±1.1 |
| Masurca/ZONA2 | 349 | (1.7%) | -2.6±1.5 |
| FCA/XIX-1 | 742 | (3.2%) | 2.3±1.2 |
| FCA/XIX-2 | 364 | (2.5%) | 0.3±1.6 |
| FCA/XIX-3 | 251 | (1.6%) | 0.0±2.0 |
| SNEAK/9C1 | 758 | (3.2%) | 0.5±1.2 |
| SNEAK/7A | 395 | (5.1%) | -6.8±1.6 |
| SNEAK/7B | 429 | (4.9%) | -0.7±1.4 |
| SNEAK/9C2 | 426 | (4.5%) | -8.2±1.5 |
| ZPR-9/34 | 667 | (2.2%) | 4.5±2.2 |
| ZPR-U9 | 725 | (2.3%) | -3.3±1.9 |
| ZPPR-21/B | 381 | (2.4%) | -7.6±2.3 |
| ZPR-6/10 | 222 | (2.3%) | 1.8±4.0 |
| Godiva | 659 | (1.5%) | -0.9±1.1 |
| Topsy | 665 | (2.0%) | 4.2±1.0 |
| Jezebel | 194 | (5.2%) | -5.7±1.6 |
| Popsy | 276 | (2.5%) | 4.7±1.7 |
| Skidoo | 290 | (3.4%) | 1.0±1.4 |
| Flattop | 360 | (2.5%) | 3.6±1.3 |

TABLE XIV. The values for $C/E - 1$ for the Rossi- α calculations. The uncertainty quoted for $C/E - 1$ includes only the statistical uncertainty of the calculation. All the cases have a thermal spectrum, except for Big Ten.

| | Experiment | | TENDL |
|---------------|----------------------|--------|---------------|
| | β_{eff} | | 2017 |
| | (pcm) | | $C/E - 1$ (%) |
| SHE/core8 | 6.53e-3 | (5.2%) | 2.4±1.0 |
| Sheba-II | 200.3e-6 | (1.8%) | -4.7±1.5 |
| Stacy/run-029 | 122.7e-6 | (3.3%) | -2.3±1.2 |
| Stacy/run-033 | 116.7e-6 | (3.3%) | 0.2±1.2 |
| Stacy/run-046 | 106.2e-6 | (3.5%) | -1.8±1.1 |
| Stacy/run-030 | 126.8e-6 | (2.3%) | -1.0±1.2 |
| Stacy/run-125 | 152.8e-6 | (1.7%) | -1.0±1.2 |
| Stacy/run-215 | 109.2e-6 | (1.6%) | 0.6±1.2 |
| Winco | 1109.3e-6 | (0.1%) | 0.6±1.0 |
| Big Ten | 117.0e-6 | (0.9%) | -0.3±1.5 |

similar to those for ENDF/B-VIII.0, which was expected because the evaluations for $^{233,235}\text{U}$ and ^{239}U in TENDL-2017 were adopted from ENDF/B-VIII.0.

D. Integral Activation Data

The study of radioactive properties of nuclear devices relies upon calculations of neutron-induced activation/-

transmutation reactions. These have resulted in a suite of experimental data for spectrum-averaged cross sections and other quantities, such as post-irradiation decay heat, gamma activity or isotopic inventory. In the development of modern activation nuclear data files, this data was assembled under the European Activation File (EAF) project [105] and comprehensively reviewed in work carried out for TENDL [106]. The resulting database was used to validate the TENDL-2017 neutron sub-library, including full re-analysis of the Japanese Fusion Neutron Source (FNS) decay heat measurements [107]. These are complemented by measurements from the Technische Universität Dresden (TUD), Forschungszentrum Karlsruhe (FZK), Frascati Neutron Generator (FNG), Jülich Nuclear Physics Group and National Physics Institute Rež.

1. JAEA FNS Decay Heat Data

Several experiments were performed by the Japan Atomic Energy Agency (JAEA) using the deuterium-tritium Fusion Neutron Source (FNS) [108, 109]. The decay heat was measured using the a Whole Energy Absorption Spectrometer (WEAS) method, taking into account both the β and γ emissions. Measurements were taken over a broad range, between a few seconds and up to thirteen months. To validate the TENDL-2017 data, full inventory simulations are performed using the FISPACT-II code [92, 93]. An example simulation is shown in Fig. 44. In this case, seven radioisotopes or isomers are responsible for the decay heat in the measured time period, and of these ^{52}V and ^{56}Mn are dominant at early and late cooling times, respectively. The reactions responsible for these are almost exclusively $^{52}\text{Cr}(n,p)$ and $^{55}\text{Mn}(n,\gamma)$, so the ratio of the total calculated decay heat (C) to the experimental decay heat (E) may be attributed to the primary reaction of the dominant radionuclide.

Comparing the results of all FNS cross section C/E ratios over the nuclide number of the target provides an overview of the results, as shown in Fig. 45. The results show several corrections due to efforts made to improve several cross sections for fusion applications [111].

2. Integro-differential Validation

The results of integral tests are not, by themselves, an indication of the quality of the library, and must be taken in context with the other available experimental data. For example, the $^{206}\text{Pb}(n,\alpha)$ cross section, which is responsible for the measured ^{203}Hg decay heat, shows a bias of a factor of 20 between the FNS measurement and TENDL prediction in Fig. 45. However, the differential data from EXFOR shows a much better agreement in this energy range, as seen in Fig. 46. This motivates a more rigorous method for testing, which must consider not only integral data, but all relevant differential and

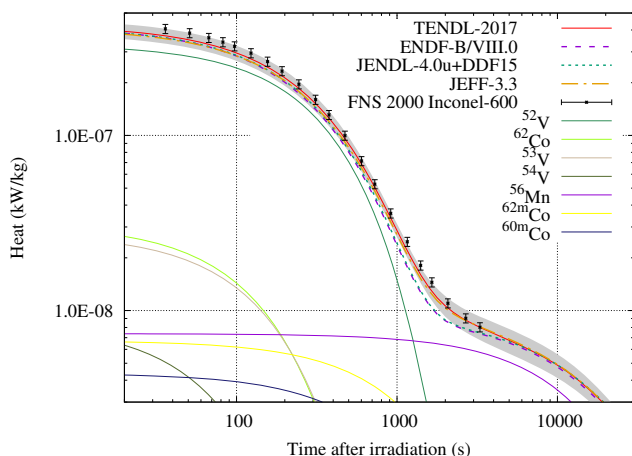


FIG. 44. (Color online) Total decay simulation for an FNS 5 minute irradiation of Inconel-600, with experimental results compared against calculated solutions using FISPACT-II with different nuclear data libraries. The grey band represents uncertainty from TENDL-2017 calculated using the full covariance data the FISPACT-II pathways-based uncertainty propagation algorithm [110]. Individual radionuclide contributions are shown for those that are dominant in the time-periods that were measured.

integral comparisons simultaneously. Statistics such as the well-known χ^2 are not shown, as they are dominated by a few reaction channels with significant disagreement. These are often also reaction channels with very limited experimental data and global statistics represent primarily these cases which are of less interest to the nuclear data community.

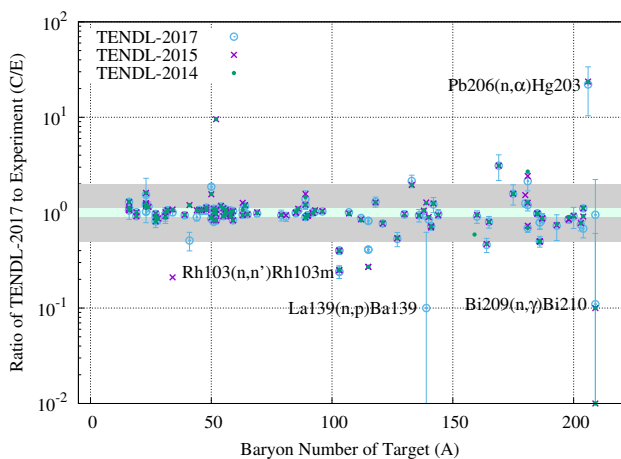


FIG. 45. (Color online) All FNS decay heat calculation (C) to experiment (E) ratios for simulations using TENDL-2014, -2015 and -2017. Uncertainty bars are from the experiments. The grey band represents a factor of 2, whilst the inner band represents a 10% range. Individual reactions with significant disagreement are labelled individually.

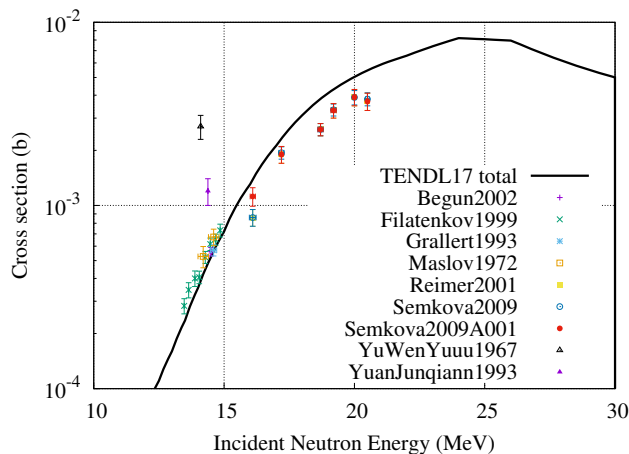


FIG. 46. (Color online) Differential cross section for $^{206}\text{Pb}(n,\alpha)$, against data from EXFOR.

The comparison of integral and differential data for each of the FNS decay heat cases, as well as a set of other fusion and accelerator-driven systems, was performed in another validation report from the UKAEA [112]. This study utilised a suite of incident neutron spectra ranging from 14 MeV deuteron-tritium sources to 150+ MeV deuteron-Li sources. The cross-comparison of both the integral and differential data provides the verification and validation of activation-transmutation cross sections that has been standard practice for years [105]. While the integral measurements have various uncertainties and systematic errors which require caution when interpreting, the global distribution of all calculation (C) to experiment (E) ratios provides a useful metric. This is shown in Fig. 47. While the distributions are quite similar, it should be noted that the EAF-2010 library was specifically tailored, with manual renormalisations performed, to match this data. Moreover, the log-mean C/E value,

$$\text{Log} \left(\overline{C/E} \right) = \frac{1}{n} \sum_{i=i}^n \text{Log} \left(\frac{C_i}{E_i} \right), \quad (26)$$

for TENDL-2017 is 1.046, while the EAF-2010 data gives 0.850. This indicates a systematic under-prediction that is intuitively due to the evaluation methodology for EAF: reaction cross sections are added when and where required, rather than automatically for all allowable reaction channels.

While there is undoubtedly more work left to improve activation nuclear data, the fact that this distribution has a relatively large variance should not necessarily be cause of concern, as the experimental uncertainties are often much larger than 20%, or likely include some significant systematic error (such as the $^{206}\text{Pb}(n,\alpha)$ FNS measurement).

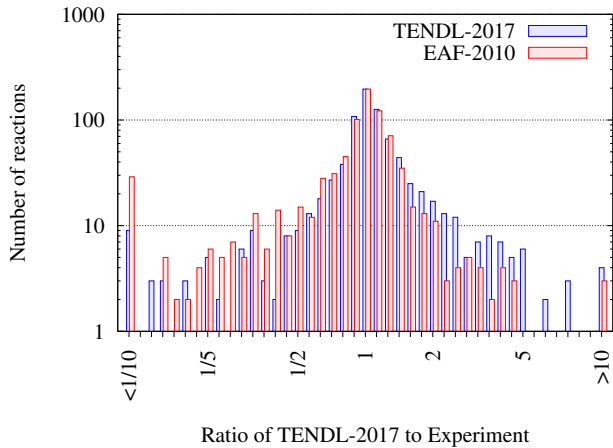


FIG. 47. (Color online) Distribution of C/E values for TENDL-2017 and EAF-2010 neutron-induced activation-transmutation cross sections, taken from [112].

IX. APPLICATIONS

The TENDL libraries (both nominal and random files) have been used over the past years in many applications. A short list is given below.

A. Use in Nuclear Software

Since its creation in 2008, TENDL has been used in many different applications, as shown in Fig. 2. In specific cases, TENDL has been directly implemented in code packages, with or without additional processing. Examples are provided below.

- FISPACT-II (for activation and transmutation, depletion burn-up, inventory and radiation damage). The complete TENDL library is now available with the FISPACT-II package [92, 93]. FISPACT-II is taking advantage of all the information included in the different reaction sections (MT) for all isotopes, as well as the covariance data. The group TENDL cross-section libraries for charged particles (from proton to alpha) and gamma are selected by default. For more details, see the above reference or Ref. [110].
- GEANT4 (toolkit for the simulation of the passage of particles through matter). GEANT4 now contains a specific database for the TENDL-2014 incident proton reactions, including 2400 isotopes up to 200 MeV. See Ref. [113] for additional details.
- MARS (Monte Carlo code for hadronic and electromagnetic cascades, muon, heavy-ion and low-energy neutron). The charged-particles sublibraries for TENDL were included in the MARS15 code package to improve the prediction of secondary

particles (neutral and charged ones), generated in proton-nucleus interactions below a few tens of MeV [114].

- CASMO (deterministic fuel assembly burnup program). The CASMO5 neutron data library is based on ENDF/B-VII.1 data files, supplemented with TENDL-2012 data [115].

This list is not exhaustive, and is based on open literature which explicitly mentions the TENDL library. As TENDL is also provided in ACE formatted files, TENDL can also be used with the MCNP or SERPENT codes: users can easily change the origin of the cross section libraries.

B. Use in Nuclear Libraries

The TENDL libraries have also been used in other nuclear data libraries. A list is provided below.

- JEFF-3.2. JEFF is the OECD Nuclear Data Bank nuclear data library. The library version 3.2 is using about 300 TENDL-2012 files out of 473 neutron evaluations.
- JEFF-3.3. The version 3.3 is the latest release of the JEFF library. All charged-particles sublibraries are coming from TENDL-2017 (alphas, deuterons, helium-3, protons and tritons), as well as the gamma sublibrary and the activation files (in EAF format). Concerning the neutron sublibrary, 312 evaluations come from TENDL-2015, out of 562 files.
- ENDF/B-VIII.0. The US library, released in 2018, includes 36 TENDL-2015 neutron evaluated files. See Ref. [4] for details.
- FENDL-3.1. FENDL is a nuclear data library for fusion application. It uses a large number of TENDL neutron files, mostly from TENDL-2010, with some isotopes updated to TENDL-2014 (in the FENDL latest version).
- IRDFF-1.05. IRDFF is an international library for reactor dosimetry and fusion application and it is making use of TENDL data by extrapolating IRDFF-2002 evaluations from 20 to 60 MeV [116].

C. Total Monte Carlo

The TMC approach was developed in 2008 and has been applied tens of times in various cases. A full list of publications is not provided here, but rather groups of examples, based on their area of application. The main advantages of the TMC method compared to other uncertainty propagation methods are (1) its simplicity and

(2) its capability to be applied in complex simulations. Of course, this comes at a computational price. Over the years, the name “TMC” was also used when producing random nuclear data libraries based on existing cross section covariance files. Even if the original TMC developments were based on random model parameters, the production of random cross sections based on existing cross section covariance files follows the same logic, even if an additional degree of approximation is implied by using a covariance file (often used in combination with the assumption of Normal distribution).

Different comparisons of uncertainty propagation methods can also be found in the literature (*e.g.* with GLLS [117], Polynomial Chaos [118], NUSS [119]) showing that under specific assumptions, results can be considered equivalent from a statistics point of view. To facilitate its application, the TENDL libraries come with a variety of random files, based on the variations of model parameters. Below are presented a few examples for specific categories.

- Assembly. A fuel assembly is a relatively simple system to study, with or without depletion calculation. For a nominal calculation (without using random nuclear data files), one has to be able to perform it in a reasonable amount of time, using either a deterministic or Monte Carlo transport code. Nowadays, this type of calculation can (almost) be performed on any computer for a two-dimensional geometry, and on a small computer cluster for a three-dimensional geometry. Additionally, no specific knowledge on a reactor core is required (such as amount of assemblies, specific histories...). For these reasons, such systems has been studied in some details. See Refs. [120–123] for specific examples.
- Criticality-safety benchmarks. As for the assembly system, some criticality-safety and shielding benchmarks can be calculated relatively easily on modern computers, therefore the application of the TMC method is also feasible. Examples can be found in Refs. [117, 124–126].
- TMC applied with fission yields. In the majority of cases, the propagation of the fission yield uncertainties is difficult to perform based on existing covariance matrices solely. The main reason is that the covariance files included in the nuclear data libraries do not contain correlation terms. A convenient solution is to use the GEF code [45] and randomly vary its parameters to produce random fission yields, available on the TENDL webpage. One can notice that other solutions exist, as presented in Refs. [127, 128]. For the application of random fission yields from the GEF code, see Refs. [81, 129, 130].
- Fusion system. Similar to the above example, the TMC method was applied to a specific MCNP model of the JET fusion machine [131] and to fusion shielding benchmarks [132].
- Full core without burn-up. This type of application presents an additional complexity due to the calculation time requirement. In this case, a convenient solution is to apply the fast-TMC method for Monte Carlo transport code [123, 133], or to use deterministic codes: see Ref. [134] for a PWR, Ref. [135] for a Sodium Fast Reactor and Refs. [136, 137] for a Lead Fast Reactor.
- Full core with burn-up. This type of simulation is obviously computational intensive and Monte Carlo transport calculation cannot be applied with uncertainty propagation for the time being. The solution lies in the use of deterministic code, with flexibility on nuclear data (ability to change them), and the availability of input models (realistic cycles, assembly histories, shutdown periods, *etc.*). Examples on such calculations with TMC-like uncertainty propagation can be found in Refs. [138, 139].
- Full core non linearity. Based on the full core calculations (with burnup), many core parameters can be calculated. Some of these parameters might be very sensitive to specific cross sections. Such an example is presented in Ref. [140] where the impact of the $^{238}\text{U}(n,\text{inl})$ cross section on the peak pin power (ppp) analysed. It was shown that a strong nonlinear behavior due to the variation of this cross section exist, indicating that smaller uncertainties for the $^{238}\text{U}(n,\text{inl})$ cross section are required to make this effect disappear. Note that the use of adjoint methods can also be investigated.
- Transient. Following the above example of steady-state calculations, the additional step towards the simulation complexity is to study the effect of nuclear data on transient systems, such as reactivity-initiated accident [141, 142].
- Spent fuel. Another type of complexity can be achieved by staying with steady-state calculations, but extending the calculation scheme towards the characteristics of spent nuclear fuels (for transport and storage). Important quantities such as decay heat and source terms can be obtained with uncertainties due to nuclear data, see for instance Refs. [143, 144]. Whereas the uncertainty propagation is performed in [143] up to the decay heat calculations of single assemblies, there is the possibility to associate such calculations with those of criticality of canister for long-term storage [144]. Such methods, combining both full-core deterministic and criticality-safety Monte Carlo approach will nevertheless require relatively important calculation power.
- dpa. The calculation of dpa (displacement per atom) and related quantities are important for the

determination of the damage of material. Dpa can also be calculated with uncertainties due to nuclear data using the TMC method, as presented in Refs. [145, 146].

D. Other Applications

The completeness of TENDL makes it usable in many applications, also outside traditional fission energy applications. The pie chart of Fig. 2 already gives an indication about this. A non-exhaustive list is

- Medical isotope production. Especially the proton and deuteron TENDL files, and to a lesser extent the photonuclear files, are used regularly for the estimate of *e.g.*, (p,n) or (p,2n) production cross sections for isotope yield estimates.
- Fusion. As discussed in this paper, the completeness in terms of activation cross sections, including isomers, makes TENDL an obvious library for activation studies of fusion reactor designs. Also the deuteron data libraries are used for IFMIF studies.
- Astrophysics. TENDL has a rather extensive nuclide range and can be used to predict reaction rates for *e.g.*, r-processes. Other applications are the study of solar flares and cosmic rays.

X. FUTURE

The future of TENDL is not as statistically secure as other file projects, where several tens of contributors deliver their isotopic data files in one place. Making the entire TENDL system open source, and thus for everyone to use, and as easy to use as *e.g.*, the TALYS code itself, is a huge challenge but necessary for survival of this concept. There are several particular issues which require special attention.

A. Systematic Evaluation of Experimental Reaction Data

The systematic approach behind TENDL takes away many deficiencies and restrictions of the so-called 'manual' data evaluation which forms the basis of the other world libraries. Nevertheless, expert knowledge of experimental data is still one of the key ingredients of the procedure. Much of this experimental knowledge, especially about older measurements is lost because opinions of experts have often not been documented or have ended up in data libraries in a way that is not recognizable, and thus not reproducible. In the community of technological analyses the adopted approach is often "That nuclear data library performs good, although we don't know exactly why anymore, and we are not going to change it". Sometimes, there exists documented quality assessment

of different experimental data sets, but then the opinion of evaluators is expressed in textual form. That is better than nothing, but a truly systematic approach would be if an evaluator would 'score' experimental nuclear data sets in an internationally agreed manner. This does not exist yet, although some global approaches have been applied [6, 111] which at least rule out the most severe outliers in EXFOR. We call for a more in-depth and systematic approach by experimental nuclear physicists who give their opinion on EXFOR subentries, realizing that this is subjective. A format for such experimental nuclear data evaluation database should be agreed upon.

B. Solving Deficiencies in Uncertainty Quantification

The approach that combines Bayesian inference and Monte Carlo is basically set, and from a statistical point of view there is no reason to doubt the approach. However, two main deficiencies enter the formulation of the χ^2 estimator which basically prevents a flawless uncertainty approach: (a) the correct experimental covariance matrix, which in addition to the aforementioned quality scoring which rules out outliers, also should address the issue of assigning correlations between data points and data sets, and (b) a robust method for handling model defects to enable evaluated curves to perfectly describe experimental data. Both aspects should lead to an effective χ^2 which can be used as a proper goodness-of-fit estimator.

C. Systematic Integral Data Evaluation

What holds for the EXFOR database also holds for integral experiments. In principle, only with a reliable covariance matrix for (perhaps all) integral benchmarks a sound validation procedure for nuclear data libraries can be used. Also here, various experts know which benchmarks are more important and more reliable than others but again this is not yet represented in a numerical table. That such a table is subjective per expert is less relevant. A WPEC subgroup is currently addressing the reliability of ICSBEP benchmarks, in particular the quoted uncertainties. For integral testing outside criticality the situation is perhaps less complicated. Here we would at least call for a complete collection of available shielding, decay heat, activation, *etc.* benchmarks which can directly be tested with TENDL, if possibly *during* and not after evaluation.

D. Upgrade to Microscopic Nuclear Models used in TALYS

One of the core assets behind the TENDL database are what we call 'best' TALYS input files per target nuclide. This means that all nuclear model parameters for TALYS have been adjusted so that an overall optimal

description of all reaction channels is obtained. So far, for all TENDL releases this is done for phenomenological models for the structure of the nucleus, such as Fermi-gas based level density models, Hill-Wheeler forms for the fission barrier and Lorentzian forms for the photon strength functions. The reason for using this is not the physics, which is actually expected to be better for several of the microscopic models, but rather the experience in adjusting the parameters for these models. However, in TALYS for all microscopic models sets of adjustable parameters are now available. Hence, as basis we can use tabulated nuclear structure ingredients coming from *e.g.*, Hartree-Fock-Bogolyubov calculations and we are able to multiply this with smooth functional parameterized forms to deviate from the original tables in order to fit the reaction data better. We feel this will increase the predictive power of TALYS, and thus TENDL, for nuclides, reaction channels and energy ranges where no experimental data is available. It should however be realized that this work is tedious since proper nuclear data evaluation is hard to automate, and new 'best' files need to be made with span the whole nuclide range.

E. Cleaning up the Software

Less is more. In the past decade, features have been added to T6 which makes it more difficult to maintain. Different codes like TALYS and TARES may be using different fundamental databases and this has not yet been streamlined completely. For some fundamental data, like the upper energy limit of the resolved and unresolved

resonance range, or values of thermal cross sections also no unified picture has been accomplished yet. Other databases may be hidden in the system which could accidentally overrule settings that we thought we were using. This is a result of adding more and more options and not sufficiently cleaning obsolete options. (Though again here, looking at other software in nuclear data, everything is relative). This is one of the reasons why TALYS-2.0 will be released at the end of 2019, which will contain the major T6 codes in one software package. The resonance parameters from TARES will be read in as a database, which could be produced on *e.g.*, a yearly basis, and no longer be produced on the fly. After that, international testing and use could lead to improved versions of TENDL and other libraries.

ACKNOWLEDGEMENTS

The authors are grateful to Arjan Plompen and Enrique Gonzalez for the coordination of the EU project CHANDA which funded TALYS and TENDL development, Ulrich Fischer for guiding the work on activation data within the EuroFusion project on nuclear data, Stephane Hilaire and Stephane Goriely for TALYS development, Stanislav Simakov for his useful feedback on the use of random TENDL files for uncertainty quantification of damage calculations, Chikara Konno and Oscar Cabellos for all their feedback on the format and processing aspects of TENDL, Jura Kopecky for his efforts on validating TENDL with differential data, Henrik Sjöstrand and Petter Helgesson for testing and applying our evaluation system on JEFF evaluations and Total Monte Carlo.

-
- [1] N. Otuka, E. Dupont, V. Semkova, *et al.*, "Towards a more complete and accurate experimental nuclear reaction data library (EXFOR)," *NUCL. DATA SHEETS* **120**, 272 (2014).
 - [2] C. Mattoon, B. Beck, N. Patel, N. Summers, G. Hedstrom, and D. Brown, "Generalized nuclear data: A new structure (with supporting infrastructure) for handling nuclear data," *NUCL. DATA SHEETS* **113**, 3145 (2012).
 - [3] A. Koning, M. Duijvestijn, and S. Hilaire, "TALYS-1.0," in *Proc. International Conference on Nuclear Data for Science and Technology*, 211 (2008). April 22-27, 2007, Nice, France, editors O.Bersillon, F.Gunsing, E.Bauge, R.Jacqmin, and S.Leray, EDP Sciences.
 - [4] D. Brown, M. Chadwick, R. Capote, *et al.*, "ENDF/B-VIII.0: The 8th major release of the nuclear reaction data library with CIELO-project cross sections, new standards and thermal scattering data," *NUCL. DATA SHEETS* **148**, 1 (2018).
 - [5] A. Koning and D. Rochman, "Towards sustainable nuclear energy: Putting nuclear physics to work," *ANNALS NUCL. EN.* **35**, 2024 (2008).
 - [6] A. Koning, "Statistical verification and validation of the EXFOR database: (n,g), (n,n'), (n,2n), (n,p), (n,a) and other neutron-induced reaction cross-sections," tech. rep., NEA (2017). OECD/NEA Data Bank report NEA/DB/DOC(2017)1.
 - [7] Y. Xu, S. Goriely, A. Jorissen, G. Chen, and M. Arnould, "Databases and tools for nuclear astrophysics applications BRUSsels Nuclear LIBrary (BRUSLIB), Nuclear Astrophysics Compilation of REactions II (NACRE II) and Nuclear NETwork GENerator (NETGEN)," *ASTRON. ASTROPHYS.* **A106**, 549 (2013).
 - [8] A. Koning and D. Rochman, "Modern nuclear data evaluation with the TALYS code system," *NUCL. DATA SHEETS* **113**, 2841 (2012).
 - [9] N. Larson, *Updated Users' Guide for SAMMY: Multi-level R-Matrix Fits to Neutron Data Using Bayes' Equations*. Oak Ridge National Laboratory (2008). Report ORNL/TM-9179/R8 ENDF-364/R2.
 - [10] J.-Ch. Sublet, P. Ribon, and M. Coste-Delcaux, *CALENDF-2010: User Manual* (2011). Report CEA-R-6277.
 - [11] D. Cullen, "PREPRO 2017 - ENDF-6 pre-processing codes," tech. rep. (2017). IAEA-NDS-39 (Rev.14), IAEA (2010).

- [12] S. Mughabghab, *Atlas of Neutron Resonances*. The Netherlands: Elsevier, 6 ed. (2006).
- [13] M. Moxon, T. Ware, and C. Dean, *REFIT-2009 A Least-Square Fitting Program for Resonance Analysis of Neutron Transmission, Capture, Fission and Scattering Data, Users' Guide for REFIT-2009-10* (2010). Report UKNSF(2010)P243.
- [14] D. Rochman, S. Goriely, A. Koning, and H. Ferroukhi, "Radiative neutron capture: Hauser Feshbach vs. statistical resonances," *PHYS. LETT. B* **764**, 109 (2017).
- [15] D. Rochman, A. Koning, J. Kopecky, J.-Ch. Sublet, P. Ribon, and M. Moxon, "From average parameters to statistical resolved resonances," *ANNALS NUCL. EN.* **51**, 60 (2013).
- [16] D. Rochman and A. Koning, "Pb and Bi neutron data libraries with full covariance evaluation and improved integral tests," *NUCL. INST. METH. PHYS. RES. A* **589**, 85 (2008).
- [17] H. Feshbach, D. C. Peaslee, and V. F. Weisskopf, "On the scattering and absorption of particles by atomic nuclei," *PHYS. REV.* **71**, 145 (1947).
- [18] R. Forrest, *SAFEPAQ-II: User Manual*. UKAEA (2007). UKAEA FUS 454, issue 7, Euratom CCFE Fusion Association Culham Science Center, UK.
- [19] J. Kopecky, M. Delfini, H. van der Kamp, and D. Nierop, *Revisions and Extensions of Neutron Capture Cross Sections in the European Activation File EAF-3* (1992). Report ECN-C-95-075, ECN, Petten, The Netherlands.
- [20] J.-Ch. Sublet, R. Blomquist, S. Goluoglu, and R. McFarlane, *Unresolved Resonance Range Cross Section, Probability Tables and Self Shielding Factors*. CEA (2009). Report CEA-R-6227, July 2009.
- [21] A. Koning and J. Delaroche, "Local and global nucleon optical models from 1 keV to 200 MeV," *NUCL. PHYS. A* **713**, 231 (2003).
- [22] P. Ribon, "The resonance self-shielding calculation with regularized random ladders," *ANNALS NUCL. EN.* **13**, 209 (1986).
- [23] G. Zerovnik, A. Trkov, R. Capote, and D. Rochman, "Influence of resonance parameters' correlations on the resonance integral uncertainty; ^{55}Mn case," *NUCL. INST. METH. PHYS. RES. A* **632**, 137 (2011).
- [24] J. Raynal, "Notes on ECIS94," tech. rep., CEA Saclay Report (1994). CEA-N-2772.
- [25] E. S. Soukhovitskii, S. Chiba, J.-Y. Lee, O. Iwamoto, and T. Fukahori, "Global coupled-channel optical potential for nucleon-actinide interaction from 1 keV to 200 MeV," *J. PHYS. G* **30**, 905 (2004).
- [26] S. Watanabe, "High energy scattering of deuterons by complex nuclei," *NUCL. PHYS.* **8**, 484 (1958).
- [27] D. Madland, "Recent results in the development of a global medium-energy nucleon-nucleus optical model potential," in *Proc. Specialists' Meeting on preequilibrium nuclear reactions* (1988). Semmering, Austria, February 10-12, 103.
- [28] V. Avrigeanu, M. Avrigeanu, and C. Manaiescu, "Further explorations of the alpha-particle optical model potential at low energies for the mass range $A=45-209$," *PHYS. REV.* **C90**, 044612 (2014).
- [29] A. Koning, S. Hilaire, and S. Goriely, "Global and local level density models," *NUCL. PHYS.* **A810**, 13 (2008).
- [30] J. Kopecky and M. Uhl, "Test of gamma-ray strength functions in nuclear reaction model calculations," *PHYS. REV.* **C41**, 1941 (1990).
- [31] R. Capote, M. Herman, P. Obložinsky, *et al.*, "RIPL - reference input parameter library for calculation of nuclear reactions and nuclear data evaluation," *NUCL. DATA SHEETS* **110**, 3107 (2009).
- [32] D. Filipescu, "Photoneutron cross sections for samarium isotopes: Toward a unified understanding of (γ, n) and (n, γ) reactions in the rare earth region," *PHYS. REV. C* **90**, 064616 (2014).
- [33] S. Hilaire, C. Lagrange, and A. Koning, "Comparisons between various width fluctuation correction factors for compound nucleus reactions," *ANN. PHYS.* **306**, 209 (2003).
- [34] A. Koning and M. Duijvestijn, "A global pre-equilibrium model from 7 to 200 MeV based on the optical model potential," *NUCL. PHYS.* **A744**, 15 (2004).
- [35] S. S. Qian, C. A. Stow, and M. E. Borsuk, "On Monte Carlo methods for Bayesian inference," *ECOL. MODEL.* **159**, 269 (2003).
- [36] A.J. Koning, "Bayesian Monte Carlo method for nuclear data evaluation," *EUR. PHYS. J. A* **51**, 184 (2015).
- [37] P. Helgesson, H. Sjöstrand, A. Koning, J. Rydén, D. Rochman, E. Alhassan, and S. Pomp, "Combining Total Monte Carlo and Unified Monte Carlo: Bayesian nuclear data uncertainty quantification from auto-generated experimental covariances," *PROG. NUCL. ENERGY* **96**, 76 (2017).
- [38] D. Smith, "A Unified Monte Carlo approach to fast neutron cross section data evaluation," *PROC. 8TH INT. TOP. MEET. ON NUCL. APPL. UTIL. ACCEL. POCATELLO, ID, JULY 29-AUG 2, 2007*, 736 (2007).
- [39] R. Capote, D. L. Smith, A. Trkov, and M. Meghizifene, "A New Formulation of the Unified Monte Carlo Approach (UMC-B) and Cross-Section Evaluation for the Dosimetry Reaction $^{55}\text{Mn}(n, \gamma)^{56}\text{Mn}$," *J. ASTM INT.* **9**, 104115 (2012).
- [40] E. Bauge and P. Dossantos-Uzarralde, "Evaluation of the Covariance Matrix of ^{239}Pu Neutronic Cross Sections in the Continuum Using the Backward-forward Monte-Carlo Method," *J. KOR. PHYS. SOC.* **59**, 1218 (2011).
- [41] G. Schnabel and H. Leeb, "Differential cross sections and the impact of model defects in nuclear data evaluation," *EPJ WEB CONF.* **111**, 09001 (2016).
- [42] R. MacFarlane and A. Kahler, "Methods for Processing ENDF/B-VII with NJOY," *NUCL. DATA SHEETS* **111**, 2739 (2010).
- [43] D. Rochman, O. Leray, G. Perret, A. Vasiliev, H. Ferroukhi, and A. Koning, "Re-evaluation of the thermal neutron capture cross section of ^{147}Nd ," *ANNALS NUCL. ENERGY* **94**, 612 (2016).
- [44] A. Wahl, "Systematics of fission-product yields," (2002). LA-13928, Los Alamos National Laboratory.
- [45] K.-H. Schmidt, B. Jurado, C. Amouroux, and C. Schmitt, "General Description of Fission Observables: GEF Model Code," *NUCL. DATA SHEETS* **131**, 107 (2016).
- [46] D. Madland and J. Nix, "New calculation of prompt fission neutron spectra and average prompt neutron multiplicities," *NUCL. SCI. ENG.* **81**, 213 (1982).
- [47] D. Rochman, E. Bauge, A. Vasiliev, H. Ferroukhi, and G. Perret, "Nuclear data correlation between different isotopes via integral information," *EPJ NUCL. SCI. TECHNOL.* **4**, 7 (2018).

- [48] A. Trkov, M. Herman, and D. Brown, "ENDF-6 formats manual: Data formats and procedures for the evaluated nuclear data file ENDF/B-VI and ENDF/B-VII," tech. rep., Brookhaven National Laboratory (2011). BNL-90365-2009 Rev. 2.
- [49] P. Talou, "Prompt fission neutrons calculations in the Madland-Nix model," (2007). LA-UR-07-8168, Los Alamos National Laboratory.
- [50] C. Dunford, "ENDF utility codes release 6.10," tech. rep. (1995). IAEA report, IAEA-NDS-29.
- [51] A. Kahler and R.E. MacFarlane, "Methods for processing ENDF/B-VII with NJOY," NUCL. DATA SHEETS **111**, 2739 (2010).
- [52] B. Beck and C. Mattoon, "FUDGE a toolkit for nuclear data management and processing," tech. rep. (2014). LLNL-PROC-64847 (2014).
- [53] A. Koning and D. Rochman, "Modern Nuclear Data Evaluation with the TALYS Code System," NUCL. DATA SHEETS **113**, 2841 (2012).
- [54] Z. Ge, H. Wu, G. Chen, and R. Xu, "CENDL project, the chinese evaluated nuclear data library," EPJ WEB CONF. **146**, 02002 (2017).
- [55] O. Cabellos, "The JEFF-3.3 nuclear data library," TO BE PUBLISHED (2018).
- [56] K. Shibata, O. Iwamoto, T. Nakagawa, *et al.*, "JENDL-4.0: A new library for nuclear science and engineering," J. NUCL. SCI. TECHNOL. **48**, 1 (2011).
- [57] E. Zsolnay, R. Capote, H. Nolthenius, and A. Trkov, "Summary description of the new international reactor dosimetry and fusion file (irdff release 1.0)," tech. rep., IAEA (2012). INDC(NDS)-0616.
- [58] J.-Ch. Sublet, L. W. Packer, J. Kopecky, R. A. Forrest, A. J. Koning, and D. A. Rochman, "Activation file: EAF-2010 neutron-induced cross section library," tech. rep., UKAEA (2010). EASY Documentation Series CCFE-R (10) 05.
- [59] N. Iwamoto, K. Kosako, and T. Murata, "Photonuclear data file," JAEA-CONF **2016-004**, 53 (2016).
- [60] "Handbook of photonuclear data for applications: Cross sections and spectra," tech. rep., IAEA (2000). IAEA-TECDOC-1178.
- [61] Y. Watanabe, "Status of JENDL high energy file," J. KOR. PHYS. SOC. **59(2)**, 1040 (2011).
- [62] "IBANDL: the Ion Beam Analysis Nuclear Data Library, <https://www-nds.iaea.org/exfor/ibandl.html>," (2015).
- [63] "Charged particle cross section database for medical isotope production," tech. rep., IAEA (2001). IAEA-TECDOC-1211.
- [64] M. Fleming, J. Eastwood, T. Stainer, J.-C. David, and D. Mancusi, "HEIR: A High-Energy Intra-Nuclear Cascade Liège-based residual nuclear data library for simulation with FISPACT-II," NUCL. INST. METH. PHYS. RES. A (2018).
- [65] C. Kalbach, "Phenomenological model for light-projectile breakup," PHYS. REV. C **C95**, 014606 (2017).
- [66] C. Kalbach, "Preequilibrium reactions with complex particle channels," PHYS. REV. C **C71**, 034606 (2005).
- [67] S. Simakov and Q. van den Berg, "Update of the alpha-n yields for reactor fuel materials for the interest of nuclear safeguards," NUCL. DATA SHEETS **139**, 190 (2017).
- [68] T. Murata, "Evaluation of the (alpha, xn) reaction data for JENDL/AN-2005," JAEA-RESEARCH **2006-052** (2006).
- [69] J. Luo, R. Liu, L. Jiang, and Z. Liu, "Cross sections for fast-neutron interaction with erbium isotopes," J. RADIOANAL. NUCL. CHEM. **289**, 455 (2011).
- [70] N. Dzysiuk, A. Kadenko, I. Kadenko, and G. Primenko, "Measurement and systematic study of (n,x) cross sections for Dysprosium (Dy), Erbium (Er), and Ytterbium (Yb) isotopes at 14.7 MeV neutron energy," PHYS. REV. C **86**, 034609 (2012).
- [71] S. Amemiya, K. Ishibashi, and T. Katoh, "Neutron activation cross section of Molybdenum isotopes at 14.8 MeV," J. NUCL. SCI. TECHNOL. **19**, 781 (1982).
- [72] P. Cuzzocrea, E. Perillo, and S. Notarrigo, "Activation cross sections of Mo isotopes for 14.1 MeV neutrons," NUCL. PHYS. A **103**, 616 (1967).
- [73] W. M. Haynes, ed., *Handbook of Chemistry and Physics*. CRC Press, edition 96 ed. (2015).
- [74] M. Fleming, J.-Ch. Sublet, J. Kopecky, D. Rochman, and A. Koning, "Probing experimental and systematic trends of the neutron-induced TENDL-2014 nuclear data library," Tech. Rep. UKAEA-R(15)30, UKAEA (2015). <http://fisfact.ukaea.uk>.
- [75] Z. Bao, H. Beer, F. Käppeler, F. Voss, K. Wisshak, and T. Rauscher, "Neutron Cross Sections for Nucleosynthesis Studies," AT. DATA NUCL. DATA TABLES **76**, 70 (2000).
- [76] I. Dillmann, M. Heil, F. Käppeler, and T. Rauscher, "KADoNiS v0.3 - The third update of the Karlsruhe Astrophysical Database of Nucleosynthesis in Stars," in *Proc. Workshop EFNUDAT Fast Neutrons - scientific workshop on neutron measurements, theory and applications*, (Geel, Belgium) (2009).
- [77] T. Rauscher and F.-K. Thielemann, "Astrophysical reaction rates from statistical model calculations," AT. DATA NUCL. DATA TABLES **75**, 1 (2000).
- [78] G. Nobre, M. Herman, S. Hoblit, A. Palumbo, R. Capote, and A. Trkov, "Fitting Prompt Fission Neutron Spectra Using Kalman Filter Integrated with Empire Code," NUCL. DATA SHEETS **118**, 224 (2014).
- [79] S. Pelloni and D. Rochman, "Cross-section adjustment in the fast energy range on the basis of an Asymptotic Progressing nuclear data Incremental Adjustment (APIA) methodology," ANNALS NUCL. EN. **115**, 323 (2018).
- [80] P. Helgesson, H. Sjostrand, A. Koning, J. Ryden, D. Rochman, E. Alhassan, and S. Pomp, "Combining Total Monte Carlo and Unified Monte Carlo: Bayesian nuclear data uncertainty quantification from auto-generated experimental covariances," PROG. NUCL. ENERGY **96**, 76 (2017).
- [81] D. Rochman, O. Leray, A. Vasiliev, H. Ferroukhi, A. Koning, M. Fleming, and J.-Ch. Sublet, "A Bayesian Monte Carlo method for fission yield covariance information," ANNALS NUCL. EN. **95**, 125 (2016).
- [82] C. De Saint Jean, P. Archier, E. Privas, G. Noguere, O. Litaize, and P. Leconte, "Evaluation of cross section uncertainties using physical constraints: Focus on integral experiments," NUCL. DATA SHEETS **123**, 178 (2015).
- [83] D. Rochman, E. Bauge, A. Vasiliev, and H. Ferroukhi, "Correlation ν_p - σ - χ in the fast neutron range via integral information," EPJ NUCL. SCI. TECHNOL. **3**, 14 (2017).
- [84] D. Rochman and A. Koning, "How to Randomly Evaluate Nuclear Data: A New Data Adjustment Method

- Applied to ^{239}Pu ,” *NUCL. SCI. ENG.* **169**, 68 (2011).
- [85] D. Rochman and A. Koning, “Evaluation and Adjustment of the Neutron-Induced Reactions of $^{63,65}\text{Cu}$,” *NUCL. SCI. ENG.* **170**, 265 (2012).
- [86] O. Leray, D. Rochman, M. Fleming, J.-Ch. Sublet, A. Koning, A. Vasiliev, and H. Ferroukhi, “Fission yield covariances for JEFF: A Bayesian Monte Carlo method,” *EPJ WEB CONF.* **146**, 09023 (2017).
- [87] E. Bauge, “Full Model Nuclear Data and Covariance Evaluation Process Using TALYS, Total Monte Carlo and Backward-forward Monte Carlo,” *NUCL. DATA SHEETS* **123**, 201 (2015).
- [88] P. Helgesson and H. Sjostrand, “Fitting a defect non-linear model with or without prior, distinguishing nuclear reaction products as an example,” *REV. SCI. INSTRUM.* **88**, 115114 (2017).
- [89] M. Salvatores, “Methods and issues for the combined use of integral experiments and covariance data,” tech. rep., Nuclear Energy Agency, OECD, NEA/WPEC-33 (2013). NEA/NSC/WPEC/DOC(2013)445.
- [90] J. Briggs, “International Handbook of evaluated Criticality Safety Benchmark Experiments,” tech. rep., Nuclear Energy Agency, OECD, Paris (2004). NEA/NSC/DOC(95)03/I.
- [91] R. E. MacFarlane, D. W. Muir, R. M. Boicourt, A. C. Kahler, J. L. Conlin, and W. Haeck, “The NJOY Nuclear Data Processing System, Version 2016,” (2018). LANL <https://github.com/njoy>.
- [92] J.-Ch. Sublet, J. Eastwood, J. Morgan, M. Gilbert, M. Fleming, and W. Arter, “FISPACT-II: An Advanced Simulation System for Activation, Transmutation and Material Modelling,” *NUCL. DATA SHEETS* **139**, 77 (2017).
- [93] M. Fleming, T. Stainer, and M. Gilbert, eds., *FISPACT-II User Manual*. No. UKAEA-R(18)001, UKAEA (2018). <https://fispact.ukaea.uk/>.
- [94] T. Goorly, M. James, T. Booth, *et al.*, “Initial MCNP6 release overview,” *NUCL. TECHNOL.* **180**, 298 (2012).
- [95] J. Leppänen, M. Pusa, T. Viitanen, V. Valtavirta and T. Kaltiaisenaho, “The Serpent Monte Carlo code: Status, development and applications in 2013,” *ANNALS NUCL. EN.* **82**, 142 (2015). Joint Inter. Conf. on Supercomputing in Nuclear Applications and Monte Carlo 2013, SNA + MC 2013. Pluri- and Trans-disciplinarity, Towards New Modeling and Numerical Simulation Paradigms.
- [96] E. Brun, F. Damian, C. Diop, *et al.*, “TRIPOLI-4, CEA, EDF and AREVA reference Monte Carlo code,” *ANNALS NUCL. EN.* **82**, 151 (2015).
- [97] M. R. Gilbert, “SPECTRA-PKA,” (2018). <https://github.com/fispact/SPECTRA-PKA>.
- [98] R. E. MacFarlane, D. W. Muir, R. M. Boicourt, and A. C. Kahler, “The NJOY Nuclear data processing system – LA-UR-12-27079,” (Version 2012-082).
- [99] M. Gilbert, J. Marian, and J.-Ch. Sublet, “Energy spectra of primary knock-on atoms under neutron irradiation,” *J. NUCL. MATER.* **467**, 121 (2015).
- [100] J. B. (Ed.), “International handbook of evaluated criticality safety benchmark experiments,” tech. rep., Nuclear Energy Agency Paris (2015). NEA/NSC/DOC(95)03/I.
- [101] “Benchmarks - sublibrary of benchmarks for FENDL validation, www.nds.iaea.org/fendl20/fen-bench.htm,” (2018).
- [102] Y. Oyama, S. Yamaguchi, and H. Maekawa, “Measurements and analyses of angular neutron flux spectra on graphite and lithium-oxide slabs irradiated with 14.8 MeV neutrons,” *J. NUCL. SCI. TECHNOL.* **25**, 419 (1988).
- [103] C. Ichihara, I. Kimura, S. Hayashi, J. Yamamoto, and A. Takahashi, “Measurement of leakage neutron spectra from a spherical pile of Zirconium irradiated with 14 MeV neutrons and validation of its nuclear data,” *J. NUCL. SCI. TECHNOL.* **40**, 417 (2003).
- [104] C. Wong, J. Anderson, P. Brown, L. Hansen, J. Kammerdiener, C. Logan, and B. Pohl, “Livermore pulsed sphere program: Program summary through July 1971,” tech. rep., Lawrence Livermore National Laboratory (1972). UCRL-51144, Rev. 1.
- [105] R. Forrest, M. Pillon, J. Kopecky, A. Klix, S. P. Simakov, J.-Ch. Sublet, P. Bém, M. Honusek, and E. Šimecková, “Validation of EASY-2007 using integral measurements,” Tech. Rep. UKAEA-FUS-547, UKAEA, United Kingdom (2008).
- [106] M. Fleming, J.-Ch. Sublet, M. Gilbert, A. Koning, and D. Rochman, “TALYS/TENDL verification and validation processes: Outcomes and recommendations,” *EPJ WEB CONF.* **146**, 02033 (2017).
- [107] M. Gilbert and J.-Ch. Sublet, “Decay heat validation, FISPACT-II & TENDL-2017, JEFF-3.3, ENDF/B-VIII.0, EAF2010, and IRDFF-1.05 nuclear data libraries,” Tech. Rep. UKAEA-CCFE-R(18)002, CCFE (2018).
- [108] F. Maekawa and Y. Ikeda, “Decay heat experiment on thirty-two fusion reactor relevant materials irradiated by 14-MeV neutrons,” *FUSION ENG. DES.* **47**, 377 (2000).
- [109] F. Maekawa, C. Konno, Y. Kasugi, Y. Oyama, and Y. Ikeda, “Data collection of fusion neutron benchmark experiments conducted at FNS/JAERI,” Tech. Rep. JAERI-Data/Code 98-021, FNS/JAERI (1998).
- [110] J. Eastwood, J. Morgan, and J.-Ch. Sublet, “Inventory Uncertainty Quantification using TENDL Covariance Data in Fispact-II,” *NUCL. DATA SHEETS* **123**, 84 (2015).
- [111] N. Dzysiuk and A. Koning, “Improving activation cross section data with TALYS,” *EPJ WEB CONF.* **146**, 02047 (2017).
- [112] M. Fleming, J.-Ch. Sublet, and J. Kopecky, “Integro-Differential Verification and Validation, FISPACT-II & TENDL-2017, nuclear data libraries,” Tech. Rep. UKAEA-R(18)004, CCFE (2018).
- [113] E. Mendoza, D. Cano-Ott, T. Koi, and C. Guerrero, “New Standard Evaluated Neutron Cross Section Libraries for the GEANT4 Code and First Verification,” *IEEE TRANS. ON NUCL. SCI.* **61**, 2357 (2014).
- [114] I. Rakhno, N. Mokhov, and K. Gudima, “Modelling proton-induced reactions at low energies in the MARS15 code,” in *12th Meeting on Shielding Aspects of Accelerators, Targets and Irradiation Facilities (SATIF-12)* (2014). April 28-30, 2014, Fermi National Accelerator Laboratory, Illinois, USA, Fermilab-Conf-14-173-APC.
- [115] B. Haugh, “Generic application of the Studsvik Scandpower core management system to pressurized water reactors,” tech. rep., Studsvik Scandpower, Wilmington, NC, USA (2017). SSP-14-P01/028-TR-NP-A, Rev. 0.
- [116] R. Capote, K. Zolotarev, V. Pronyaev, and A. Trkov, “Updating and Extending the IRDF-2002 Dosimetry Library,” *J. ASTM INT.* **9**, 1 (2012).

- [117] D. Rochman, A. Vasiliev, H. Ferroukhi, T. Zhu, S. van der Marck, and A. Koning, "Nuclear data uncertainty for criticality-safety: Monte Carlo vs. linear perturbation," *ANNALS NUCL. EN.* **92**, 150 (2016).
- [118] L. Gilli, D. Lathouwers, J. Kloosterman, T. van der Hagen, A. Koning, and D. Rochman, "Uncertainty quantification for criticality problems using non-intrusive and adaptive Polynomial Chaos techniques," *ANNALS NUCL. EN.* **56**, 71 (2013).
- [119] T. Zhu, A. Vasiliev, H. Ferroukhi, D. Rochman, and A. Pautz, "Testing the Sampling-Based NUSS-RF Tool for the Nuclear Data Related Global Sensitivity Analysis with Monte Carlo Neutronics Calculations," *NUCL. SCI. ENG.* **184**, 69 (2016).
- [120] D. D. Cruz, D. Rochman, and A. Koning, "Uncertainty analysis on reactivity and discharged inventory due to $^{235,238}\text{U}$, $^{239,240,241}\text{Pu}$, and fission products: Application to a Pressurized Water Reactor Fuel assembly," *NUCL. TECHNOL.* **185**, 174 (2014).
- [121] D. da Cruz, D. Rochman, and A. Koning, "Quantification of Uncertainties due to $^{235,238}\text{U}$, $^{239,240,241}\text{Pu}$ and Fission Products Nuclear Data Uncertainties for a PWR Fuel Assembly," *NUCL. DATA SHEETS* **118**, 531 (2014).
- [122] D. Rochman and C. Sciolla, "Nuclear data uncertainty propagation for a typical PWR fuel assembly with burnup," *NUCL. ENG. TECHNOL.* **46**, 353 (2014).
- [123] D. Rochman, O. Leray, M. Hursin, *et al.*, "Nuclear Data Uncertainties for Typical LWR Fuel Assemblies and a Simple Reactor Core," *NUCL. DATA SHEETS* **139**, 1 (2017).
- [124] D. Rochman, A. Koning, and S. van der Marck, "Uncertainties for criticality-safety benchmarks and k_{eff} distributions," *ANNALS NUCL. EN.* **36**, 810 (2009).
- [125] T. Zhu, D. Rochman, A. Vasiliev, H. Ferroukhi, W. Wieselquist, and A. Pautz, "Comparison of Two Approaches for Nuclear Data Uncertainty Propagation in MCNPX for Selected Fast Spectrum Critical Benchmarks," *NUCL. DATA SHEETS* **118**, 388 (2014).
- [126] A. Vasiliev, D. Rochman, M. Pecchia, and H. Ferroukhi, "On the options for incorporating nuclear data uncertainties in criticality safety assessments for LWR fuel," *ANNALS NUCL. EN.* **116**, 57 (2018).
- [127] N. Terranova, O. Serot, P. Archier, C. D. S. Jean, and M. Sumini, "Covariance Matrix Evaluations for Independent Mass Fission Yields," *NUCL. DATA SHEETS* **123**, 225 (2015).
- [128] L. Fiorito, A. Stankovskiy, G. V. den Eynde, C. Diez, O. Cabellos, and P. Labeau, "Generation of fission yield covariances to correct discrepancies in the nuclear data libraries," *ANNALS NUCL. EN.* **88**, 12 (2016).
- [129] G. Noguere, J. Tommasi, E. Privas, K. Schmidt, and D. Rochman, "Systematics of Nd cumulative fission yields for neutron-induced fission of ^{235}U , ^{238}U , ^{238}Pu , ^{239}Pu , ^{240}Pu and ^{241}Pu ," *EUR. PHYS. J. PLUS* **133**, 99 (2018).
- [130] O. Leray, D. Rochman, M. Fleming, J.-Ch. Sublet, A. Koning, A. Vasiliev, and H. Ferroukhi, "Fission yield covariances for JEFF: A Bayesian Monte Carlo method," *EPJ WEB CONF.* **146**, 09023 (2017).
- [131] H. Sjöstrand, S. Conroy, P. Helgesson, A. Hernandez, A. Koning, S. Pomp, and D. Rochman, "Propagation of nuclear data uncertainties for fusion power measurements," *EPJ WEB CONF.* **146**, 02034 (2017).
- [132] D. Rochman, A. Koning, and S. van der Marck, "Exact nuclear data uncertainty propagation for fusion neutronics calculations," *FUSION ENG. DES.* **85**, 669 (2010).
- [133] D. Rochman, S. van der Marck, A. Koning, *et al.*, "Uncertainty Propagation with Fast Monte Carlo Techniques," *NUCL. DATA SHEETS* **118**, 367 (2014).
- [134] D. da Cruz, D. Rochman, and A. Koning, "Uncertainty on feedback coefficients and key core parameters for a pressurized water reactor due to nuclear data uncertainties," in *Proceedings of ICONE-23* (2015). ICONE23-1685, 23rd International Conference on Nuclear Engineering May 17-21, 2015, Chiba, Japan.
- [135] D. Rochman, A. Koning, and D. da Cruz, "Uncertainties for the kalimer sodium fast reactor: Void reactivity coefficient, k_{eff} , β_{eff} , depletion and radiotoxicity," *J. NUCL. SCI. TECHNOL.* **48**, 1193 (2011).
- [136] E. Alhassan, H. Sjöstrand, P. Helgesson, M. Osterlund, S. Pomp, A. Koning, and D. Rochman, "Selecting benchmarks for reactor simulations: An application to a lead fast reactor," *ANNALS NUCL. EN.* **96**, 158 (2016).
- [137] E. Alhassan, H. Sjöstrand, P. Helgesson, A. Koning, M. Osterlund, S. Pomp, and D. Rochman, "Uncertainty and correlation analysis of lead nuclear data on reactor parameters for the European Lead Cooled Training Reactor," *ANNALS NUCL. EN.* **75**, 26 (2015).
- [138] O. Cabellos, E. Castro, C. Ahnert, and C. Holgado, "Propagation of nuclear data uncertainties for PWR core analysis," *NUCL. ENG. TECHNOL.* **46**, 299 (2014).
- [139] O. Leray, H. Ferroukhi, M. Hursin, A. Vasiliev, and D. Rochman, "Methodology for core analyses with nuclear data uncertainty quantification and application to Swiss PWR operated cycles," *ANNALS NUCL. EN.* **110**, 547 (2017).
- [140] D. Rochman, A. Vasiliev, H. Ferroukhi, H. Dokhane, and A. Koning, "How inelastic scattering stimulates nonlinear reactor core parameter behaviour," *ANNALS NUCL. EN.* **112**, 236 (2018).
- [141] D. da Cruz, D. Rochman, and A. Koning, "Total Monte Carlo method applied to the assessment of uncertainties in a reactivity-initiated accident," (2014). PBNC2014-205, The 19th Pacific Basin Nuclear Conference (PBNC 2014), Hyatt Regency Hotel, Vancouver, British Columbia, Canada, August 24-28, 2014.
- [142] A. Dokhane, G. Grandi, A. Vasiliev, D. Rochman, and H. Ferroukhi, "Validation of PSI best estimate plus uncertainty methodology against SPERT-III reactivity initiated accident experiments," *ANNALS NUCL. EN.* **118**, 178 (2018).
- [143] D. Rochman, A. Vasiliev, H. Dokhane, and H. Ferroukhi, "Uncertainties for Swiss LWR spent nuclear fuels due to nuclear data," *ACCEPT. EUR. J. PHYS. N* (2018).
- [144] D. Rochman, A. Vasiliev, H. Ferroukhi, and M. Pecchia, "Consistent criticality and radiation studies of Swiss spent nuclear fuel: The CS₂M approach," *J. HAZARD. MATER.* **357**, 384 (2018).
- [145] P. Griffin, D. Rochman, and A. Koning, "Characterization of the energy-dependent uncertainty and correlation in silicon neutron displacement damage metrics," *EPJ WEB CONF.* **146**, 02008 (2017).
- [146] J.-Ch. Sublet, I. Bondarenko, V. Khryachkov, *et al.*, "Neutron-induced damage simulations: Beyond defect production cross-section, displacement per atom and iron-based metrics," unpublished (2018).